EFFECT OF SURFACE IMPERFECTIONS ON THE STABILITY OF COMPRESSIBLE LAMINAR BOUNDARY LAYERS.

by

R. C. Krishna

Thesis submitted to the Faculty of the

Virginia Polytechnic Institute and State University

in partial fulfillment of the requirements for the degree of

Master of Science

in

Engineering Science and Mechanics

APPROVED:

Dr. S. A. Ragab, Chairman

Dr. A. H. Nayfeh

Dr. R. A. Heller

May, 1988

Blacksburg, Virginia

EFFECT OF SURFACE IMPERFECTIONS ON THE STABILITY OF COMPRESSIBLE LAMINAR BOUNDARY LAYERS.

by

R. C. Krishna

Dr. S. A. Ragab, Chairman

Engineering Science and Mechanics

(ABSTRACT)

The accuracy of the compressible interacting boundary-layer computations is investigated and their limitations are established by comparison with solutions to the Navier-Stokes equations both for the mean flow profiles and for the stability characteristics. The instabilities of flows around smooth forward and backward facing steps are investigated. Results presented include the effect of computational grid refinement, geometrical parametres such as heights and slopes of steps, Mach number and Reynolds number on the mean flow as well as the stability characteristics.

A proper grid should be chosen to predict accurately the mean flow profiles, including their first and second derivatives. The study has shown that the heights of the steps are more influential in triggering transition than their slopes. Increasing the Mach number reduces the growth rates and amplification factors but the presence of small separation bubbles, which increase in size with increasing Mach number, partially offset this benefit.

Attention Patron:

Page iii is missing
from all copies

Acknowledgements

The author would like to take this opportunity to place on record his deep sense of gratitude to Professors Saad. A. Ragab and A. H. Nayfeh for their continuous guidance and assistance in the pursuance of this work. Thanks are also due to Professor R. A. Heller for serving on his committee and for contributing to his education.

Thanks are due to Prof. J. N. Reddy for all his support and encouragement.

Thanks are due to the author's parents and to his sisters Aruna and Shanti for their inspiration, love, support and sacrifice.

Finally, the author appreciates all the help of Mr. William Richardson with the computer facilities.

This work was supported by the NASA Langley Research Center, under Grant No. NAG-1-714.

Table of Contents

List of Illustrations

Chapter 1

1. INTRODUCTION

Present efforts to use Natural Laminar Flow (NLF) for high performance aircraft design stem from the progress made in recent years in the field of laminar flow aerodynamics and its proven achievability on modern airframe surfaces over a range of cruise flight conditions (Ref.1). The substantial drag benefits with NLF have prompted further indepth analyses of ways and means of achieving NLF on geometries of aerodynamic interest in various flow regimes and flight conditions.

Surface imperfections strongly influence the location of transition. The location of transition in the flow field in turn influences the performance of NLF geometries. Existing manufacturing techniques and tools can control the smoothness of the surfaces which are compatible with NLF. However, in all practical situations the designer is still faced with the problem of having to accommodate some unavoidable imperfections in the form of bulges, steps and gaps and three-dimensional roughness elements . The imperfections due to installation of various components of the aircraft, such as, doors and windows on fuselages and leading-edge panels on wings and nacelles, which are unavoidable, also need to be accommodated. Thus

criteria to limit the sizes of these imperfections so that NLF can be maintained need to be established.

The mechanisms by which these imperfections cause transition include laminar flow separation, amplification of Tollmien-Schlichting (TS) waves and cross-flow vorticity, acoustic disturbances, and the enhancement of receptivity due to free-stream turbulence. Any interaction between any of the above mechanisms may also trigger transition. Empirically based criteria that result in either laminar separation or amplification of TS waves was established first by Fage (Ref.3) and Carmichael (Ref.4). Fage established the critical heights of bulges, hollows and ridges in incompressible flows based on the results of experiments carried out on flat plates with these imperfections by Walker and Greening. Carmichael (Ref. 5, 6) included the effects of compressibility, suction, pressure gradients, multiple imperfections and wing sweep to establish criteria for allowable sizes of bulges and sinusoidal waviness. The flight experiments of Holmes et al (Ref.1) demonstrate the strong influence of shapes of steps on transition location and hence on the allowable heights of such imperfections. They found that by rounding a forward-facing step the critical Reynolds number increases from 1800 to 2700.

The effect of compressibility on the shapes of manufacturing imperfections still needs to be explored in detail. The Mach number range just above the drag rise Mach number is one of the most efficient regimes in flight. The past applications of NLF for drag reduction were mainly concerned with lifting surfaces. For non-lifting surfaces such as fuselages and engine nacelles, the effect of compressibilty is equally important for the application of NLF. Vijgen et al (Ref.7) have investigated the effect of compressibility on the design of subsonic fuselages. They showed that increasing the free-stream Mach number from low subsonic to 0.60 and to 0.80 incrases the TS stability of the laminar boundary layers over the geometries they analyzed. Hastings et al (Ref.2) carried out experiments on an NLF engine nacelle fairing. They reported achievability of NLF on a surface that is within the vicinity of engine noise. They observed that natural laminar flow extended as far aft as 37% on a NLF fairing installed on a turbofan nozzle.The application of NLF to bodies at high subsonic flows is affected by

compressibility through development of density gradients in the boundary layers in a direction normal to the surface and due to its effect on pressure gradients in the flow. Density gradients become dominant in high subsonic and supersonic flow regimes. These provide additional damping of two-dimensional and axisymmetric TS waves. The attainment of NLF takes advantage of this effect, resulting in an overall drag reduction. However, the enhancement of the adverse pressure gradients caused by the increasing Mach number will offset this advantage due to the increase in the size of the separation bubbles for flows over surface imperfections like those aforementioned.

Inspite of all these investigations, understanding of stability characteristics of flow fields around surface imperfections is still incomplete . With this in mind, we have carried out a study of the influence of forward and backward facing steps on two-dimensional stability. We have used a combination of linear stability theory and the exp(N) criterion for transition correlation. The linear stability theory of these types of flows is well established. The important aspect in this investigation is the accurate prediction of the mean flows over these imperfections.

As for the mean flow, a conventional boundary layer formulation would suffice when smooth surfaces are under consideration. However, it cannot predict the flow over surfaces with imperfections such as suction strips and slots, waviness and bulges, steps and gaps at junctions and the three-dimensional roughness elements because of strong viscous and inviscid interaction. Instead, one has to use a triple-deck formulation, an interactive boundary-layer formulation, or a Navier-Stokes solver. For smooth imperfections one can use either a triple-deck or an interactive boundary-layer formulation. However the accuracy of the triple-deck formulation, which is an asymptotic theory for large Reynolds numbers for laminar flows, may not be accurate enough for finite Reynolds number. For large and/or nonsmooth imperfections, one has to use a Navier-Stokes solver. However, they involve prohibitive computation costs. The high costs and and the large number of cases to be investigated naturally justifies the lookout for an interactive boundary-layer solution for flows which do not

involve massive separation and/or vortex shedding. When using the Navier-Stokes solvers care must be taken to choose a proper grid which is fine enough to capture the important flow structures and avoid the contamination of the solution by reflections from far field boundaries especially for high Mach number flows. The grid should also be fine enough to determine accurately the magntitudes of mean velocity and temperature profiles, including their first and second derivatives, so that the stability characteristics of these flows can be accurately determined.

The mean flow over small humps and steps have been considered by many authors using the triple-deck and interactive boundary-layer formulations. The problem of flow over humps was first considered by Smith using the triple deck theory (Ref.8). Ragab and Nayfeh (Ref.9) presented a second-order triple-deck theory for predicting flows over a hump and presented a comparison of the solution with those obtained by the interactive boundary-layer formulation. Carter and Wornom (Ref.10,11) presented a viscous-inviscid interaction technique in which the inviscid solution is solved inversely by prescribing the pressure obtained from the boundary-layer solution and the new displacement thickness is obtained as the solution of the Cauchy integral.

One of the purposes of the present work is to check the accuracy of mean flows computed by the interactive boundary-layer formulation in the compressible regime. In Chapter 2 a compressible interactive boundary-layer formulation for flows with small imperfections is presented. Davis (Ref.12) presented a similar treatment for interacting boundary-layer equations for subsonic and supersonic flows. Mean flows using a Navier-Stokes formulation have been obtained by the code ARC2D which has been acquired from NASA Ames. The method of solution is that presented by Pulliam and Schaussee (Refs.13,14). Following the work of Nayfeh (Ref.15,16) a linear stability model is presented in chapter 3 for the analysis of stability characteristics.

To check the present code, we compare its results with those of Carter and Wornom for incompressible laminar flows over an indented plate in chapter 4. Veldman (Ref.17,18) and Henkes and Veldman (Ref.19) presented a method for calculating boundary layers with strong viscid-inviscid interaction using an interactive boundary condition that describes the outer potential flow. A comparison of our results with Veldman's calculations is presented in chapter 4. Comparisons between Navier-Stokes and Interacting boundary layer results for the mean profiles as well as the stability characteristics such as the growth rates and amplification factors of linear stability waves for two Mach numbers for flows over smooth forward and backward steps are also presented. The geometries of the steps are given by Smith and Merkin (Ref.20).The results presented in chapter 4 also enunciate the importance of grid refinement for both compressible and incompressible flows.

The effect of humps and dips on the stability characteristics of incompressible flow was considered by Nayfeh et al (Ref.21). They studied the effect of hump/width ratio and hump location on the growth rates of 2-D TS waves and the corresponding N-factors. They found a significant dependence of the amplification factor on the height-to-width ratio. Nayfeh and Ragab (Ref.22) extended the work of Nayfeh et al to consider the effect of secondary instabilities. The objective of the present work is also to consider the effect of surface imperfections, in the form of smooth forward-and backward-facing steps and humps on the stability of compressible flows. In chapter 5, results are presented that show the effect of the geometrical parametres of the imperfections, Mach number and Reynolds number. The work ends with conclusions and recommendations in chapter 6.

Chapter 2

2. INTERACTIVE BOUNDARY LAYER MODEL

2.1 Introduction

We consider viscous compressible flows over a flat plate with small backward-and forward-facing steps. In our analysis we have also considered the case of viscous incompressible flows over flat plates with small indentations. Evaluating the response of the boundary layer to these types of imperfections is necessary for studying their effects on the transition from laminar to turbulent flows. In high speed regimes these protrusions and indentations also contribute significantly to the overall drag increase of flight vehicles. This analysis also can be extended to three-dimensional atmospheric boundary-layer flows for similar types of landscapes.

The problem of flows over steps was first anlyzed by Smith and Merkin (Ref.20) using triple deck theory. Carter and Wornom (Ref.10) formulated the subsonic interaction problem in terms of the vorticity and stream function. They used a linearized potential theory to calculate

the pressure over the displacement body. They obtained solutions over a dip with small separation bubbles using the method of finite differences. Veldman (Refs.17,18) presented a method for calculating boundary layers with strong viscous - inviscid interactions. He used a boundary condition which describes the outer potential flow instead of specifying pressure. In the present analysis, the problem is formulated in terms of the Levy-Lees variables (ξ, η, F, V, Q) and the interaction with the outer flow is accounted for by the Veldman's procedure for both compressible and incompressible flows. Davis (Ref. 12) considered a similar treatment for subsonic and supersonic flows over parabolic humps.

2. 2 Mathematical Model

The governing equations are the compressible boundary-layer equations. In terms of the Levy - Lees variables, the problem is given by

$$2\xi FF_\xi + VF_\eta - \frac{\partial}{\partial\eta}(\theta\frac{\partial F}{\partial\eta}) + \beta_0(F^2 - Q) = 0 \tag{2.1}$$

$$2\xi F_\xi + V_\eta + F = 0 \tag{2.2}$$

$$2\xi FQ_\xi + VQ_\eta - \frac{\partial}{\partial\eta}(\frac{\theta}{Pr}\frac{\partial Q}{\partial\eta}) - \alpha\theta F_\eta^2 = 0 \tag{2.3}$$

subject to the boundary conditions

$$F = 0, V = 0 \qquad \text{at } \eta = 0$$

$$F = 1 \qquad \text{as } \eta \to \infty \tag{2.4}$$

$$F = F(\xi_0, \eta) \quad \text{at } \xi = \xi_0$$

$$Q = Q_w \quad \text{at } \eta = 0$$

$$Q = 1 \qquad \text{as } \eta \to \infty$$

$$Q = Q(\xi_0, \eta) \quad \text{at } \xi = \xi_0$$

where

$$\xi(x) = \int_0^x \rho_e \mu_e U_e \, dx \tag{2.5}$$

$$\eta(x, y) = \frac{U_e}{\sqrt{2\xi}} \int_0^y \rho \, dy \tag{2.6}$$

$$F(\xi, \eta) = U(x, y)/U_e(x) \tag{2.7}$$

$$V(\xi, \eta) = \frac{\sqrt{2\xi}}{\rho_e U_e \mu_e} [\rho v + \eta_x \sqrt{2\xi} F] \tag{2.8}$$

$$Q(\xi, \eta) = \frac{T(x, y)}{T_e(x)} = \frac{\rho_e(x)}{\rho(x, y)} \tag{2.9}$$

$$\theta = \frac{\rho \mu}{\rho_e \mu_e} \tag{2.10}$$

$$\alpha = (\gamma - 1) M_\infty^2 U_e^2 / T_e \tag{2.11}$$

Here, x and y are body oriented coordinates and $\rho_\bullet$, $\mu_\bullet$ and $U_\bullet$ are the inviscid density, coefficient of viscosity, and surface inviscid velocity, respectively. The displacement thickness is given by

$$\delta = \frac{1}{\sqrt{Re}} \frac{\sqrt{2\xi}}{\rho_e \mu_e} \int_0^\infty (Q - F) \, d\eta \tag{2.12}$$

and the friction coefficient is defined by

$$C_f = \tau_w^\circ / \frac{1}{2} \rho^\circ U_e^{\circ 2} \tag{2.13}$$

All the above variables are nondimensionalized with respect to a reference length L°, reference velocity U_∞°, and pressure $\rho_\infty U_\infty^{\circ 2}$. Compressible and incompressible flows are obtained over the step specified by the equation

$$f = \frac{1}{2} h(1 + \text{erf}\,\bar{x}) \tag{2.14}$$

where

$$\bar{x} = Re^{-\frac{3}{8}} \lambda^{\frac{5}{4}} (x - 1) \tag{2.15}$$

Re is the Reynolds number based on the distance from the leading edge to the step center ($x = 1.0$) and $\lambda = 0.332057$. The equation for the dip for the incompressible study is given by

$$f = (-0.003) \frac{1}{\cosh(4x - 10)} \tag{2.16}$$

The interaction law relates the edge velocity U_e to the displacement surface given by equation (2.12). Using thin airfoil theory we obtain

$$U_e = \bar{U}_e + \frac{1}{\beta\pi} \int_{L.E}^{\infty} U_e \delta \frac{\frac{d \ln \rho_e}{dt}}{x - t} dt + \frac{1}{\beta\pi} \int_{L.E}^{\infty} \frac{d \frac{U_e \delta}{dx}}{x - t} dt \tag{2.17}$$

where

$$\beta = \sqrt{1 - M_\infty^2}$$

and $\bar{U}_e$ is the inviscid surface velocity in the absence of the boundary layer . Letting $T = f + \bar{U}_e\delta$ we can rewrite Eq. (2.17) as

$$U_e = 1 + \frac{1}{\beta\pi}\int_{L.E}^{\infty} \frac{\frac{dT}{dt}}{x-t}\,dt + \frac{1}{\beta\pi}\int_{L.E}^{\infty} U_e\delta \frac{\frac{d\ \ln\ \rho_e}{dt}}{x-t}\,dt \tag{2.18}$$

The principal values of the Cauchy integrals in Eq. (2.18) are assumed. Equations (2.1) to (2.4) are solved simultaneously following the procedure of Veldman (Ref.18) . Veldman integrated Eq. (2.18) by parts to obtain a second derivative for T and expressed U_e as a linear combination of the values of δ at the nodes. However, we perform the integration by parts to eliminate the derivative of T and assume T to be linearly varying over the differencing intervals to result in a second-order accurate scheme. The finite-difference scheme for solving the equations employs a three-point backward-differencing scheme for the ξ derivatives and a central differencing for the η derivatives. The distribution of the mesh points on the surface of the steps and dip are such that they honor the triple-deck scalings. The lower deck is resolved using a mesh with a variable step size in the η direction so that a larger number of points could be employed near the wall than in the rest of the boundary layer. Before substituting a linear expression of T, we decompose the first integral in the interaction law (2.18) as follows:

$$I = \frac{1}{\beta\pi}\int_{L.E}^{\infty} \frac{\frac{dT}{dt}}{x-t}\,dt = \frac{1}{\beta\pi}\lim_{\varepsilon\to 0}\left(\int_{L.E}^{x_l} + \int_{x_l}^{x_l-\varepsilon} + \int_{x_l+\varepsilon}^{x_r} + \int_{x_r}^{\infty}\right)\frac{\frac{dT}{dt}}{x-t}\,dt \tag{2.19}$$

Integrating the second and the third integrals by parts we have

$$I = \frac{1}{\beta\pi}\left(\int_{L.E}^{x_l} + \int_{x_r}^{\infty}\right)\frac{\frac{dT}{dt}}{x-t}\,dt + \frac{1}{\beta\pi}\left(\frac{T(x_r)}{x-x_r} - \frac{T(x_l)}{x-x_l}\right)$$

$$+ \frac{1}{\beta\pi}\lim_{\varepsilon\to 0}\left(\frac{T(x-\varepsilon)+T(x+\varepsilon)}{\varepsilon} + \int_{x_l}^{x-\varepsilon}\frac{T\,dt}{(x-t)^2} - \int_{x+\varepsilon}^{x_r}\frac{T\,dt}{(x-t)^2}\right) \tag{2.20}$$

Substituting a linear expression for T in Eq. (2.18) and using Eq. (2.20) we obtain

$$U_e(x_i) = 1 + \frac{\lambda}{\pi\beta}\{\frac{\Delta x}{4}\frac{T_1}{2x_l\sqrt{\xi_1\xi_i}}\ln(\frac{\sqrt{\xi_l}+1}{\sqrt{\xi_i}-1}) + \frac{T_m}{2x_r\sqrt{\zeta_m\zeta_i}}\ln(\frac{1-\sqrt{\zeta_i}}{\sqrt{\zeta_i}+1})\}$$

$$+\frac{\lambda}{\pi\beta}\{+\frac{T_m}{\sqrt{x_m x_r}}\frac{1}{\zeta_i - 1} - \frac{T_1}{\sqrt{x_1 x_l}}\frac{1}{\xi_i - 1}\}$$

$$+\frac{\lambda}{\pi\beta}\{\sum_{j=1}^{m} D_k T_j + \sum_{j=1}^{m} E_k(T_{j+1} - T_{j-1})\} \qquad (2.21)$$

where

$$k = |i - j|$$

$$D_k = (1 - 4k^2)^{-1},\ E_k = \frac{1}{2}kD_k - \frac{1}{8}\ln(2k-1)/(2k+1),\ \xi_i = \frac{x_i}{x_l},\ \zeta_i = \frac{x_i}{x_r},\ \lambda = \frac{4Re^{\frac{-1}{2}}}{\Delta x}$$

and x_l and x_r are given by

$$x_l = x_1 - \frac{1}{2}\Delta x,\ x_r = x_m + \frac{1}{2}\Delta x$$

Here x_1 and x_m are the first and last nodal points.The third term in Eq (2.18) is added explicitly. Integrating the continuity equation with respect to η and denoting η at infinity by η_N and V by V_N we have

$$V_N + K\eta_N = \sqrt{2\xi}\frac{d(\rho_e U_e \delta_e)}{d\xi} \qquad (2.22)$$

where

$$k = \int_0^{\eta_e}(Q + 2\xi\frac{\partial Q}{\partial \xi})d\eta$$

Equation (2.21) is rewritten in the following form for convenience:

$$U_e(x_i) = \lambda G_i + \lambda\Gamma(\rho_e U_e \delta)_i \tag{2.23}$$

Using three-point backward differencing, and Eqs. (2.2), (2.12) and (2.23) and defining the pressure-gradient parameter as

$$\beta_0 = \frac{2\xi}{U_e}\frac{dU_e}{d\xi},$$

we rewrite the interaction law as

$$V_N + \phi\beta_{0i} = \psi \tag{2.24}$$

where

$$\phi = (\sqrt{2\xi_i}/\lambda\Gamma)a_0\tilde{u}_{ei}/(2\xi_i a_0 - \beta_{0i}) \tag{2.25a}$$

$$\psi = -k\eta_N + \sqrt{2\xi_i}\,a_0\ X\left(\frac{\alpha}{\lambda\Gamma} - \frac{G_i}{\Gamma} + \frac{a_1}{a_0}T_{i-1} + + \frac{a_2}{a_0}T_{i-2}\right) \tag{2.25b}$$

$$\alpha = -\frac{u_{ei}\beta_{0i} + 2\xi_i(a_1 U_{ei-1} + a_2 u_{ei-2})}{2\xi_i a_0 - \beta_{0i}} \tag{2.25c}$$

$$a_0 = \frac{1}{\xi_i - \xi_{i-1}} + \frac{1}{\xi_i - \xi_{i-2}} \tag{2.25d}$$

$$a_1 = \frac{\xi_i - \xi_{i-2}}{(\xi_i - \xi_{i-1})(\xi_{i-1} - \xi_{i-2})} \tag{2.25e}$$

$$a_2 = \frac{\xi_i - \xi_{i-1}}{(\xi_i - \xi_{i-2})(\xi_{i-1} - \xi_{i-2})} \tag{2.25f}$$

Equations (2.1) to (2.4) along with the interaction law are solved simultaneously using the scheme described previously.The flow upstream of the interaction region is taken to be the Blasius flow.

Chapter 3

3. LINEAR STABILITY OF COMPRESSIBLE FLOW

3. 1 The Mathematical Model

In this section we consider a two-dimensional, compressible boundary - layer flow such as the flow over backward-or forward-facing steps. In order to study the stability of these basic states or the mean flow we superimpose small disturbances on the mean flow to obtain the total flow

uantities. These quantities are then substituted into the Navier Stokes equations. In order to obtain the governing equations for the disturbance quantities, we subtract the mean flow and linearize the resulting equations. These equations are then nondimensionalized and the Reynolds number and Prandtl number are given by $\mathrm{Re} = \frac{U_\infty^\circ \delta^\circ}{\nu_\infty^\circ}$ and $\mathrm{Pr} = \frac{\mu_\infty^\circ C_p^\circ}{\kappa_\infty^\circ}$. Here U_∞° is the dimensional velocity of the free stream , ν_∞° is the dimensional kinematic viscosity, δ° is a reference length given by $\sqrt{\nu_\infty^\circ \frac{x^\circ}{U_\infty^\circ}}$, μ_∞° is the dimensional dynamic viscosity, C_p° is the dimensional specific heat at constatnt pressure, and κ_∞° is the dimensional thermal conductivity.

The basic assumptions made are the following:

(1) quasi parallel mean flow

(2) constant γ, C_p, Pr

(3) the viscosity μ and conductivity κ are functions of temperature only

The assumption of constant Pr and C_p will affect the accuracy of the stability results only to a small extent because we are limiting our calculations to slightly compressible flows, where the Mach number is less than one. Since the Prandtl number and C_p are constants, we take $\kappa = \mu$.

The continuity equation for the total flow is given by

$$\frac{\partial \overline{\rho}}{\partial t} + \frac{\partial \overline{\rho}\overline{u}}{\partial x} + \frac{\partial \overline{\rho}\overline{v}}{\partial y} = 0 \tag{3.1}$$

where

$$\begin{aligned} \overline{\rho} &= R + \rho \\ \overline{u} &= U + u \\ \overline{v} &= v \end{aligned} \tag{3.2}$$

Substituting Eq. (3.2) into Eq. (3.1), cancelling the mean flow, and neglecting the nonlinear terms, we have

$$\frac{\partial \rho}{\partial t} + U\frac{\partial \rho}{\partial x} + \frac{dR}{dy}v + R\left(\frac{\partial u}{\partial x} + \frac{\partial v}{\partial y}\right) = 0 \tag{3.3}$$

The x- momentum equation for the total flow is given by

$$\bar{\rho}\left(\frac{\partial \bar{u}}{\partial t}+\bar{u}\frac{\partial \bar{u}}{\partial x}+\bar{v}\frac{\partial \bar{v}}{\partial y}\right)+\frac{\partial \bar{p}}{\partial x}-\frac{1}{Re}\left(\frac{\partial \bar{\tau}_{xx}}{\partial x}+\frac{\partial \bar{\tau}_{xy}}{\partial y}\right)=0 \tag{3.4}$$

where

$$\bar{\tau}_{xx}=\bar{\lambda}\left(\frac{\partial \bar{u}}{\partial x}+\frac{\partial \bar{v}}{\partial y}\right)+2\bar{\mu}\frac{\partial \bar{u}}{\partial x} \tag{3.5}$$

$$\bar{\tau}_{xy}=\bar{\mu}\left(\frac{\partial \bar{u}}{\partial y}+\frac{\partial \bar{v}}{\partial x}\right)$$

and

$$\bar{p}=P+p$$

$$\bar{\mu}=M+\mu \tag{3.6}$$

$$\bar{\lambda}=\Lambda+\lambda$$

where M is the viscosity of the basic state.

The bulk viscosity κ is defined by

$$\kappa=\lambda+\frac{2}{3}\mu$$

Substituting Eqs. (3.2), (3.5) and (3.6) into Eq. (3.4), cancelling out the mean flow, and neglecting the nonlinear terms, we finally have

$$R\left(\frac{\partial u}{\partial t}+U\frac{\partial u}{\partial x}+\frac{dU}{dy}v\right)+\frac{\partial p}{\partial x} \tag{3.7}$$

$$-\frac{1}{Re}\frac{\partial}{\partial x}\left[(\Lambda+2M)\frac{\partial u}{\partial x}+\Lambda\left(\frac{\partial v}{\partial y}\right)\right]$$

$$-\frac{1}{Re}\frac{\partial}{\partial y}[M(\frac{\partial u}{\partial y}+\frac{\partial v}{\partial x})]=0$$

Because $\bar{\mu}$ and $\bar{\lambda}$ are functions of temperature only, we have

$$\lambda=\frac{d\Lambda}{d\bar{T}}T$$

and

$$\mu=\frac{dM}{d\bar{T}}T$$

Proceeding in a similar way, we obtain the following from the y- momentum equation:

$$R(\frac{\partial v}{\partial t}+U\frac{\partial v}{\partial x})+\frac{\partial p}{\partial y} \tag{3.8}$$

$$-\frac{1}{Re}\frac{\partial}{\partial y}[(\Lambda+2M)\frac{\partial v}{\partial y}+\Lambda(\frac{\partial u}{\partial x})]$$

$$-\frac{1}{Re}\frac{\partial}{\partial x}[M(\frac{\partial v}{\partial x}+\frac{\partial u}{\partial y})]=0$$

At this stage we define the following two prameters

$$r=2+m \tag{3.9}$$

and

$$m=\frac{\bar{\lambda}}{\bar{\mu}}$$

where m is constant and is equal to $\frac{\Lambda}{M}=\frac{\lambda}{\mu}$. Substituting these into the x-momentum and y-momentum equations, we rewrite the x- momentum as

$$R\left(\frac{\partial u}{\partial t} + U\frac{\partial u}{\partial x} + \frac{dU}{dy}v\right) + \frac{\partial p}{\partial x} \tag{3.10}$$

$$= \frac{1}{Re}\frac{\partial}{\partial x}\left[rM\frac{\partial u}{\partial x} + mM\frac{\partial v}{\partial y}\right]$$

$$+ \frac{1}{Re}\frac{\partial}{\partial y}\left[M\left(\frac{\partial u}{\partial y} + \frac{\partial v}{\partial x}\right) + \mu\frac{dU}{dy}\right]$$

and the y-momentum as

$$R\left(\frac{\partial v}{\partial t} + U\frac{\partial v}{\partial x}\right) + \frac{\partial p}{\partial y} = \tag{3.11}$$

$$\frac{1}{Re}\frac{\partial}{\partial y}\left[rM\frac{\partial v}{\partial y} + mM\frac{\partial u}{\partial x}\right]$$

$$+ \frac{1}{Re}\frac{\partial}{\partial x}\left[M\left(\frac{\partial u}{\partial y} + \frac{\partial v}{\partial x}\right) + \mu\frac{dU}{dy}\right]$$

The energy equation for the total flow is

$$\frac{\partial \overline{\rho}\overline{E}}{\partial t} + \frac{\partial}{\partial x}\left[(\overline{\rho}\overline{E} + \overline{p})\overline{u}\right] + \frac{\partial}{\partial y}\left[(\overline{\rho}\overline{E} + \overline{p})\overline{v}\right] \tag{3.12}$$

$$- \frac{\partial}{\partial x}\left(\overline{u}\overline{\tau}_{xx} + \overline{v}\overline{\tau}_{xy} - \overline{q}_x\right)$$

$$- \frac{\partial}{\partial y}\left(\overline{u}\overline{\tau}_{xy} + \overline{v}\overline{\tau}_{yy} - \overline{q}_y\right) = 0$$

where

$$\overline{E} = \overline{e} + \frac{1}{2}(\overline{u}^2 + \overline{v}^2)$$

and $\overline{e}$ is the specific internal energy,

and

$$(\bar{q}_x, \bar{q}_y) = -\frac{\kappa}{(\gamma - 1)M_\infty^2 RePr}\left(\frac{\partial \bar{T}}{\partial x}, \frac{\partial \bar{T}}{\partial y}\right)$$

Substituting Eqs. (3.2), (3.5), and (3.6) into Eq. (3.12), cancelling out the mean flow, and neglecting the nonlinear terms, we obtain the energy equation as

$$R\left(\frac{\partial T}{\partial t} + U\frac{\partial T}{\partial x} + \frac{d\bar{T}}{dy}v\right) - (\gamma - 1)M_\infty^2\left(\frac{\partial p}{\partial t} + U\frac{\partial p}{\partial x}\right) \tag{3.13}$$

$$= \frac{M}{RePr}\left(\frac{\partial^2 T}{\partial x^2} + \frac{\partial^2 T}{\partial y^2}\right) + \frac{1}{RePr}\frac{\partial \mu}{\partial y}\frac{d\bar{T}}{dy} +$$

$$\frac{1}{RePr}\frac{dM}{dy}\frac{dT}{dy} + \frac{(\gamma - 1)M_\infty^2 \phi}{Re} + \frac{\mu}{RePr}D^2\bar{T}$$

where

$$\phi = 2M\left[\left(\frac{\partial u}{\partial y} + \frac{\partial v}{\partial x}\right)\frac{dU}{dY}\right] + \mu\left(\frac{dU}{dy}\right)^2$$

The linearized equation of state for a perfect gas is

$$\gamma M_\infty^2 p = RT + \rho\bar{T} \tag{3.14}$$

or

$$\rho = (\gamma M_\infty^2 p - RT)/\bar{T}$$

The boundary conditions for the disturbance equations (3.3), (3.10), (3.11) and (3.13) are given by

$$u = v = T = 0 \quad \text{at} \quad y = 0 \tag{3.15}$$

$$u, v, p, T \to 0 \quad \text{as} \quad y \to \infty$$

We now consider disturbances or instabilities in the form of propagating waves given by

$$q = \hat{q}(y) \exp\{i\int \alpha \, dx - i\omega t\} + CC. \tag{3.16}$$

where q stands for the disturbance quantities (velocities, pressure etc.), α is a complex wavenumber, and ω is a real frequency. These are the conditions for spatial stability. For temporal stability α is real and ω is complex. For spatial stability, $-\alpha_i$ is the growth rate. The subscript i indicates the imaginary part of a complex number. We now drop the hat from the $\hat{q}$ for convenience and define

$$\Omega = \omega - \alpha U \tag{3.17}$$

Substituting Eq. (3.16) into Eq. (3.3), we have

$$-i\Omega\rho + vDR + R(i\alpha u + Dv) = 0 \tag{3.18}$$

which upon rearranging and using Eq. (3.14) we obtain

$$Dv = -i\alpha u + \frac{D\bar{T}}{\bar{T}} v + \frac{i\Omega p}{P} - \frac{i\Omega T}{\bar{T}} \tag{3.19}$$

Substituting Eq. (3.16) into Eq. (3.10), defining $M_T = \frac{dM}{d\bar{T}}$ and $\mu = \frac{dM}{d\bar{T}} T$ we obtain

$$D^2u = \left(\frac{-iRe\Omega R}{M} + \alpha^2\right) u \tag{3.20}$$

$$+ \left(\frac{-M_T D\bar{T}}{M}\right) Du + \left[\frac{ReRDU}{M} - i\frac{\alpha M_T D\bar{T}}{M} - \frac{i(1+m)\alpha D\bar{T}}{\bar{T}}\right]$$

$$+ \left(\frac{iRe\alpha}{M} + (1+m)\alpha\frac{\Omega}{P}\right) p$$

$$-\left(\frac{(1+m)\alpha\Omega}{\bar{T}}+\frac{DM_TDU}{M}+M_T\frac{D^2U}{M}\right)T$$

$$-\frac{M_TDU}{M}DT$$

Following the same procedure as above and defining $\chi^{-1}=\frac{Re}{M}-ir\frac{\Omega}{P}$, we obtain the following from the y momentum equation:

$$\chi^{-1}Dp=-i\alpha\left(r\frac{D\bar{T}}{\bar{T}}+2\frac{M_T}{\mu}D\bar{T}\right)u-i\alpha Du \tag{3.21}$$

$$+\left(\frac{iRe\Omega}{\mu\bar{T}}-\alpha^2+r\frac{D^2\bar{T}}{\bar{T}}+\frac{rM_T(D\bar{T})^2}{\mu\bar{T}}\right)v$$

$$+i\frac{r}{P}\left[\Omega\left(\frac{D\bar{T}}{\bar{T}}+\frac{M_T}{M}D\bar{T}\right)-\alpha DU\right]p$$

$$+\left[i(\alpha DU)\left(\frac{M_T}{M}+\frac{r}{\bar{T}}\right)-\frac{ir\Omega M_TD\bar{T}}{M}\right]T$$

$$-\frac{ir\Omega}{\bar{T}}DT$$

The energy equation yields

$$D^2T=\left[b-2(\gamma-1)M_\infty^2PrDU\right]Du \tag{3.22}$$

$$+\left[RePr\frac{RD\bar{T}}{M}-2i(\gamma-1)M_\infty^2Pr\alpha DU\right]v$$

$$+i(\gamma-1)M_\infty^2PrRe\frac{\Omega}{M}p$$

$$+\left[-RePri\Omega\frac{R}{M}+\alpha^2-M_{TT}\frac{(D\bar{T})^2}{M}-M_T\frac{D^2\bar{T}}{M}-(\gamma-1)M_\infty^2Pr\frac{M_T}{M}(DU)^2\right]T-2M_T\frac{D\bar{T}}{M}DT$$

The symbol D stands for $\frac{d}{dy}$. The system of equations (3.18) to (3.21) is subject to the boundary conditions

$$u = v = T = 0 \quad \text{at} \quad y = 0 \tag{3.23a}$$

and

$$u, v, p, T, \rightarrow 0 \quad \text{as} \quad y \rightarrow \infty \tag{3.23b}$$

Equations (3.19) to (3.22) can be written as a system of six first-order equations of the form

$$D\xi = F\xi \tag{3.24}$$

where

$$\xi^T = \{u \quad Du \quad v \quad p \quad T \quad DT\}^T$$

The boundary conditions (3.23) can be written as

$$\xi_1 = \xi_3 = \xi_5 = 0 \quad \text{at} \quad y = 0 \tag{3.25a}$$

$$\xi_n \rightarrow 0 \quad \text{as} \quad y \rightarrow \infty \tag{3.25b}$$

The system of equations (3.24) subject to the boundary conditions (3.25) constitutes an eigenvalue problem. For a given Reynolds number and mean flow profiles , we determine the dispersion relation

$$\omega = \omega(\alpha, \mathrm{Re}) \tag{3.26}$$

employing a numerical procedure. For the spatial stability problem considered here, we specify ω and an initial guess for the eigenvalue α. We numerically integrate the system (3. 24) from $y = y_{max}$ to $y = 0$, where y_{max} indicates a value of y larger than the boundary layer thickness. In performing these calculations we made use of the computer code 'SUPORT' developed by Scott and Watts (Ref. 23). This code, which is based on the method of Gudonov,

solves stiff two-point boundary-value problems . It uses the Runge-Kutta-Fehlburg scheme for integrating the equations and uses the Gram - Schmidt orthonormalization schemes to keep the solution vectors linearly independent. Normally , our guess of the eigenvalue is incorrect and therefore one of the boundary conditions at $y=0$ is not satisfied. Then we employ a Newton-Raphson scheme on this unsatisfied boundary condition to iterate and obtain the correct eigenvalue. Once having found the growth rates, we compute the N- factor as

$$N = -\int_{R_{e0}}^{Re} 2\alpha_i dRe$$

where R_{e0} corresponds to the Reynolds number at branch I of the neutral stability curve.

Chapter 4

4.NAVIER-STOKES AND INTERACTIVE BOUNDARY LAYER SOLUTIONS

The number of cases to be considered in which viscid-inviscid interactions play a dominant role are numerous. Seeking Navier-Stokes solutions for all the cases that will be encountered is seemingly a prohibitive task. An alternative is to model these flow fields using an interactive boundary-layer formulation (IBL). However, the solutions obtained by the IBL, for compressible and incompressible flow regimes, need to be validated using a Navier-Stokes solver. This chapter addresses this task.

In section 4.1, the incompressible code used here is validated against the results obtained for the flows over the standard Carter-Wornom trough for various Reynolds numbers and computational grids . In section 4.2., the results obtained for compressible flows over a smooth backward facing step using the IBL are compared with those obtained using a thin layer Navier-stokes solver "ARC2D" . Once we have a satisfctory comparison, we can use the IBL with confidence to all the flow cases which have small separation bubbles, in both

compssilble and incompressible flow regimes. However, cases which have very large seperated region or involve vortrex shedding must be excluded.

4.1 Incompressible Flow Results.

In this section the results obtained by the present IBL code are compared with the results obtained by Carter and Wornom for incompressible flows. As noted earlier in Chapter 2, the present IBL method employs a three point backward difference scheme for the ξ derivatives and a central differencing for theη derivatives. The equation of the trough is as specified by equation (2.26) in Chapter 2. The three Reynolds numbers that have been considered are Re = 180000, 360000 and 550000. A step size study is also provided to see the effect of the grid size on the solution. Four grids have been considered for this investigation with Δx = 0. 05, 0. 025, 0. 0125 and 0. 01. In order to cluster more points near the wall than in the rest of the boundary layer, a variable step size in the η - direction with an expansion ratio of R = 1.02 and initial grid spacing of $\Delta\eta_0 = 0.01$ has been employed for all the four grids.

Figures 1 and 2 show comparison of the coefficients of pressure and skin friction, respectively, with those obtained by Carter (Ref.10), Veldman (Ref. 17) and the present IBL code. The Reynolds number for this case is Re = 180000. The Cp is in excellent agreement with that of Carter but differ considerably from that of Veldman. However the C_f is in good agreement with both Carter and Veldman . Figure 1 suggests that a constant shift of Veldman's result upwards would make them coincidewith Carter's and the present results. The reason for this discrepancy of Veldman's result is unknown. Figure 3 provides a comparison of the displacement thickness obtained by Carter with that obtained using the present method.As evident from the figure, a good agreement exists. Next we consider a case of a higher Reynoldsnumber, namely, Re = $36X10^4$.Figures 4 and 5 show the pressure and skin friction

coefficients, respectively, for all the four grids considered. As can be seen from the figures, grid3 and grid4 with $\Delta x = 0.0125$ and 0.01, respectively, converge to the same solution. Also presented on these plots are the solutions obtained by Veldman. Again we observe a difference in the pressure coefficients obtained by both methods. The skin friction coefficient is in agreement with the present results except near the large spike where Veldman's results show a lower negative coefficient of friction peak . Figure 6 shows the displacement thickness computed for the four grids using the IBL. As observed for the friction and pressure coefficients, the displacement thickness also becomes independent of the mesh size after grid 3 indicating a converged solution.

The next set of results presented correspond tothe Reynolds number $Re = 55X10^4$. Figures 7 and 8 show the pressure and skin friction coefficients for grids with $\Delta x = 0.05$ and 0.025. Figures 9 and 10 correspond to the pressure and friction coefficients for $\Delta x = 0.0125$ and 0.01. From these figures it can be seen that refining of the grid, the negative pressure and friction peaks grow and in the separated regions oscillations start to develop. Further attempts to solve the problem with finer grids resulted in a convergence failure. As is evident from the figures the deviation is only in the separated regions, while the other parts of the flow converge to one solution with the grid refinement. Figures 11 and 12 show the displacement thickness corresponding to the above cases. The behavior of the solution is the same as that observed for the other two Reynolds numbers and we do not see any unusual oscillations as observed in the pressure and skin friction coefficients.

4. 2 Compressible Flow Results.

In this section the solutions for flow over smooth backward and forward steps obtained using the Navier-Stokes solver and the IBL are compared for compressible flows. The Mach num-

bers considered for the comparison are M=0. 5 and M=0. 8. The comparisons are made for the mean flows as well as their stability characteristics such as the growth rates and the N-factors. To predict the flow field and its stability accurately, we need to be careful to choose a proper grid, which is fine enough to capture the important flow structures. The far field boundary also plays an important role in the determination of the solution. The boundary must be far enough to prevent the contamination of the solution from the reflections there , especially in the high Mach number flows.

Figure 13 shows a typical computational grid employed in the present investigation. The y coordinates are multiplied by a factor of 20 for the purpose of illustration. The first case considered is for a Mach number of 0.5. Four computational grids are choosen. They are grid1 (136x70), grid2(136 x 98), grid3(136x99), grid4(166x120). The far field boundary is at 0.4 for all the grids and Δy_0 is 0.00015 for grid1, 0.00008 for grid2 and is 0.00003 for the last two grids. Figures 14 and 15 show a comparison of the pressure and wall-shear coefficient for these four grids. The results obtained using grid2, grid3, and grid4 are close enough to conclude their independence of the grid refinement. However these results show a marked improvement over the solution obtained using grid1 and are also in closer agreement with the IBL solutions. The agreement between the Navier-Stokes and IBL is good throughout the flow field except in the separated flow region. Figures 16 and 17 show a comparison of the growth rates and N-factors. The prediction of the stability characteristics improves drastically in the upstream of the step as the grid is refined. The mean flow is predicted within acceptable limits of accuracy even for the coarsest of the grids employed but as figures 16 and 17 indicate, the stability calculations for this grid are way off from those calculated using the IBL profiles. The results improve with the refinement of the grid to a great extent only in the upstream region. There is only a marginal improvement in the separated flow region. Figures 18 to 24 show the velocity profiles around six locations of the step. The agreement between the IBL and the Navier Stokes profiles is good ahead of the step and around the unseparated flow regions. There is however some difference in the results of both methods as we enter the separated

flow regions. The sensitivity of the T. S wave instability to the first and second derivatives can be guessed from figures 16 and 17. As we refine the grid more and more, the derivatives are better predicted and hence an improvement in the stability results. The difference in the separated flow regions can be attributed to the difference in the prediction of the magnitude of the velocity . the mean flow itself. Therefore we may conclude that for an accurate prediction of the mean flow as well as its stability characteristics simultaneously, the grid choosen must be fine enough to accurately predict the magnitude of the mean flow as well as its first and second derivatives. The improvement in the mean flow as well as its derivatives with grid refinement can be seen in figures 25 to 27 which correspond to the station X=0.64 .

Having found the satisfactory grid , results have been sought for the Mach number M=0. 8 over this grid with the hope of satisfying both the mean flow and stability considerations. Figures 28 and 29 show the pressure and friction coefficients respectively. The results came out as a surprise initially. This case is marked with a larger separation bubble due to larger adverse pressure gradients created by a larger Mach number. The comparison of the Navier Stokes solution with that of IBL was better in the separation region than for the M=0. 5 case. Also, in contrast, the flow upstream of the step was better predicted for M=0.5 than for M=0.8. Figure 30 shows the displaced bodies for both Mach numbers. The improvement seen in the separated region for M=0. 8 can now be argued to be due to the reduction in the curvature and slope of the displacement body in this region. Figures 31 and 32 show the growth rates and the N-factors for M=0.8. There is a very good agreement with the stability of the IBL profiles, and suggests further improvement, as we have seen for M=0. 5, with a grid refinement. However additional refinement in the grid would result in prohibitive computational cost, not commensurate with the accuracy that we might achieve. With the results presented above, we are now in a position to accept the accuracy offered by IBL at least upto M=0.8 and hence conclude it to be a viable alternative to the Navier Stokes solvers.

The discrepancy observed at the upstream of the step for M=0.8 . suggests that the reflections from the far-field boundarymay affect the solution. In order to investigate the effect

of the far field boundary, additional cases for M=0. 8 had been considered. The far field boundary was shifted from 0.4 to 0.6 and 0.8. This resulted in a further improvement of the skin friction prediction in the separated flow, as shown in Fig.29, but remained insensitive upstream of the step. However, the pressure coefficient did improve a lot as shown in Fig. 28. Here grid4 corresponds to the far field boundary at 0. 4, grid4E and grid4EE correspond to far field boundaries at 0. 6 and 0. 8 respectively. The number of computational cells remain the same for all the four cases at 166 X 120. A similar exercise with M=0. 5, of extending the far field boundary to 0. 8 resulted only in a marginal improvement of the solution in the separated flow region. The pressure and skin friction coefficients remained practically unaltered upstream of the step. This is shown in Figures 33 and 34 . In Figures 35 and 36, the skin fricton coefficients are plotted at the leading edge of the plate for both the IBL and the Navier-Stokes formulation for M=0.5 and M=0.8, respectively. Evident from these figures is that for M=0.8, we have a larger disturbance at the leading edge which is propagated downstream. The step however has no influence on this disturbance till we reach the strong adverse pressure gradients where it vanishes for M=0. 8. For M=0. 5, this disturbance dies down soon to match the IBL solution ahead of the step itself. The fact that the step has no influence is clear from the figures 37 and 38, which show the leading edge region of the Blasius flow for Mach numbers 0.5 and 0.8, respectively. The Blasius flow has the same behavior as that of the step, suggesting that this leading edge discrepancy is not related to the step. In order to study this disturbance, the leading edge is refined in the x direction. Figure 39 shows the effect of this refinement. There is only a marginal improvement at the leading edge, but this disturbance continues to persist as before. The effect is also marginal over the entire flow field as is seen from figure 40. This suggests that we also need to refine the grid in the y direction in order to resolve the boundary layer accurately in this region . Since the boundary layer is extremely thin here, we could employ a parabolic grid to cluster more points around the leading edge.

Another imortant parameter to be considered is dissipation . Sufficient amount of dissipation needs to be added in order to obtain a converged solution free of unphysical oscil-

lations. In figures 41 and 42 the effect of changing the fourth order dissipation in the solution procedure is presented. The fourth order dissipation terms are reduced from 0. 8 to 0. 5 in the x direction and from 0. 3 to 0. 2 in the y direction. This results in unphysical oscillations in the pressure and skin friction coefficients, indicating the importance of the right amount of dissipation to be added in order to have a meaningful solution. The oscillations observed for the above cases were only in the separation region.

Figure 43 shows the number of iterations needed to obtain an acceptable, converged value of Cf. Even though the average and maximum residuals are extremely small beyond 4000 iterations, as evident in figure 44, we need to iterate at least 9000 iterations before we can claim convergence.

After noting that the grid refinement plays a key role in the accurate determination of the mean flows and their stability characteristics for the above cases, we decided to go one step further, of obtaining a solution with an extremely refined grid. We employed a grid of size 176 X 153, with the far field boundary at 0.8. Fig. 45 and 46 show the pressure and skin friction coefficients, respectively. Presented in figures 47 and 48 are the stability characteristics. As observed before there is an improvement in both the mean flows and stabilty. The improvement can be clearly seen if we compare the figures 48 and 17.

Chapter 5

5. IBL COMPUTATIONS AND THEIR HYDRODYNAMIC STABILITY

Having established the accuracy of the IBL solutions in Chapter 4. we now proceed to use this method to calculate the mean flows over smooth forward and backward steps in which the flow fields are characterised with strong viscid-inviscid interactions. Results have been obtained for the mean flow over forward and backward steps specified by eq.(2.14) for different heights and slopes, Mach numbers and Reynolds numbers. The center of the steps is at Xm =1.00. We have considered four backward facing steps with heights H=-0.002 to H=-0.005 with an increment of -0.001 and with the slopes fixed at SL=-4. 34695 degrees. Also considered in the backward step case are four steps with the height fixed at H=-0. 003 and the slopes incremented by -1.0 degree starting with the value of SL=-3. 34695. As for the forward steps, three steps with heights H=0.005, 0.007 and 0.009 with the slope fixed at 10 degrees and three steps with slopes SL=8, 10 and 12 degrees with the height fixed at H=0. 007 are considered. Effect of compressibility is studied by considering three Mach numbers M=0.8, 0.5 and 0.0, for both forward and backward steps. The Reynolds number is fixed at

Re=1000000.The effect of Reynolds number has been studied for the backward-step case with the height and slope fixed at H=-0. 003 and SL=-5. 34695 degrees respectively.

5.1. *Mean Flow Characteristics.*

5.1.1 Backward Facing Step Rresults

Figures 49 and 50 correspond to the pressure and skin friction coefficients for the case of fixed slope and varying heights. The flow field contains a separation bubble for all the cases considered. The increase in height increases the size of this separation bubble significantly. The increase in the suction peak at x=0.9 upto x=1.0 is due to the large increase in favorable pressure gradients with the increase in heights. At x=1.0 the flow separates as the boundary-layer encounters an adverse pressure gradient. The point at which it meets a favorable pressure gradient downstream also shifts quite considerably. Beyond the value of H=-0. 005, we may expect a vortex shedding at which point the interactive boundary-layer formulaton will fail to predict the mean flow. Figures 51 through 54 show a similar behavior of the pressure and friction coefficients for steps with varying slopes and a fixed height and for varying Mach numbers. The the effect is less pronounced for changes in the slope when compared with changes in the heights. However, compressibility does enhance the adverse pressure gradients in the downstream . This can be inferred from the increase in the size of the separation bubble as the Mach number is increased.

5.1.2 Forward Facing Step Results

The effect of changes in the slopes and heights on the pressure and friction coefficients is presented in figures 55 through 58 . The flow encounters an adverse pressure gradient till we reach x=0.95. Then we have a favorable pressure gradient over a short range of x=0. 95 upto x=1. 00. The suction peak increases with the increase in the heights as well as the slopes. As observed in the backward step case the influence of the slope is less than changes in the heights. The Mach number enhances the adverse pressure gradients downstream in comparison with the incompressible case. This can be seen in figures 59 and 60.

5. 2 Stability Characteristics

5. 2.1 Backward Facing Step Results

The growth rates and the N-factors for steps with constant slopes and varying heights are shown in figures 61 and 62. The frequencies for which these characteristics are computed, correspond to the most amplified frequencies throughout this chapter. The most amplified frequency has been defined to be that frequency for which the N factor reaches the value of 9 first as we march along the x direction. This is obtained by calculating the N factors over the entire range of frequencies and determining, as to which one triggers transition first. This is illustrated in figure 75 which corresponds to the case of a forward facing step of a height H = 0.007 and a slope of 10 degrees. Both the growth rates and its integrated effect - the N-factor, change sharply with height increase. The N-factors reach the value of 9 around R=1000 and shoot beyond this value over a short range for all the steps except the smallest

step of H=-0.002, thereby indicating a turbulent flow. Figures 63 and 64 show the growth rates and N-factors for steps with changing slopes and a fixed height. Evident from these figures is the insensitivity of the stability to the slope. Near the reattachment where we encounter favorable pressure gradients a slight decrease inthe growth rates is observed. The flow is also stable just before the value of R=1000, till we reach the point of separation. The growth rates decrease significantly with an increase in Mach number around R=1000. However, they start building up again in the reattchment region due to the increase in adverse pressure gradients in this region, due to the Mach number increase. The overall effect is a decrease in the N-factor and hence an increased stability. These results are depicted in figures 65 and 66

Evident from figure 67 is the effect of moving the step upstream - in other words-the effect of Reynolds number. The steps have been placed at three upstream stations. When they are placed at R=316 and R=548 they have no effect on the stability and the flow field is Blasius like . Placing the steps at R=707 and R= 836 delays the transition . When placed at R= 1000, we can see that transition sets in almost at the center of the step. We have also considered a step of smaller height (H=-0.002) with the center of the step at R=707 and at R=836. The results indicate that a smaller hump is more dangerous than a bigger one. This can be explained by the larger downstream favorable pressure gradient caused by the bigger step than the small one . Thus, although the bigger steps increase the local growth rates just around the step, they have a stabilising effect downstream.

5.2.2 Forward Facing Step Results

Results for changes in heights with the slope fixed are presented in figures 68 and 69. There is an increase in the growth rates and the N -factors all along till around R=900. The growth rates start falling till we reach the center of the step. Beyond R=1000, we encounter adverse pressure gradients and an increase in the growth rates. For the two cases of heights H=0.007

and H=0.009 transition sets in ahead of the step. There is a decrease in the N factors around R=900 upto R=1000 because of the decrease in the growth rates around this region. The N-factors reach a value beyond 14, indicating that we have essntially a turbulent flow. The case of H=0.005 shows that although the N- factor does not reach the value of 9 ahead of the step it eventually reaches a value of 13 downstream . Thus even if transition is avoided initially, the flow eventually becomes turbulent over a short downstream region. Shown in figures 70 and 71 is the effect ofthe slope. As in the backward step case the effect of changes in the slope is less significant than those of changes in the height. With a step of H=0.007 and a slope of 8 degrees we see that transition is delayed slightly. For the other two cases of SL=10.00 and SL=12.00, the N factor reaches a value of 9 very close to R=1000 followed by a decrease, further downstream, the growth rates and hence the N-factors increase. Though increasing the Mach number decreases the growth rates due to the increased density gradients around R=900 upto R=1000 this benefit is lost due to the large adverse pressure gradients created simultaneosly both due to the Mach number and due to the effect of geometry. Figures 72 and 73 depict the effect of Mach number on the growth rates and the N-factors, respectively. All the results presented are for geometries that are only slight deviations from plate geometries. For the sake of completeness the neutral stability curves for the Blasius flows for various Mach numbers are presented in Figure 74 .

Chapter 6

6. CONCLUSIONS AND RECOMMENDATIONS.

There are two objectives of this work. The first one was to validate the IBL against Navier-Stokes solvers. The approach taken was to compare the results obtained by a thin layer Navier- Stokes solver "ARC2D" with the results obtained by a compressible IBL code developed here for flows over smooth backward facing steps. The results obtained using the incompressible code was compared with the results obtained by other researchers for flows over flat plates with small indentations. In the process of comparing the Navier-Stokes with the IBL, an attempt to obtain the most appropriate grid with proper far field boundaries and dissipation parameters was made.

The second objective is to study the stability of the boundary layers over surface imperfections. After ascertaining the accuracy of the IBL computations, we used this formulation to obtain the mean flows over smooth forward facing and backward facing steps for various geometrical and flow parameters. Then we investigated the stability of these mean flows using a linear theory. The conclusions based on the above work are the following:

1. When using the Navier Stokes solvers, a proper grid must be chosen to predict the mean flows as well as their stability. Proper care must be taken in choosing the far field boundary and dissipation parameters to avoid the contamination of the solution. Proper leading edge resolution is also necessary, espeacially for higher Mach numbers to avoid the larger disturbances created there and their downstream propagation.

2. An excellent agreement between the IBL and the Navier-Stokes solutions exist at least till M=0. 8, in the entire flow field, except for a negligible deviation in the separation and reattachment regions.

3. The computatinal time incurred for the Navier- Stokes computations is about 6 hours as compared to one minute for IBL on the IBM 3090 machine for an acceptable level of accuracy. Hence, IBL can be proposed with confidence as an alternative to the Navier-Stokes solvers.

4. The stability of steps is more sensitive to small changes in heights than small changes in slopes over the range of 8 to 12 degrees for forward facing steps and -3.34695 to -6.34695 degrees for backward facing steps. The insensitivity to small changes in slopes is more noticable for backward steps.

5. Higher Mach numbers provide additional stability because of the additional damping of the TS waves due to increased density gradients. This advantage is partially offset due to the adverse pressure gradients created by the geometries and their associated increase in the separation bubbles as the Mach number increases. This offset is more noticable in the case of forward facing steps because of the additional adverse pressure gradients in the flow fields due to its geometry.

6. If a critical step (i.e. a step which causes transition to occur just downstream of the step) is displaced upstream, transition may be delayed. However, if a step smaller than a critical one is moved upstream, transition may be promoted.

As can be observed from the large values of the N-factors reached for both forward and backward steps, the flow fields associated with these types of flows are highly unstable. The stability characteristics associated with various geometrical parameters considered also indicate that nonparallel effects may not be negligible. The following recommendations for further study could lead to a better understanding of the stability of flow fields on these types of geometries.

- Nonlinear effects, including secondary instabilities
- Effects of non-parallelism on the stability.
- Effect of heat and mass transfer in controlling the stability of these flow fields.

Chapter 7

References

1. Holmes, B. J. , Obara, C. J. , Martin , G. L. and Domack, C. S, **"Manufacturing Tolerences For Natural Laminar Flow Airframe Surfaces",** SAE paper 850863, 1985.

2. Hastings, E. C. , Schoenster, J. A, Obara, C. J, Dodbele, S. S, **Flight Research On Natural Laminar Flow Nacelles: A Progress Report",** AIAA paper No 86-1629

3. Fage, A. **Smallest Seize Of Spanwise SUrface Corrugation Which affects Boundary Layer Transition On An Airfoil,** R&M No. 2120, Brit. A. R. C. , 1943.

4. Carmichael, B. H. , Whites, R. C. and Pfenninger, W. , **"Low Drag Boundary Layer Suction Experiments In Flight On The Wing Glove Of An F-94 A Airplane ",** Northdrop Aircraft Inc. Rep. No NOR-59-438 (BLC - 123) , 1975.

5. Carmichael. , B. H. , **"Surface Waviness Critria For Swept And Unswept Laminar Suction Wings",** Norair Rep. No. NOR-59-438(BLC-123), 1959.

6. Carmichael, B. H. and Pfenninger, W. , **"Surface Imperfection Experiments On A Swept Laminar Suction Wing"**, Norair Rep, No. NOR-59-454(BLC-124), 1959.

7. Vijgen, P.M.H.W. , Dodbele, S.S. , Holmes, B.J. and Vandam, C.P, **"Effects Of Compressibility On The Design Of Subsonic Natural Laminar Flow Fuselages"**, AIAA paper -86-1825 CP.

8. Smith, F. T. , **Laminar Flow Over A Small Hump On A Flat Plate "**, J. Fluid Mech. , 57, 803-824, 1973.

9. Ragab, S. A, Nayfeh, A. H. , **"A Comparison Of The Second Order Triple-Deck Theory With Interacting Boundary Layers"**, In Numerical and Physical Aspects Of Aerodynamic Flows, ED. T. Cebeci, Springer Verlag, Newyork, 1982.

10. Carter, J. E. and Wornom, S. F, **"Solution For Incompressible Seperated Boundary Layers Including Viscous-Inviscid Interaction "**, ANSA SP 347, Aerodynamic Analysis Requiring Advanced Computers, Part 1 125 - 150, 1975.

11. Carter, J. E. and Wornom, S. F, **"Forward Marching Procedure For Seperated Boundary Layer Flows"**, AIAA J 13, 1101 - 1103, 1975.

12. Davis, R. T. , **" A Procedure For Solving The Compressible Interacting Boundary Layer Flows Over Equations For Subsonic And Supersonic Flows"**, AIAA paper No-84-1614, 1984.

13. Pulliam T. H. , **"Euler and Thin Layer Navier - Stokes codes: ARC2D, ARC3D"**, Notes For Comp. Fluid Dyn. , User's Workshop, The University Of TN Space Institute, TN1984.

14. Pulliam, T. H and Chaussee, D. S, **" A Diagonal form Of An Implicit Approximate Factorization Algorithm"**, Journal Of Comp. Physics, 39, 1981, P347.

15. Nayfeh, A. H. , **"Stability Of Three-Dimensional Boundary Layers "**, AIAA Journal , Vol. 19, PP 406-416, 1980.

16. Nayfeh, A. H. , **"Three-Dimensional Stability Of Growing Boundary Layers"**, International Union Of Theoretical and Applied Mechanics Symposium On Laminar-Turbulent Transition, (E. Eppler and H. fasel, Ed.), Springer Verlag, Berlin, PP. 201-217, 1980.

17. Veldman, A. E. P, **" A Numerical Method For Calculation Of Laminar, Incompressible Boundary Layers With Strong Viscid Inviscid Interaction"**, Report NLR TR 79023, National Aerospace Lab. , The Netherlands, 1979.

18. Veldman , A. E. P. , **" New Quasi Simultaneous Method For Calculating Interacting Boundary Layers "**, AIAA paper No. 81-4010, 1980.

19. Henkes, R. A. W. M. Veldman, A. E. P, **" On The Breakdown Of The Steady And Unsteady Interacting Boundary Layer Description "**, J. Fluid Mech. (1987), Vol 179, PP 513-529.

20. Smith F. T. , Merkin, J. H. , **" Triple- Deck Solutions for Subsonic Flow Past Humps, Steps, Concave Or Convex Corners and Wedged Trailing Edges"**, Journal Of Comp. Physics, 10 1982, pp 7-25.

21. Nayfeh, A. H. , Ragab, S. A. , Al-Maaitah, A. , **" Effect of Bulges On The Stability Of The Boundary Layers"**, To Appear In The Physics Of Fluids, 1988.

22. Nayfeh, A. H. , Saad. A, Ragab, **" Effect Of A Bulge On The Secondary Stability Of Boundary Layers"**, AIAA paper No 87-0045, 1987.

23. Scott, R. R, and Watts, H. A. , **" Computation Solution Of Linear Two Point Boundary Value Problems Via Orthonormalization"**, SIAM J.Num.Anal. 14, 40-70, 1977. Also

SUPORT -A Computer Code For Two Point Boundary Value Problems Via Orthonormalization", SAND 75-0198.

Figures

BLANK PAGE

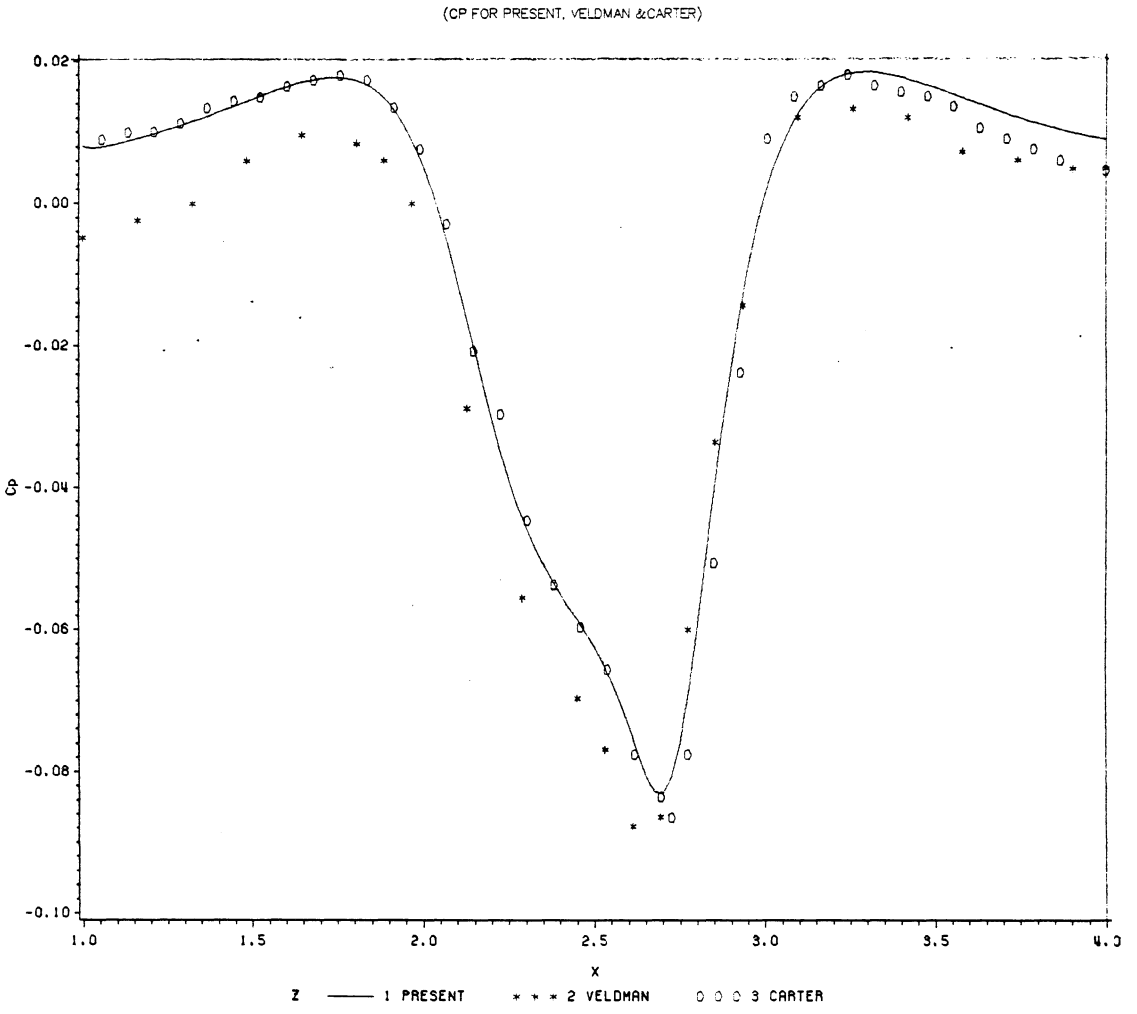

Figure 1. Cp of IBL,Carter and Veldman (Re=180000)

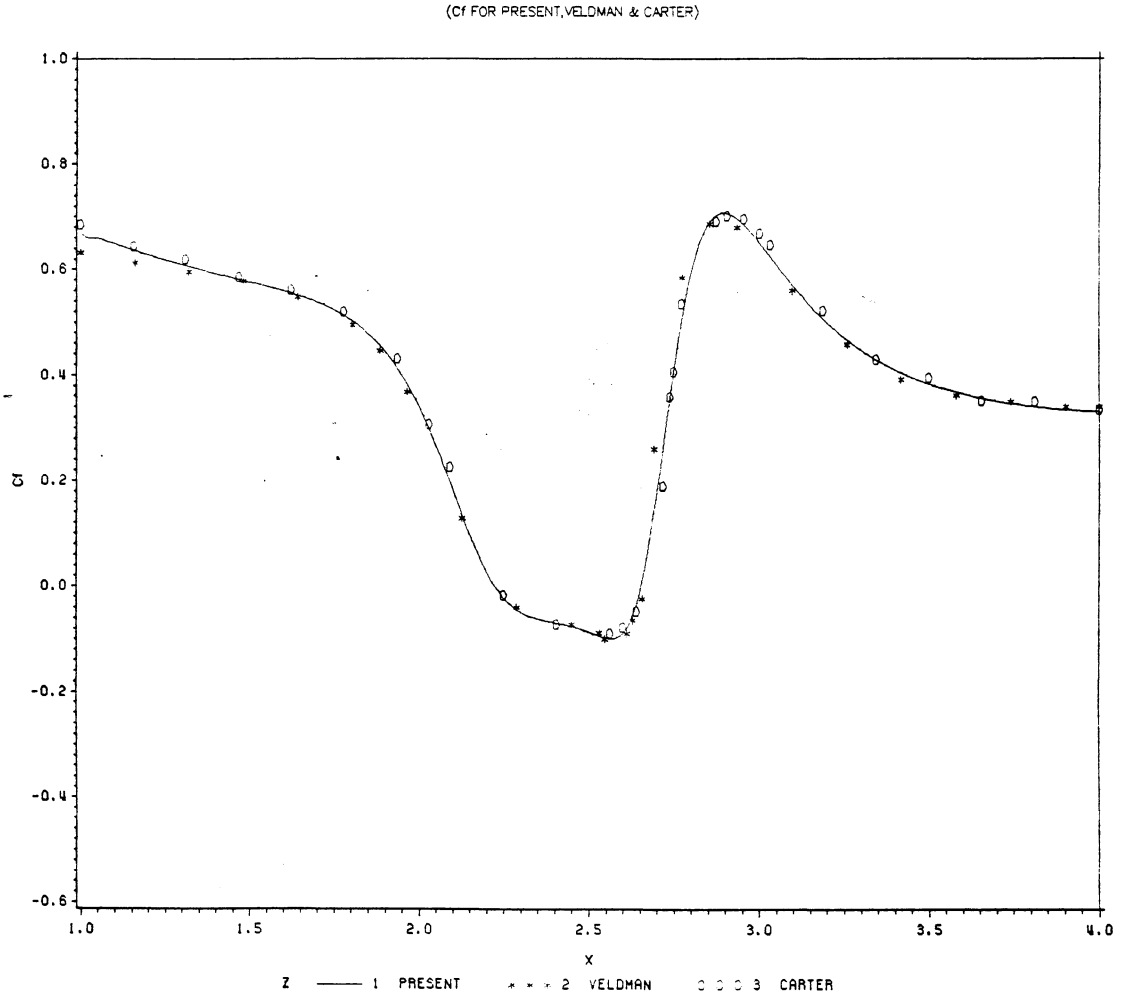

Figure 2. Cf of IBL,Carter and Veldman (Re=180000)

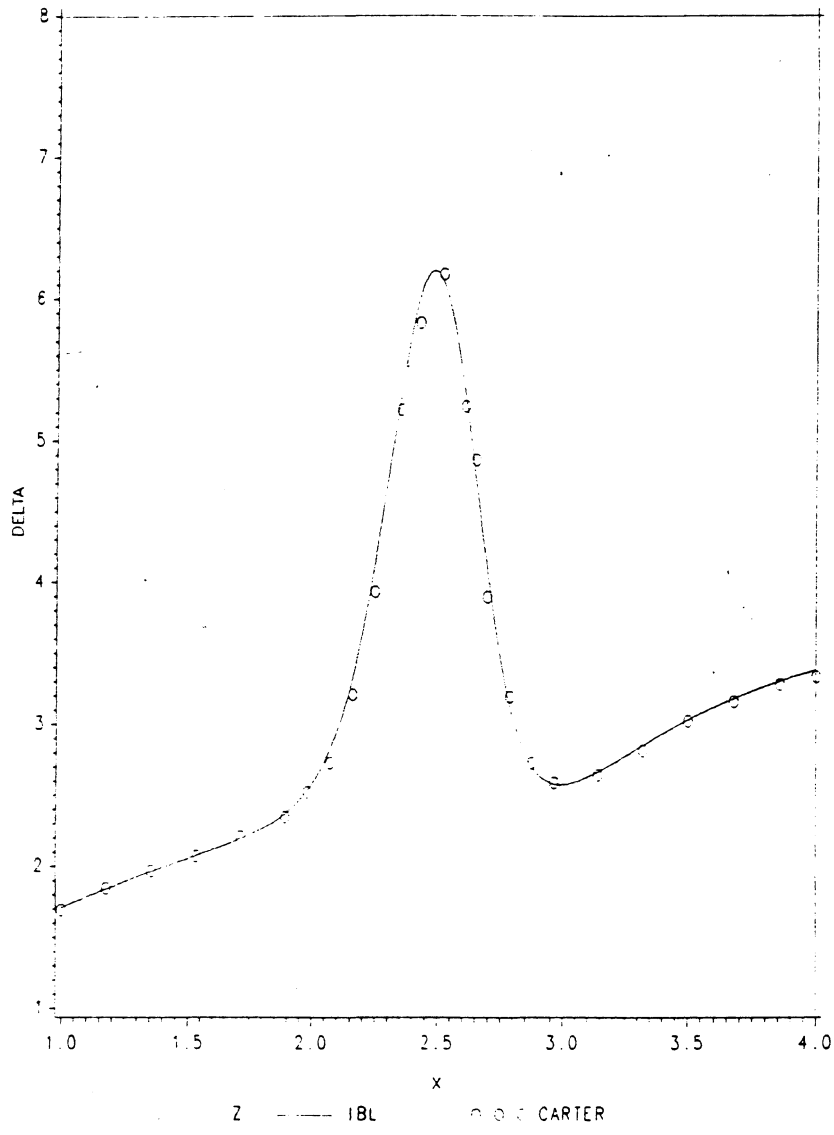

Figure 3. 3.3. Comparison of Displacemnt thickness (IBL Vs. Carter).

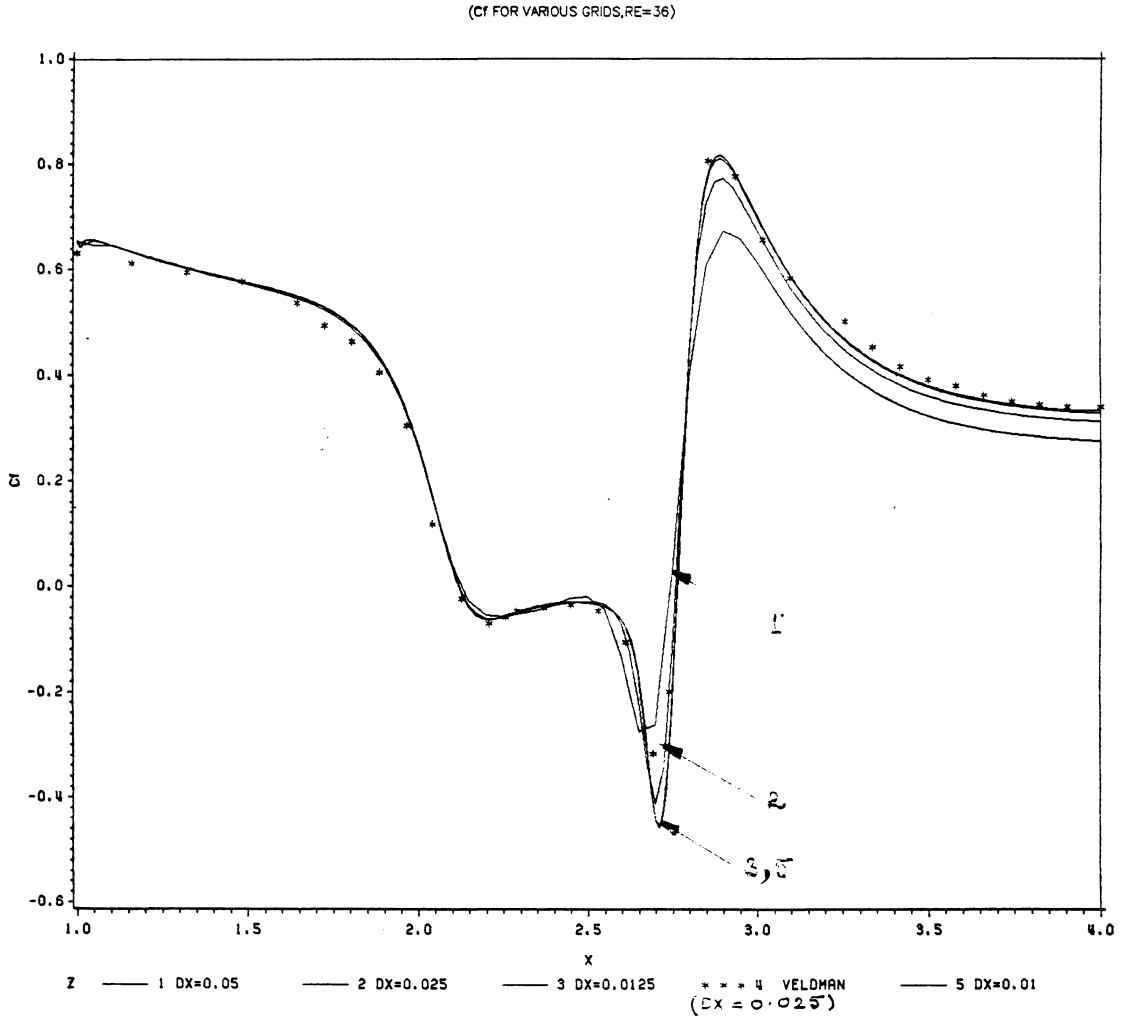

Figure 4. C of IBL, and Veldman (Re=360000)

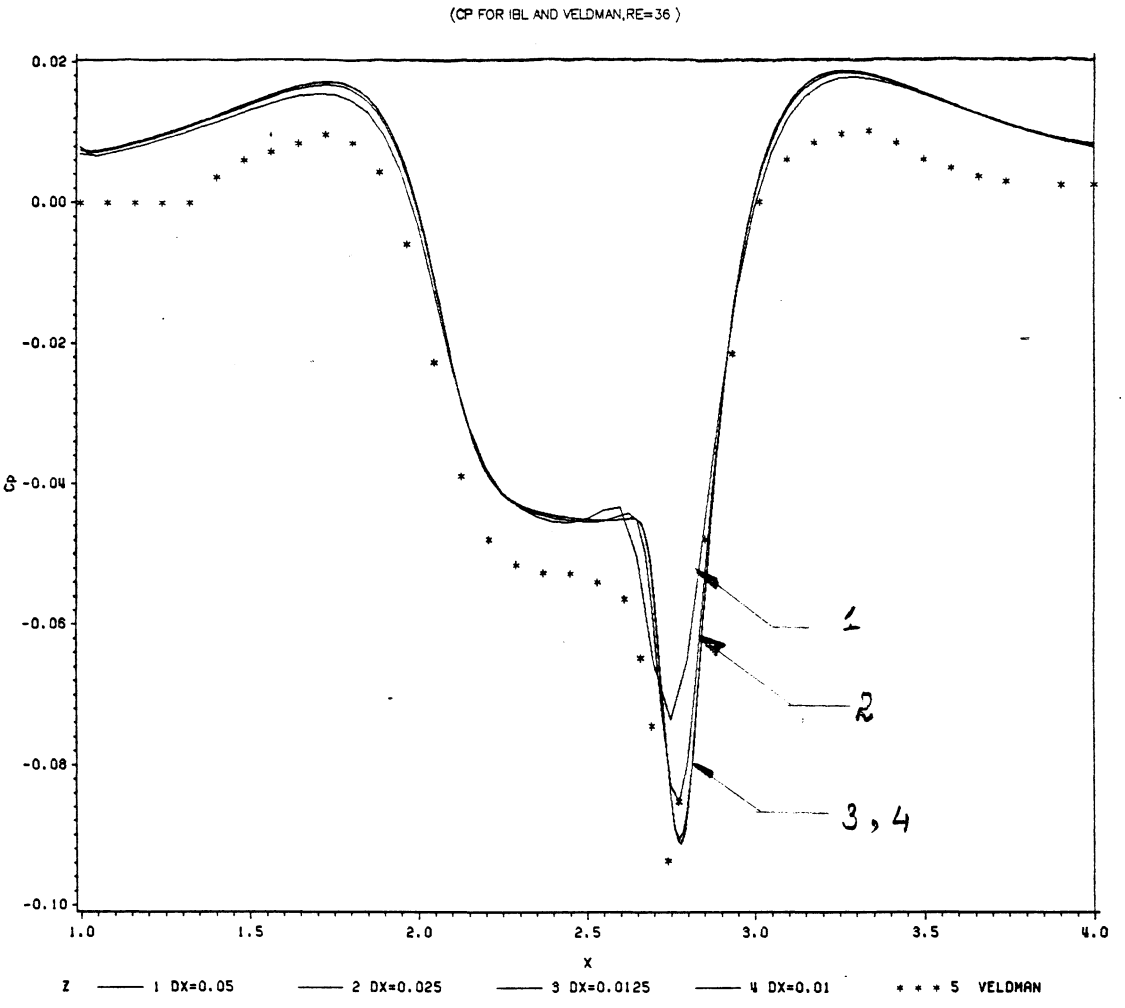

Figure 5. C of IBL, and Veldman (Re=360000)

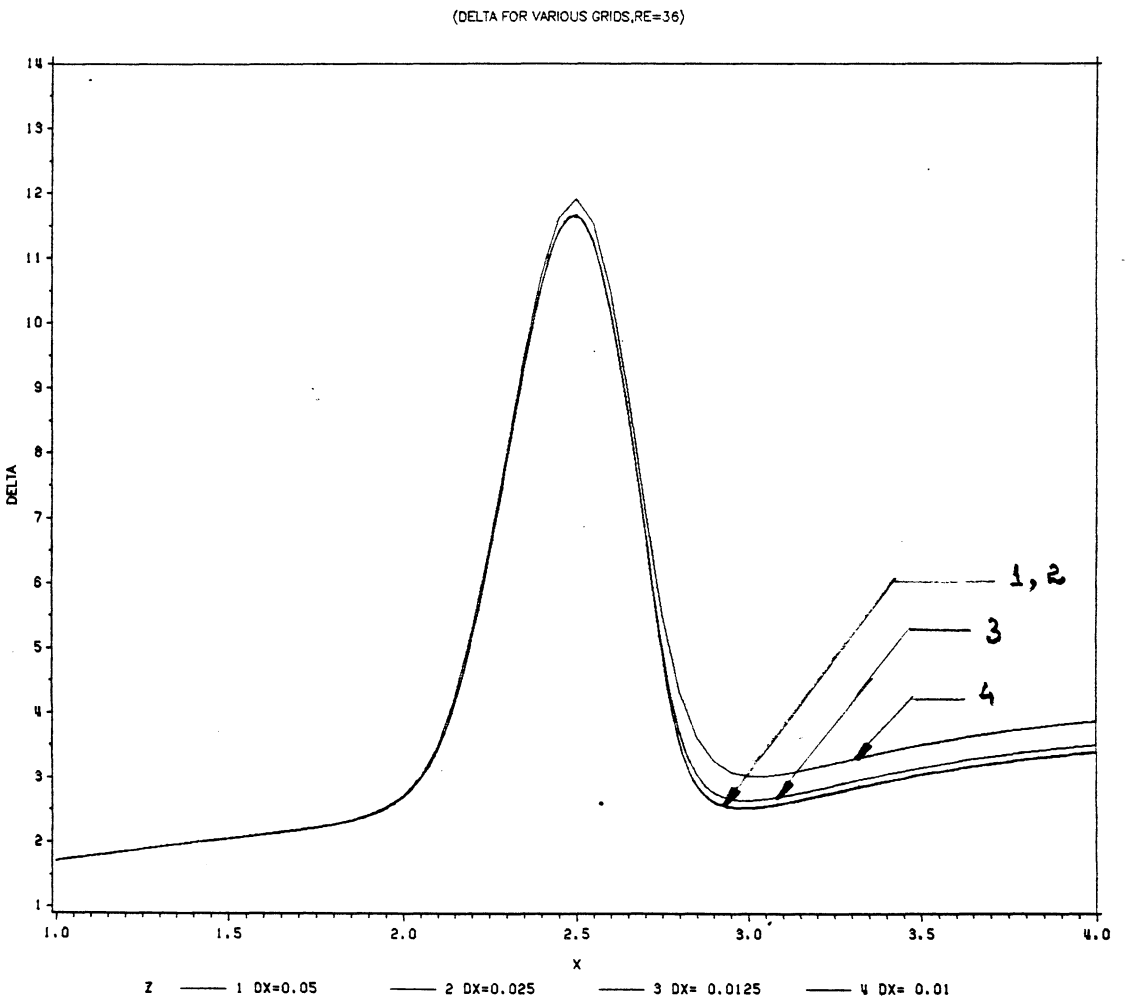

Figure 6. Displacemnt thickness (IBL)for various grids (Re=36000)

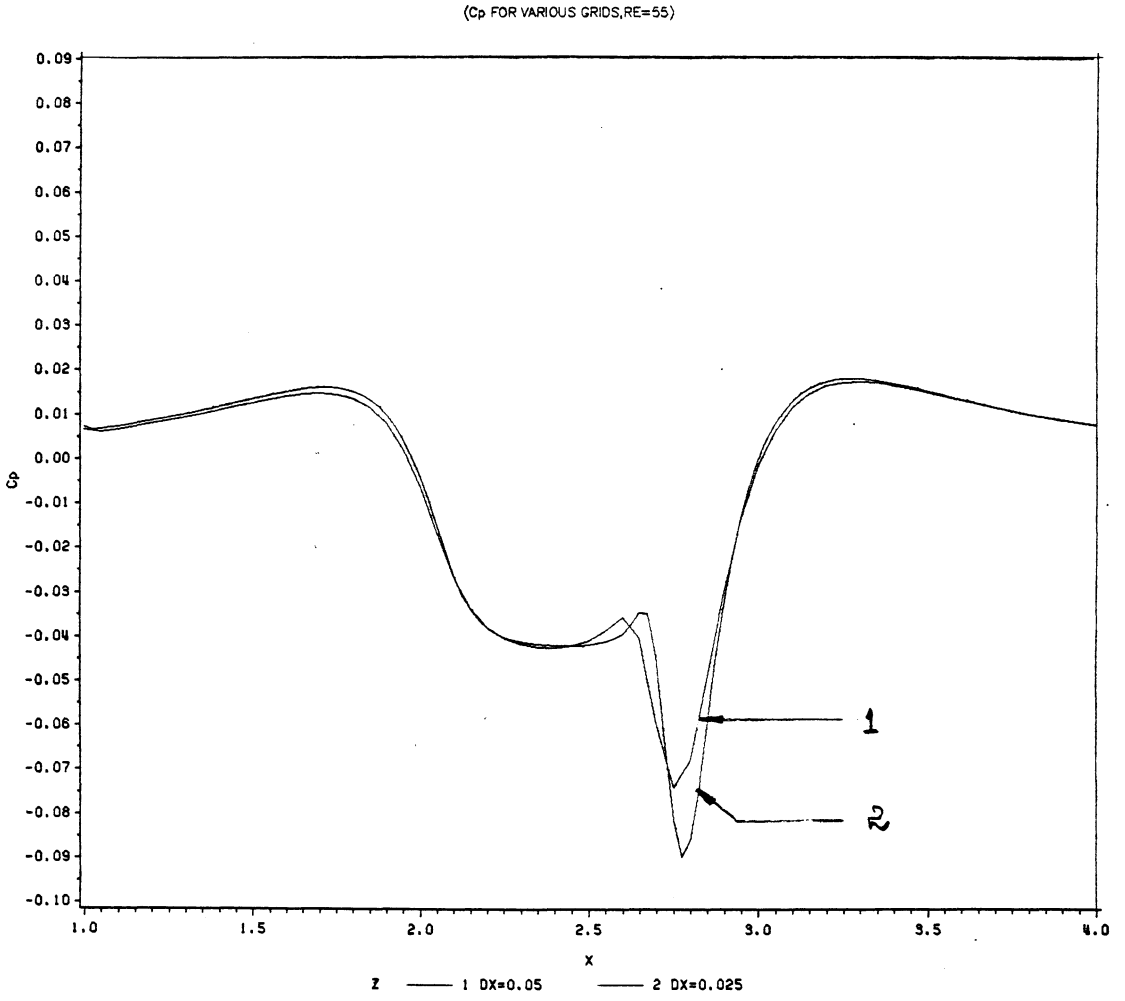

Figure 7. Cp (IBL) for coarser grids (Re=550000)

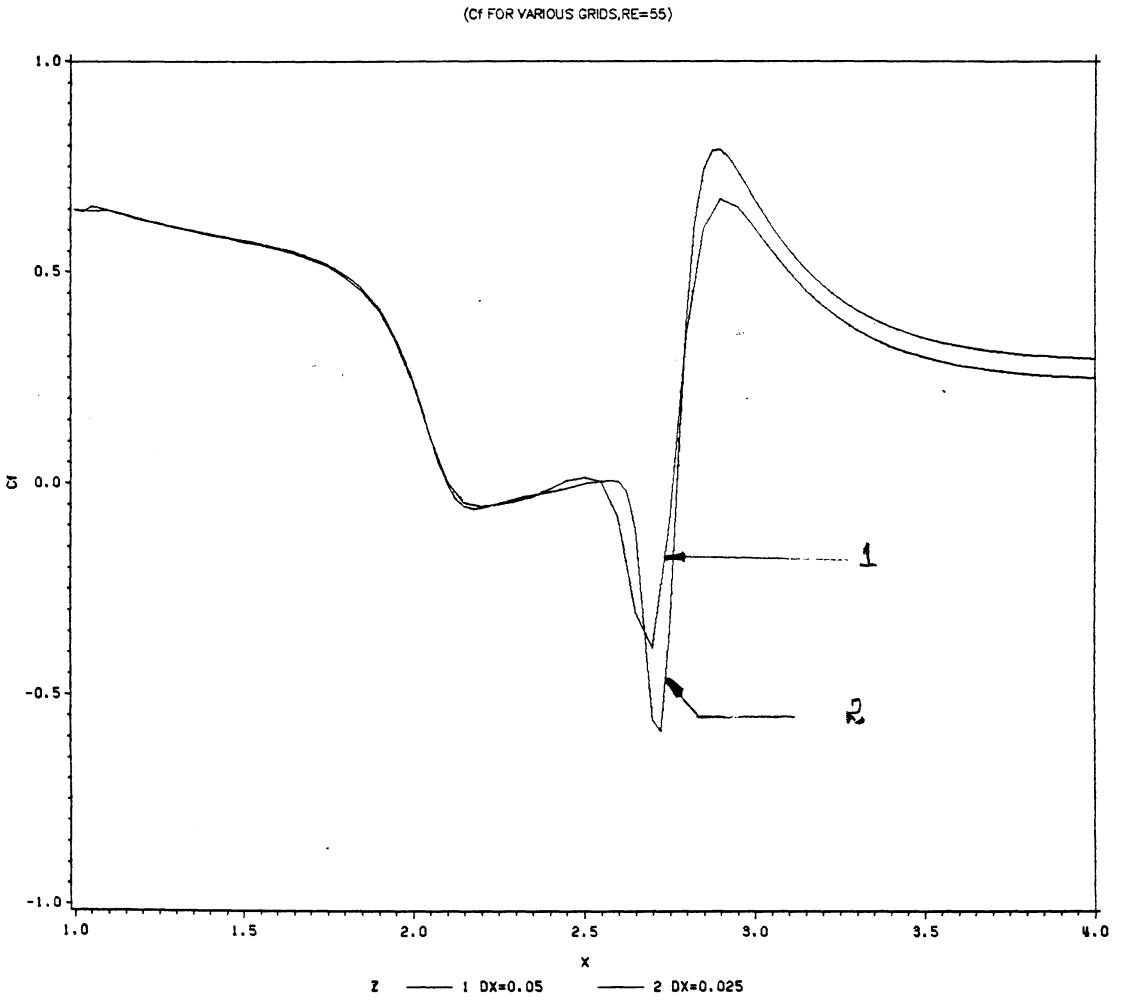

Figure 8. Cf (IBL) for coarser grids (Re=550000)

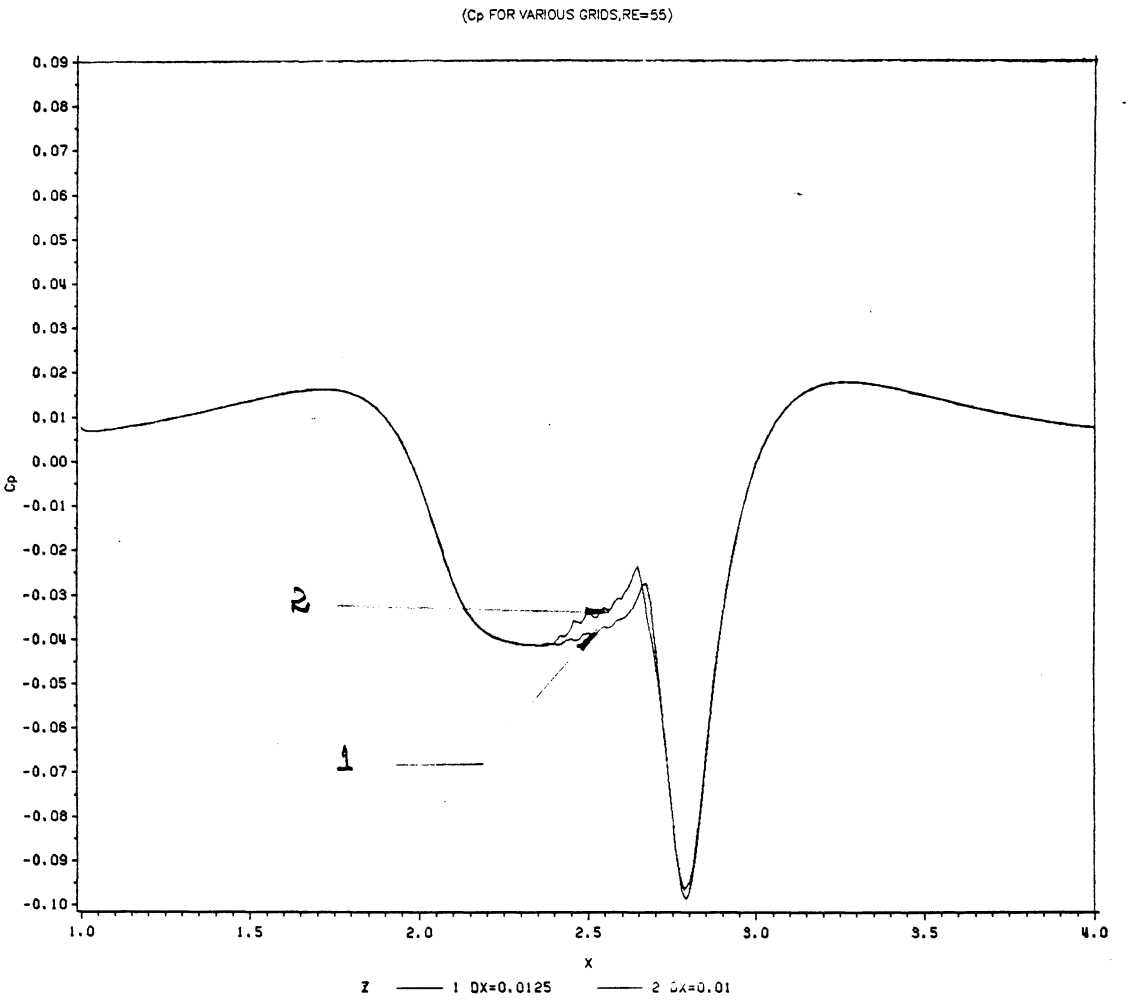

Figure 9. Cp (IBL) for finer grids (Re=550000)

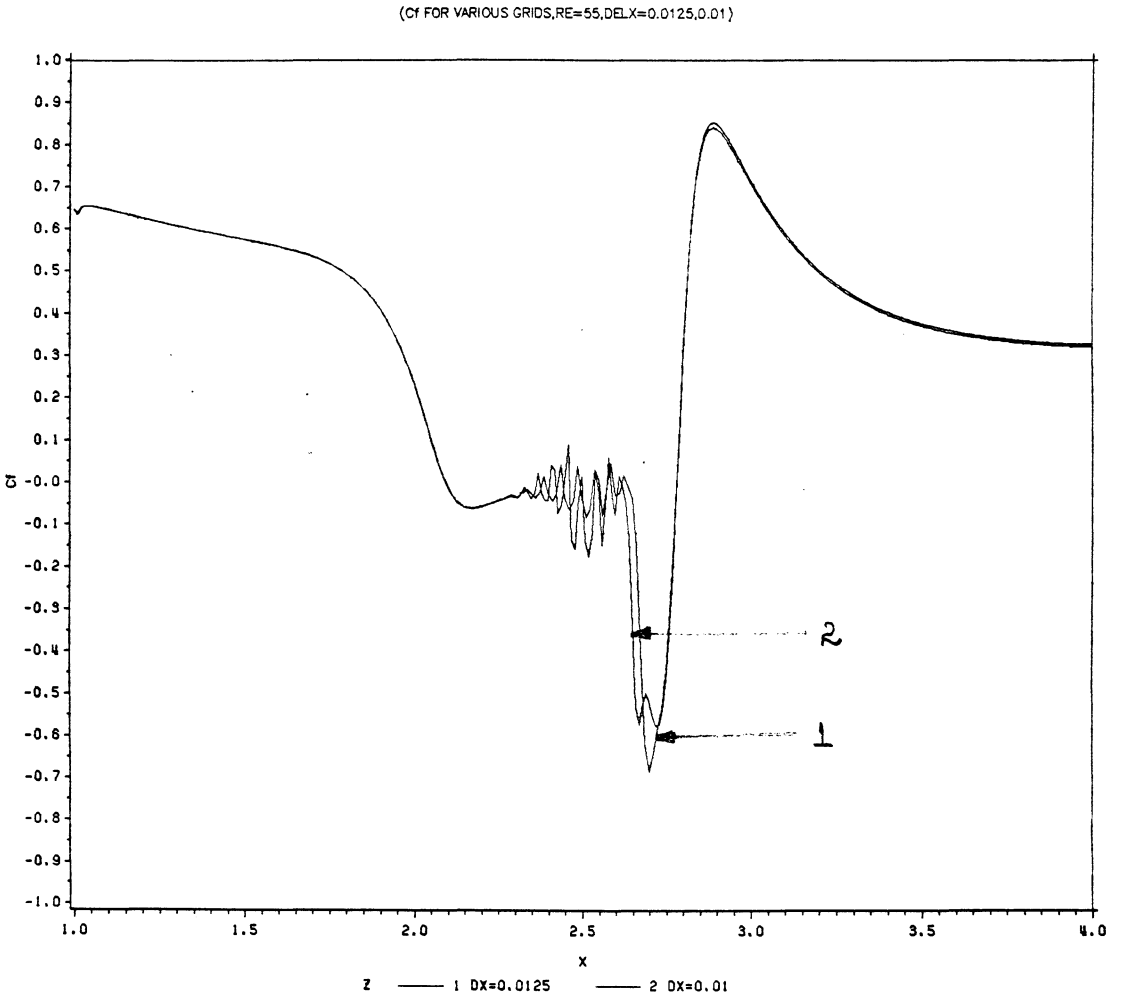

Figure 10. Cf (IBL) for finer grids (Re=550000)

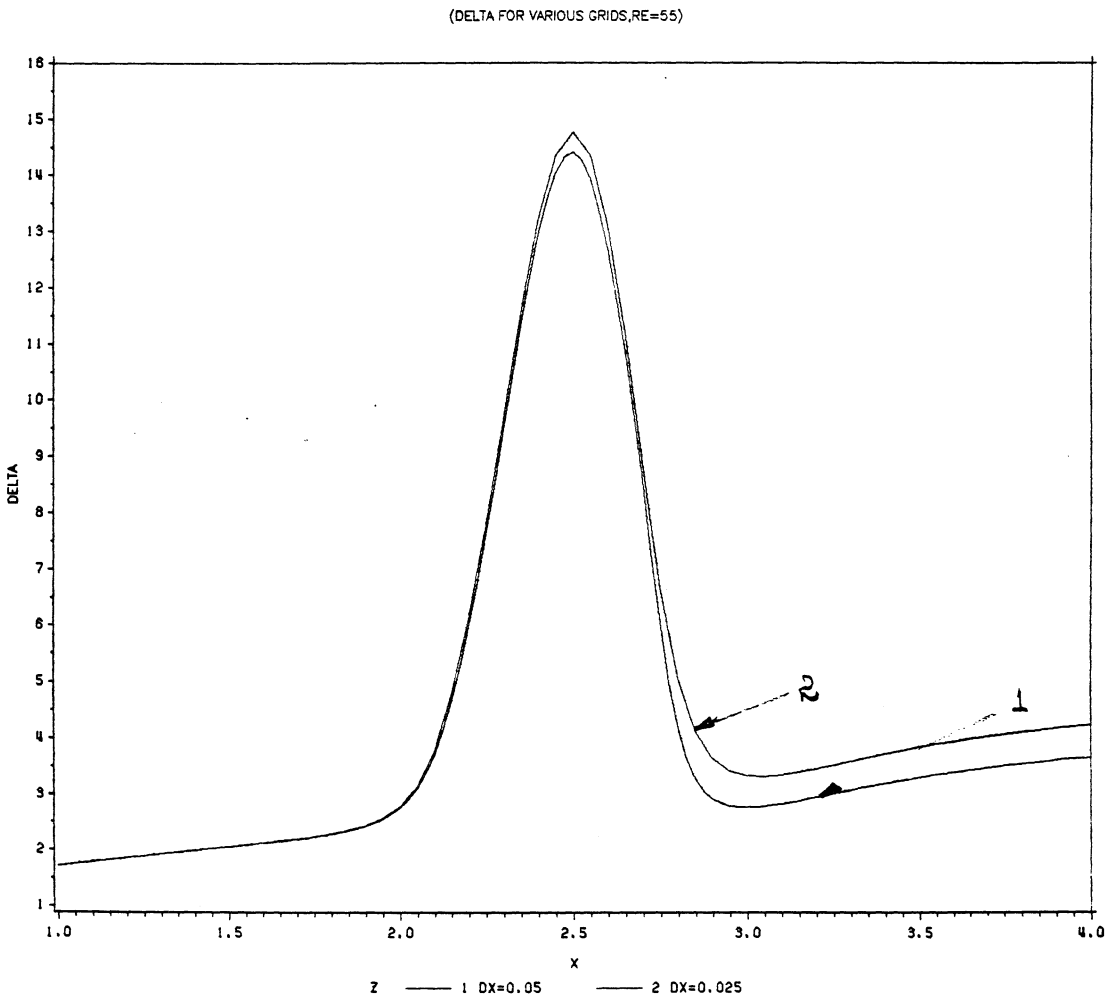

Figure 11. Displacemnt thickness(IBL)for coarser grids (Re=550000)

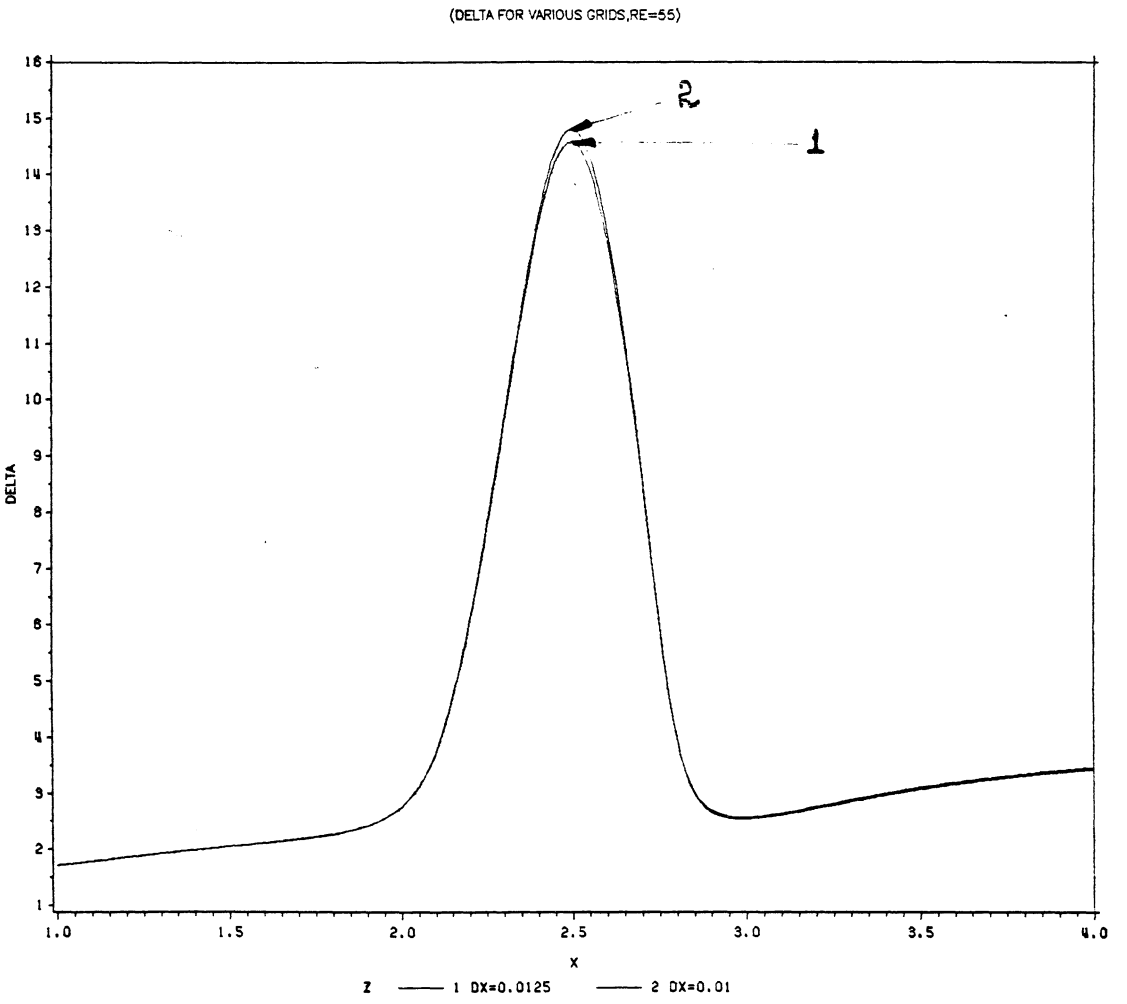

Figure 12. Displacemnt thickness(IBL)for finer grids (Re=550000)

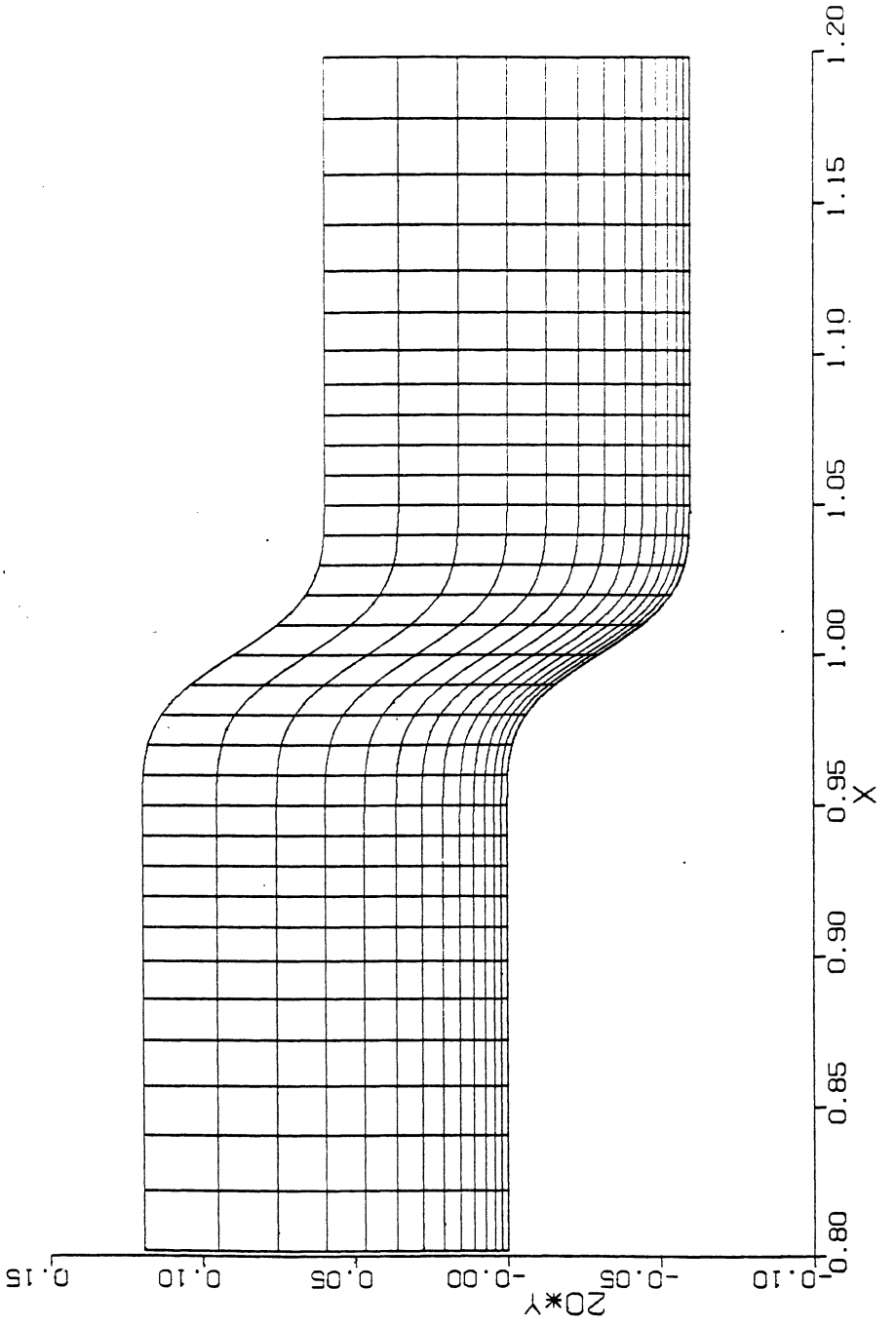

Figure 13. A Typical Computational grid .

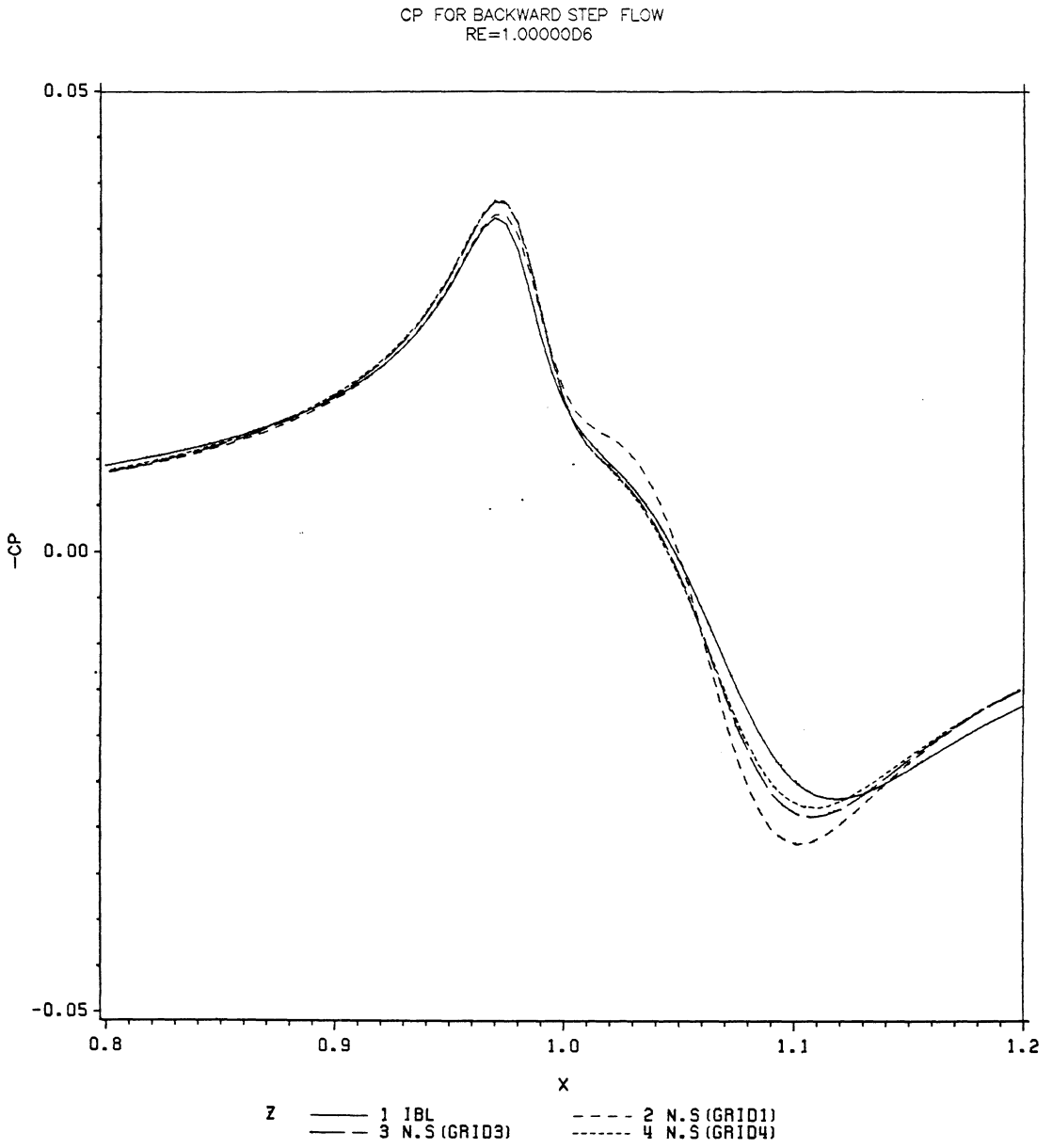

Figure 14. **Cp for Backward step (M=0.5) for various Grids.**

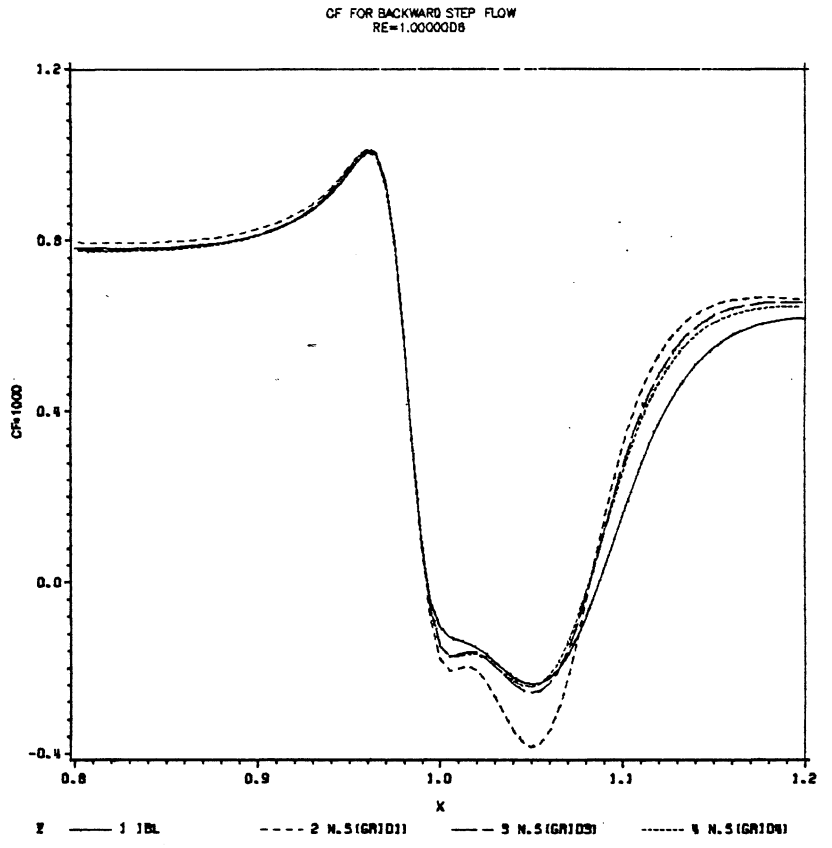

Figure 15. Cf for Backward step (M=0.5) for various Grids.

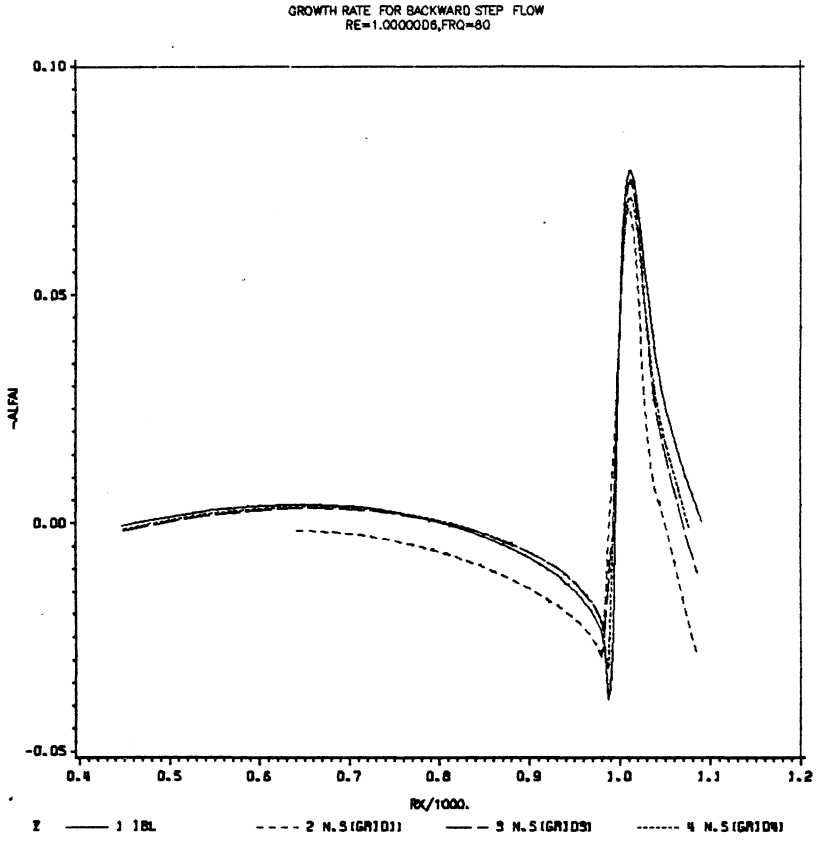

Figure 16. Growth Rate for backward step (M=0.5) for various Grids.

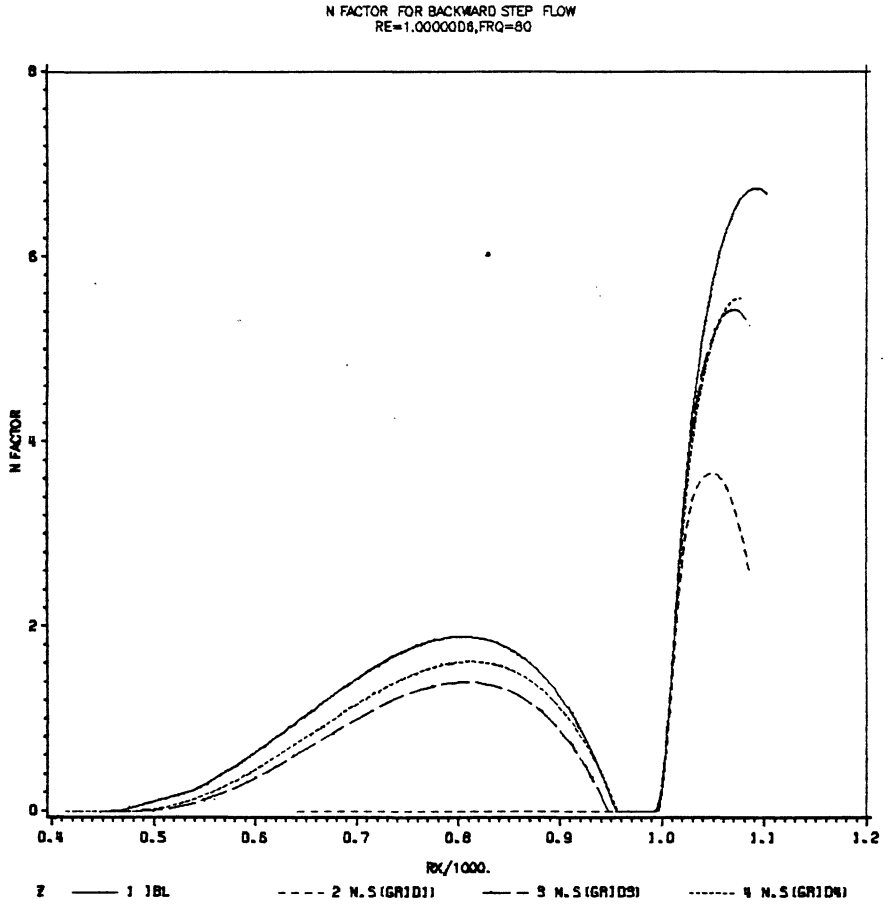

Figure 17. N-factor for backward step (M=0.5) for various Grids.

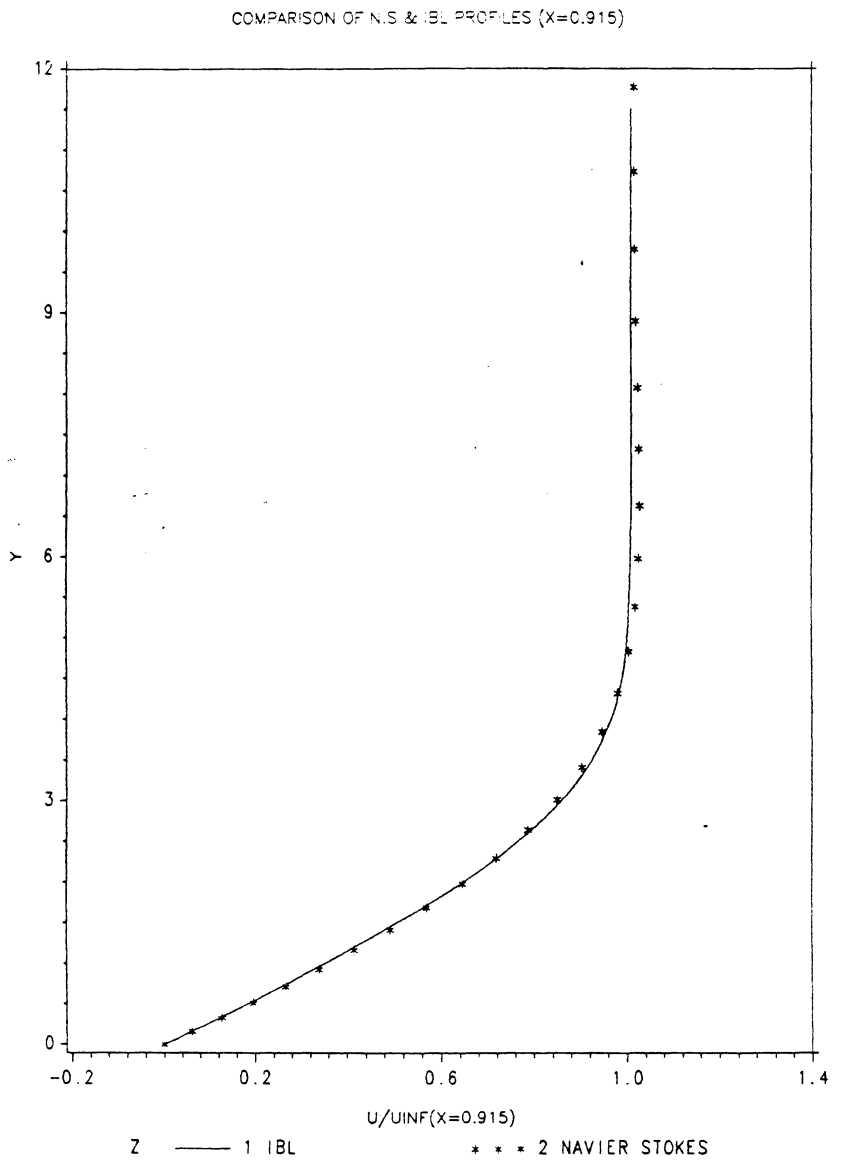

Figure 18. Comparison of Velocity profiles for IBL and Navier Stokes

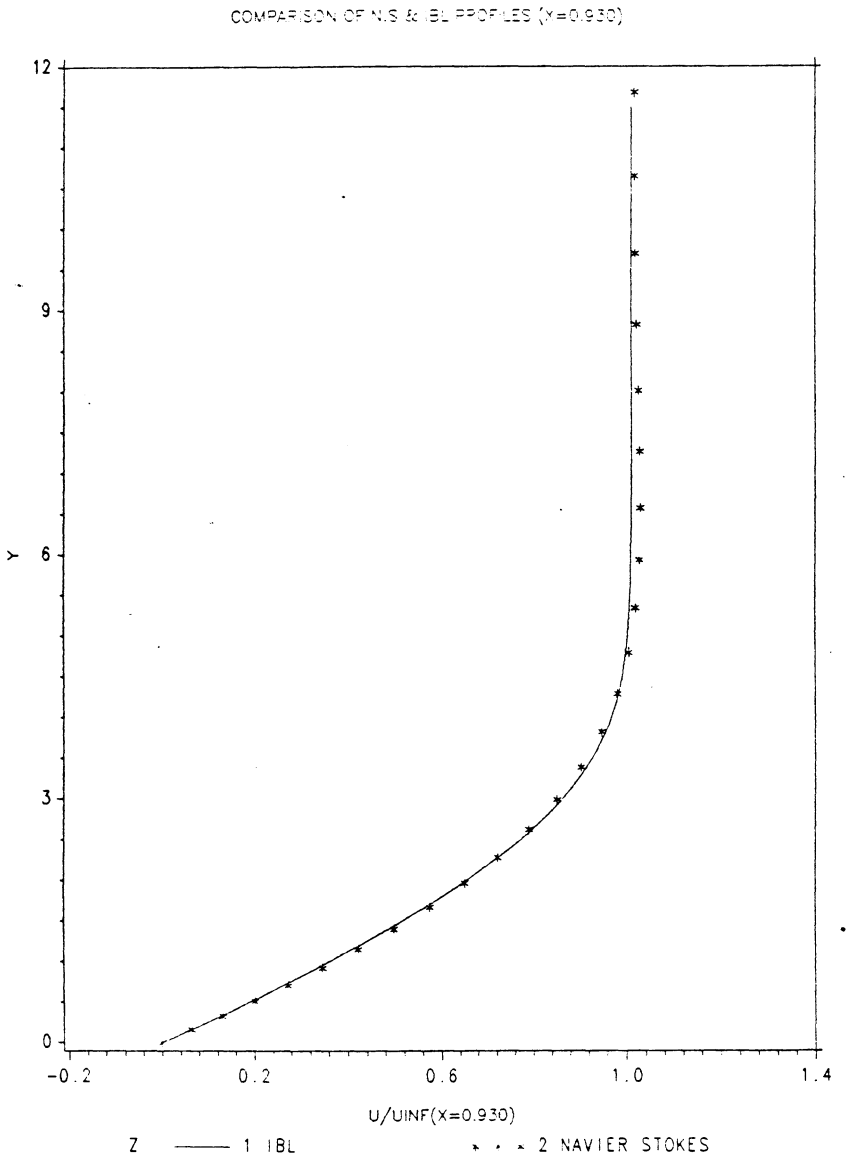

Figure 19. Comparison of Velocity profiles for IBL and Navier Stokes

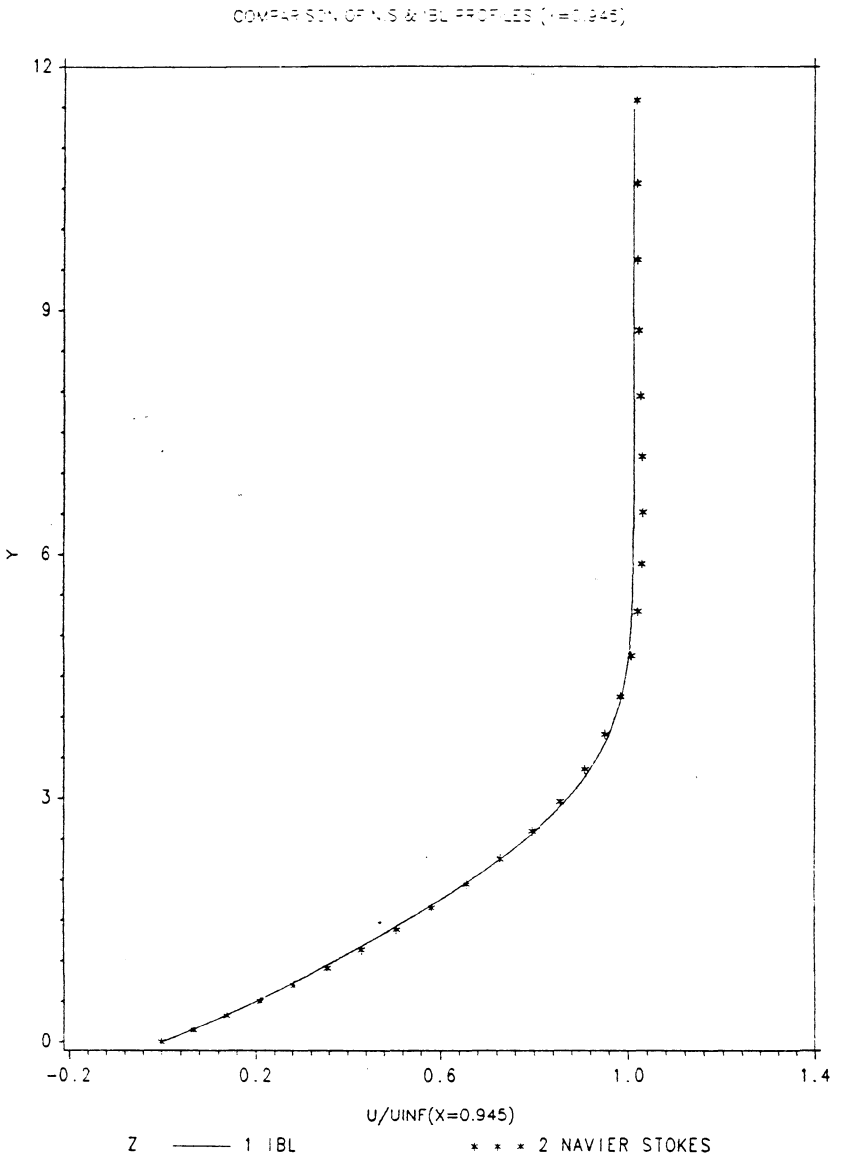

Figure 20. Comparison of Velocity profiles for IBL and Navier Stokes

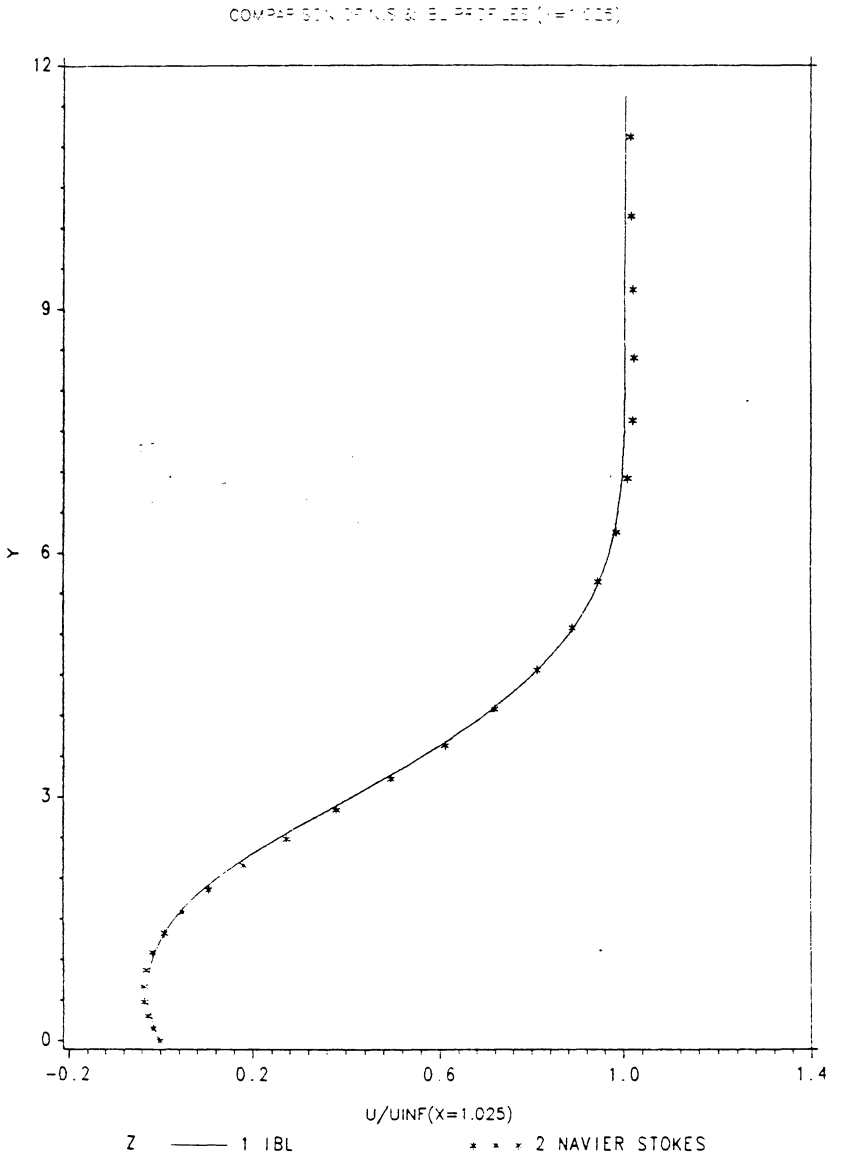

Figure 21. Comparison of Velocity profiles for IBL and Navier Stokes

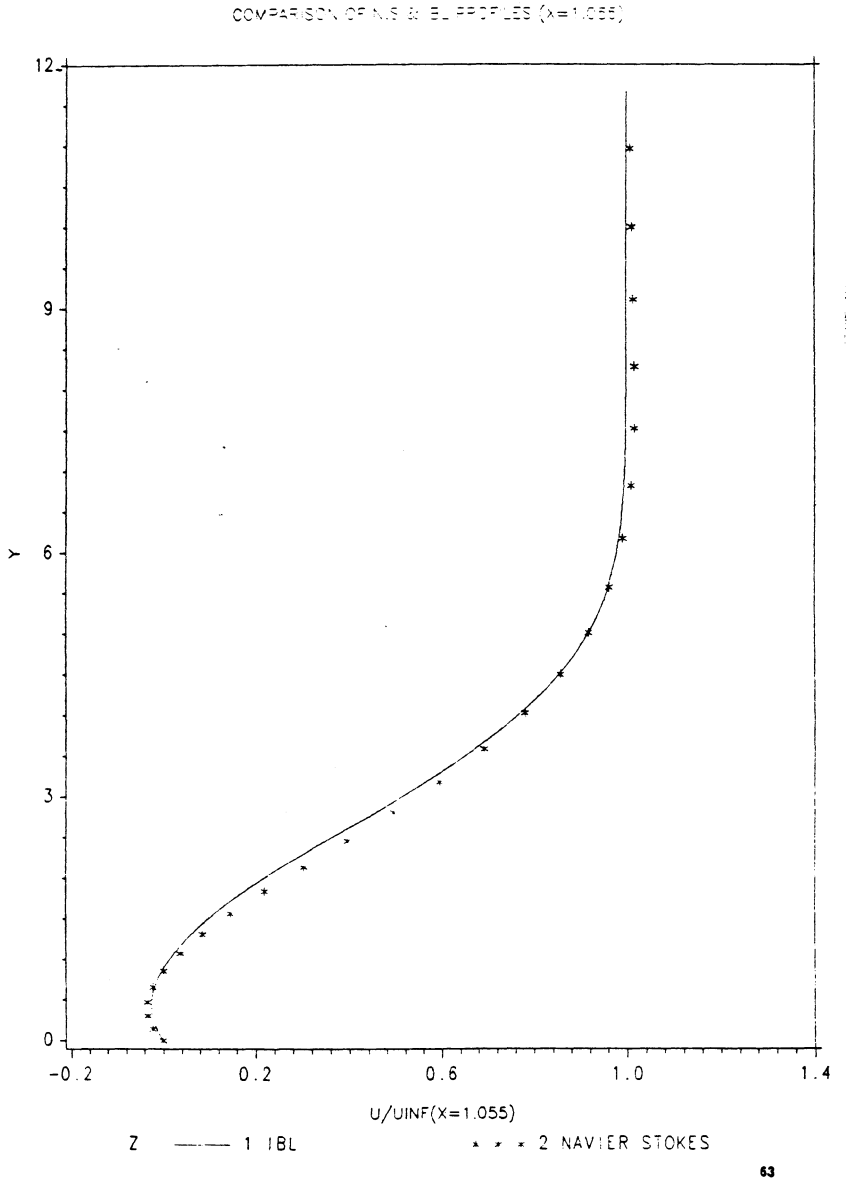

Figure 22. Comparison of Velocity profiles for IBL and Navier Stokes

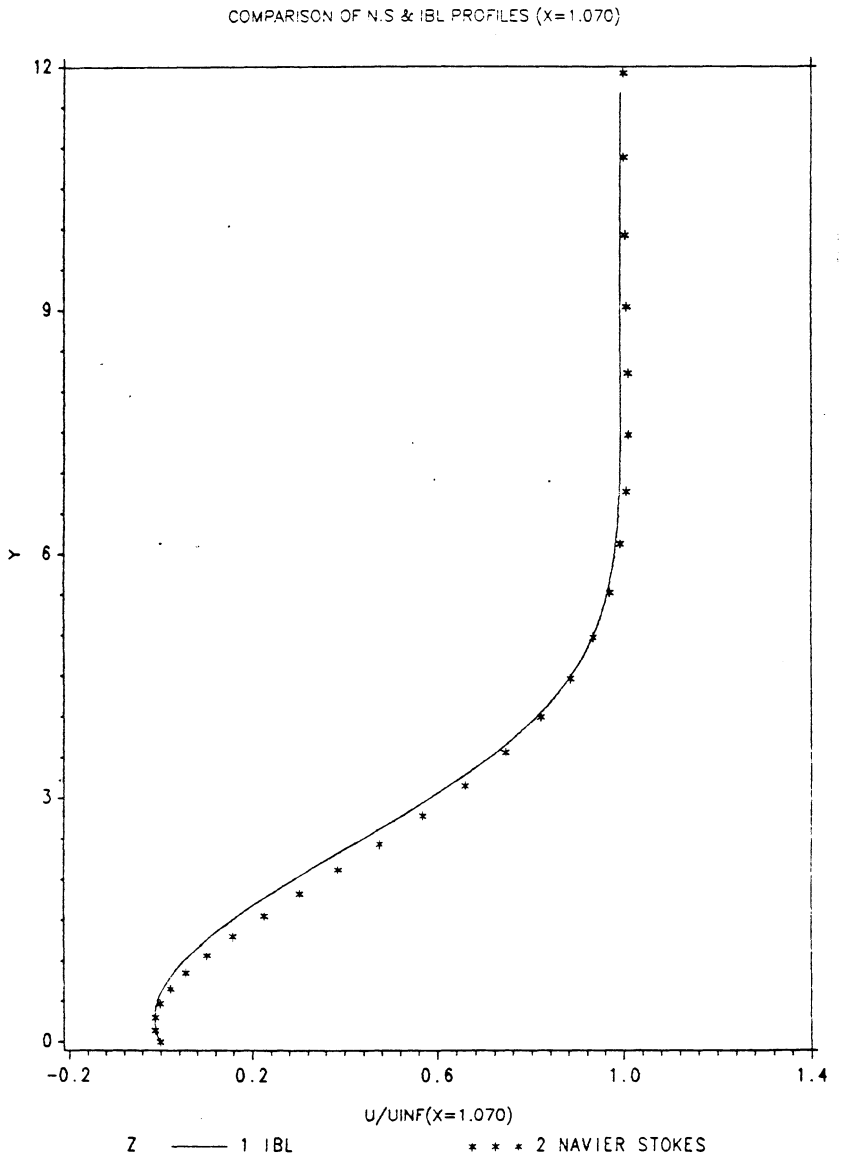

Figure 23. Comparison of Velocity profiles for IBL and Navier Stokes

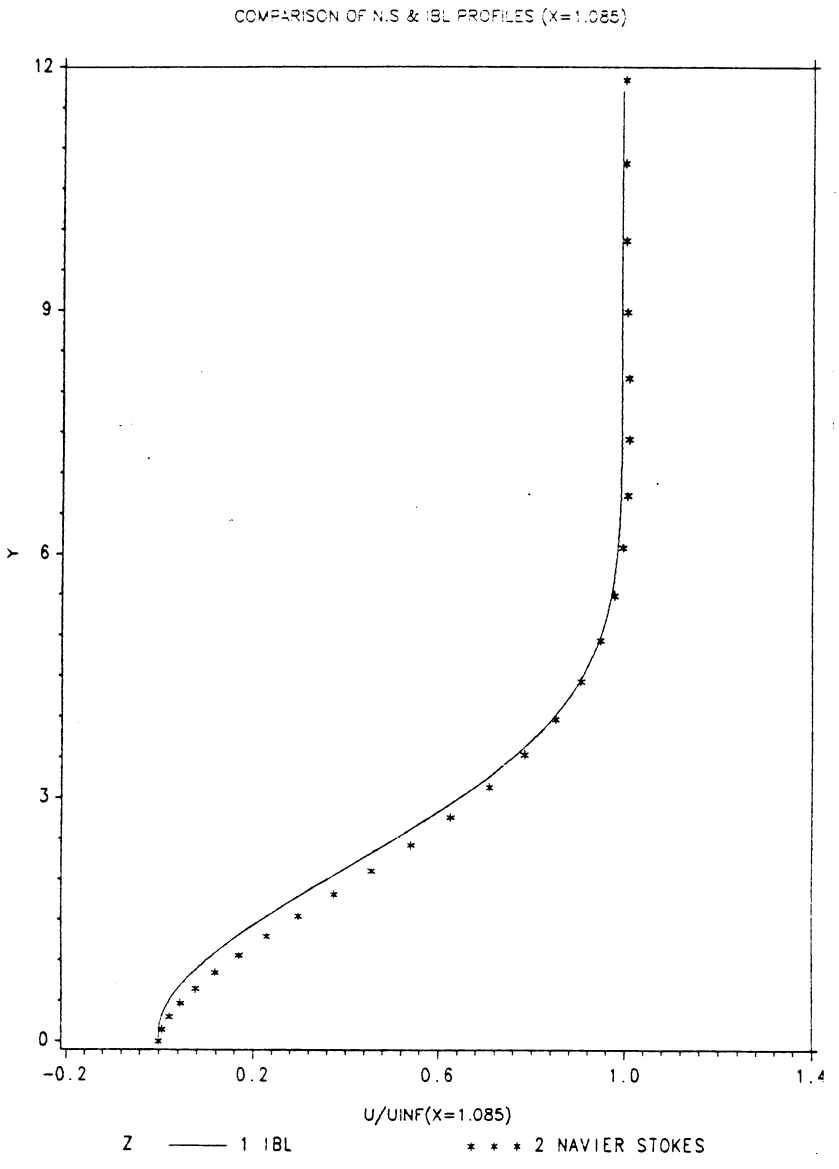

Figure 24. Comparison of Velocity profiles for IBL and Navier Stokes

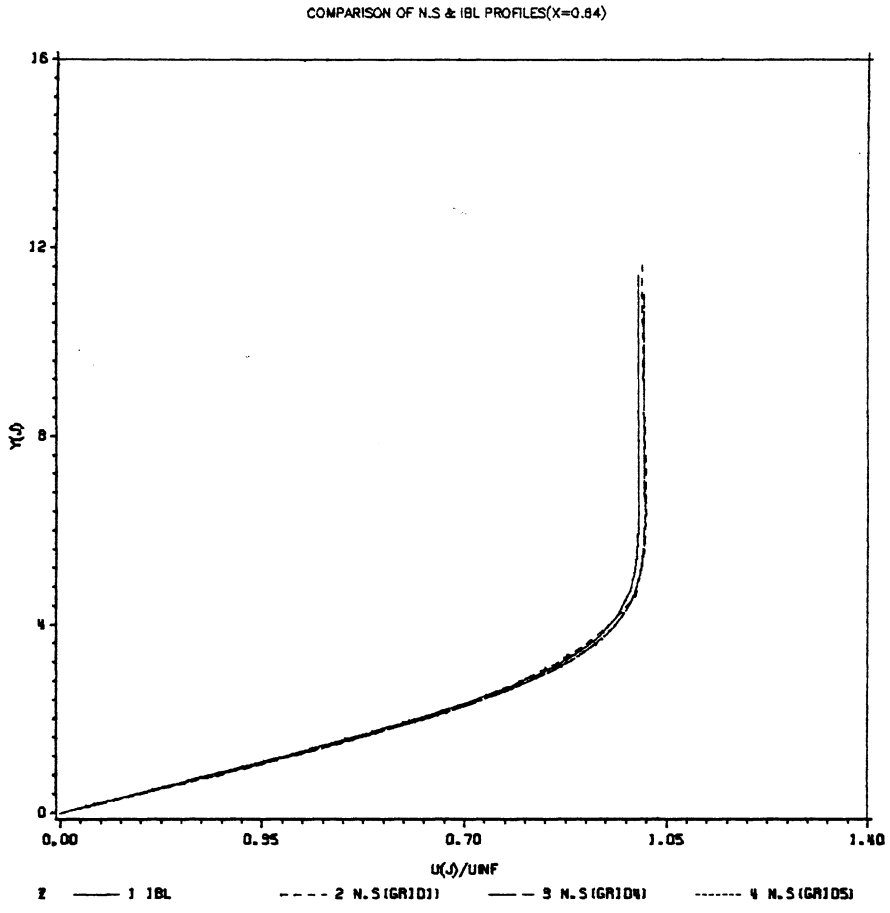

Figure 25. Comparison of Velocity profiles for various grids (X=0. 64)

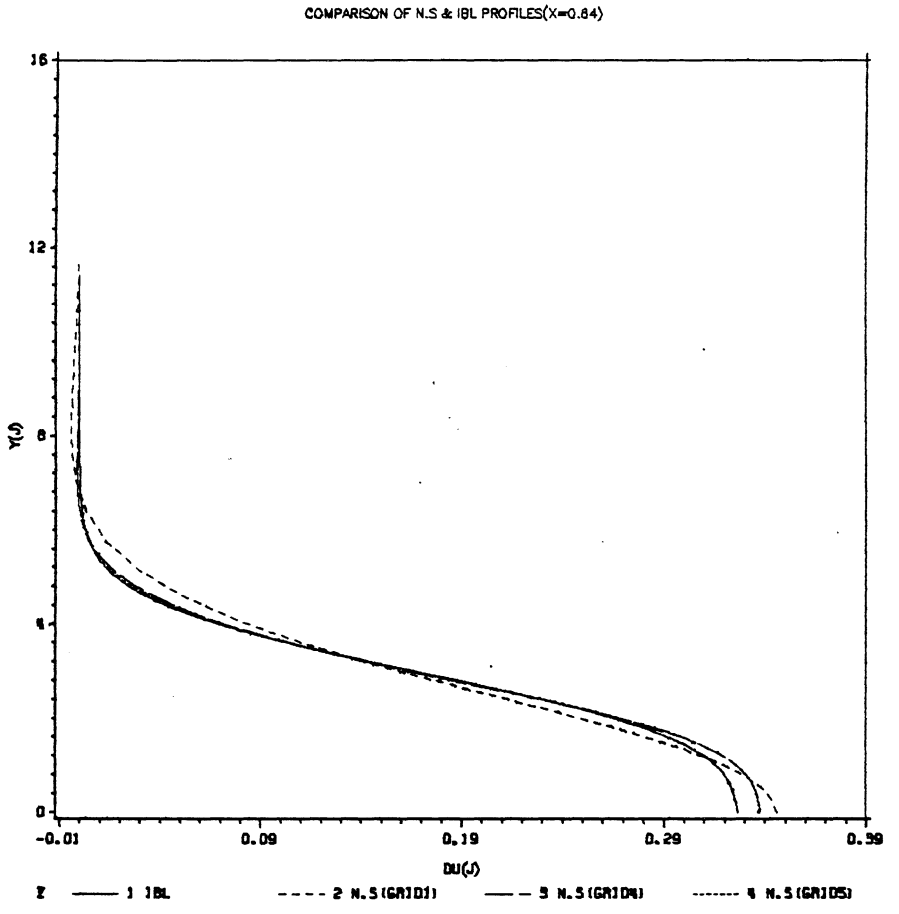

Figure 26. First dervative of velocity for various grids (X=0. 64)

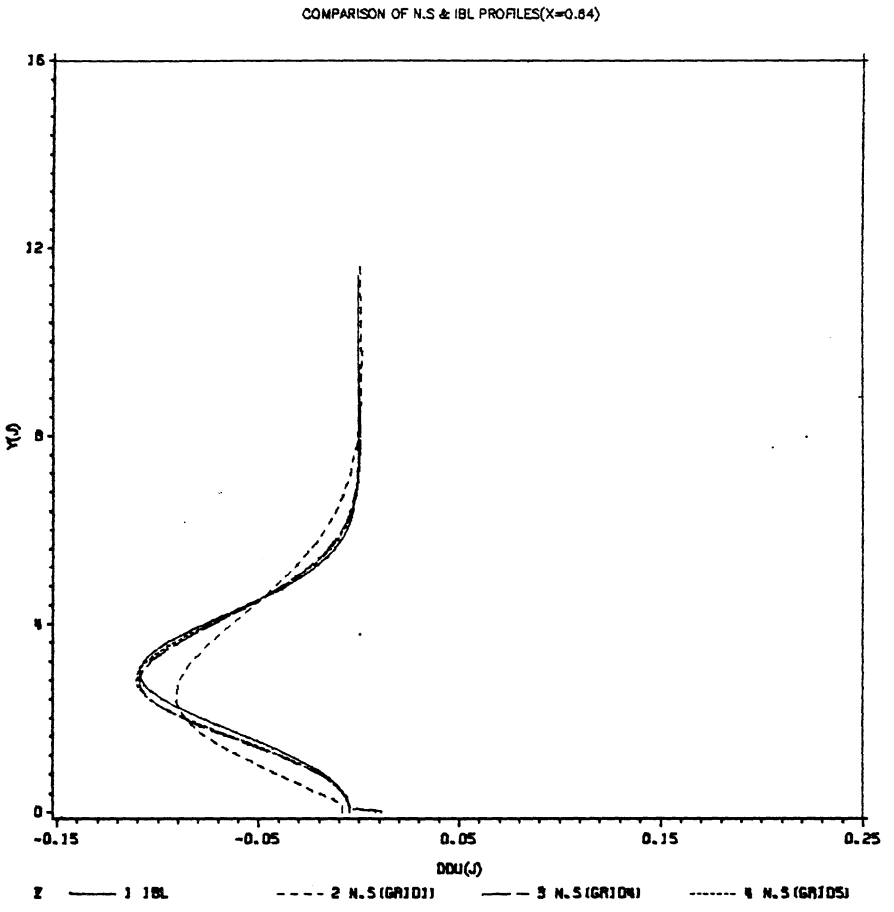

Figure 27. Second derivative for velocity for various grids(X=0. 64)

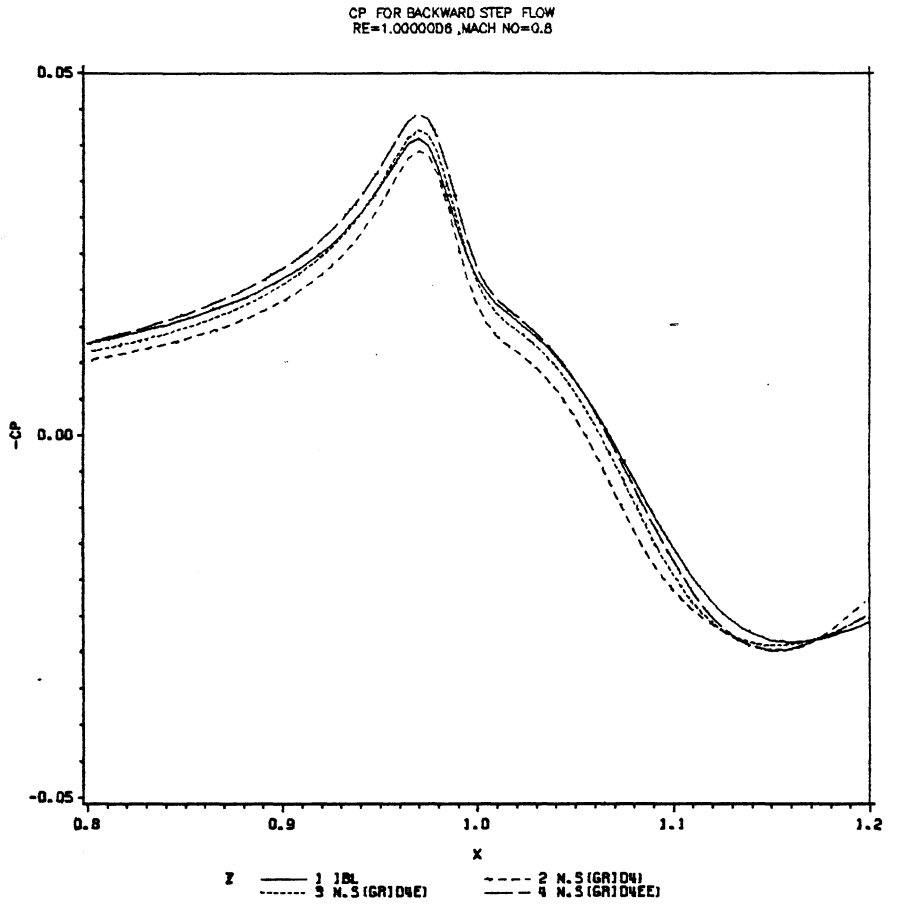

Figure 28. **Cp for Backward step (M = 0.8) for various outer boundaries**

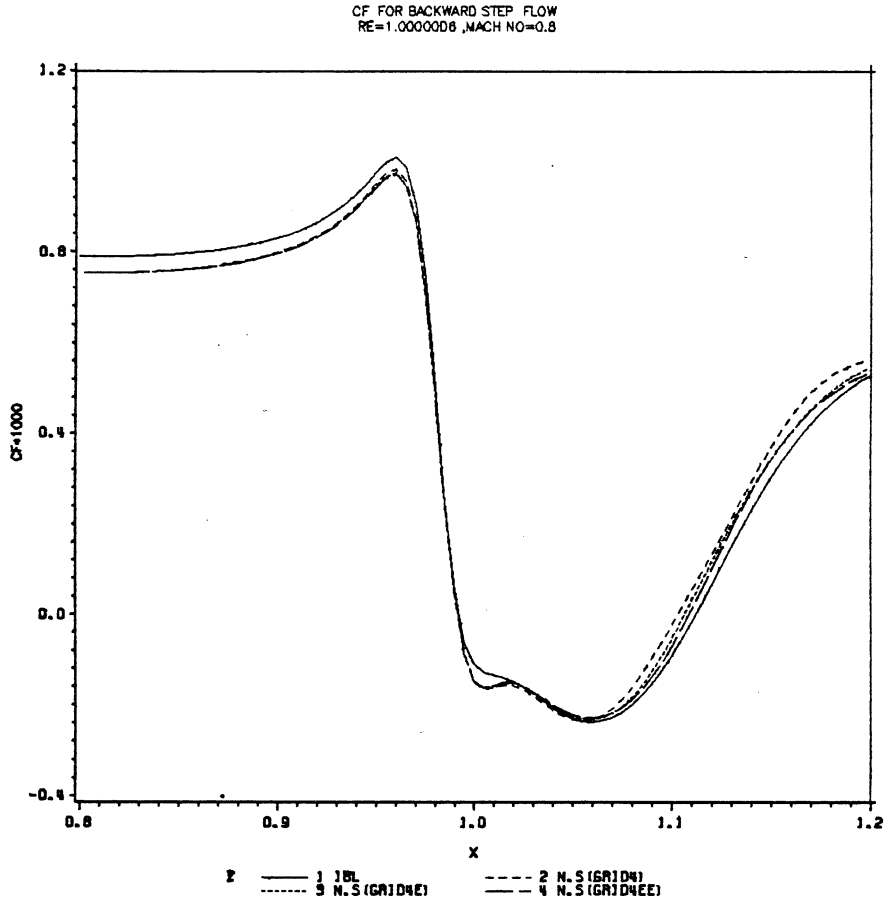

Figure 29. **Cf for Backward step (M=0.8) for various outer boundaries**

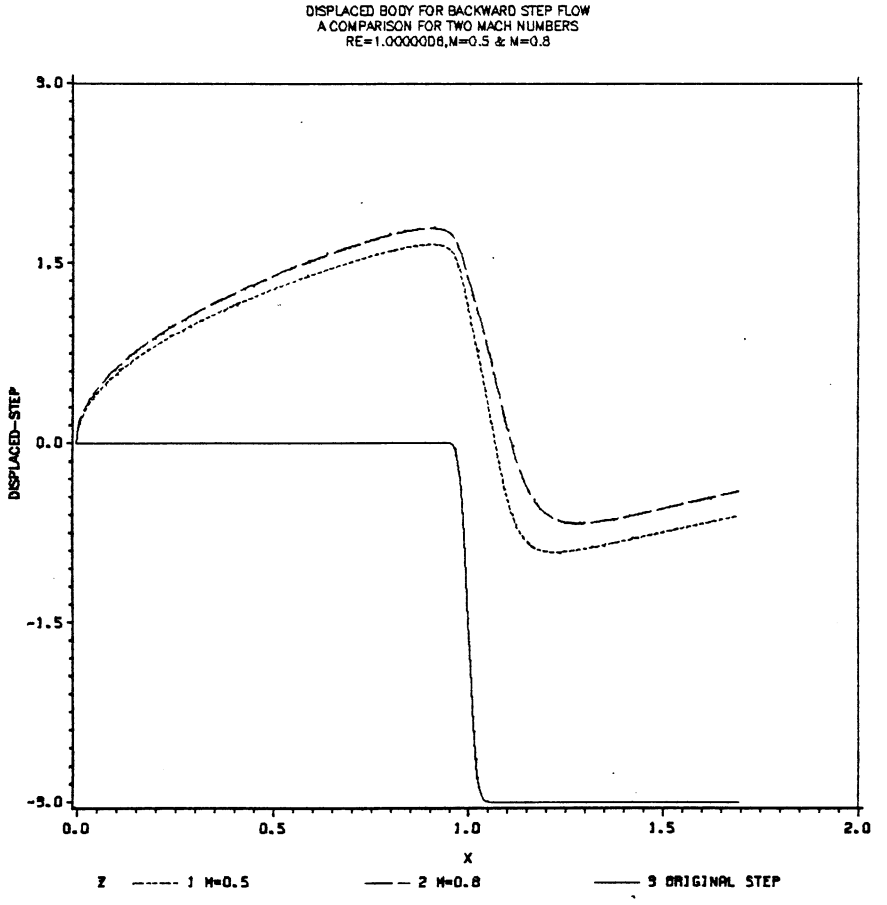

Figure 30. Comparison of displacement Thickness for M = 0.5 and M = 0.8

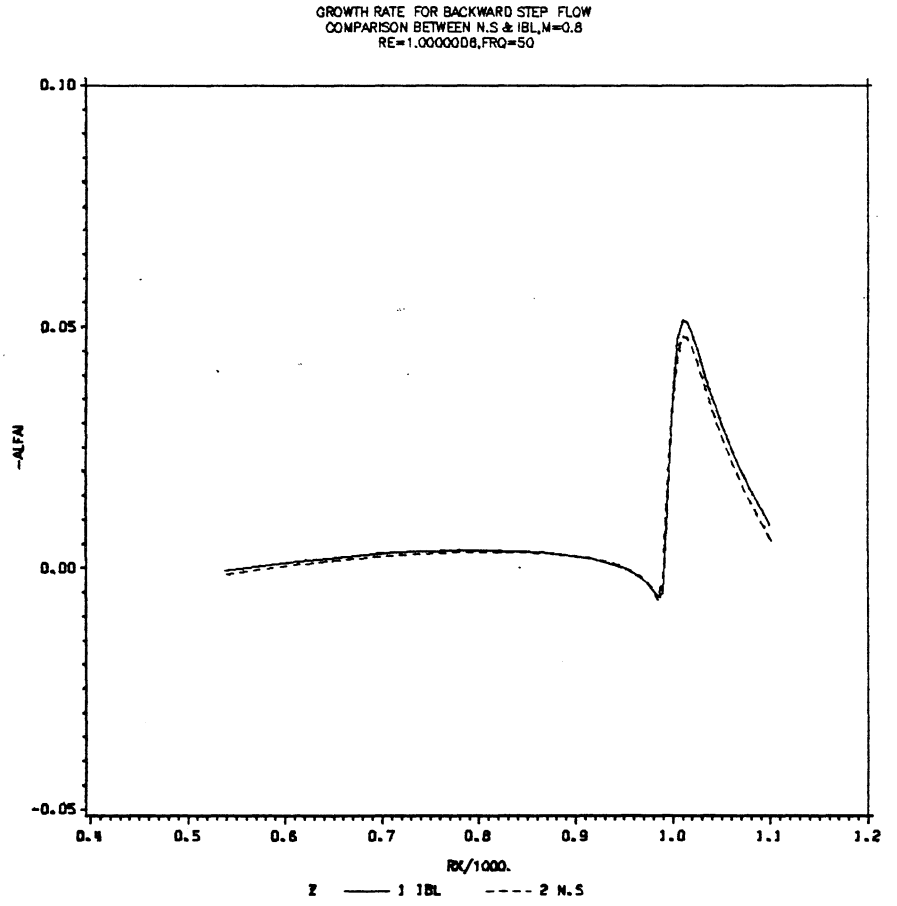

Figure 31. Growth Rate for backward step (M=0.8) for various Grids.

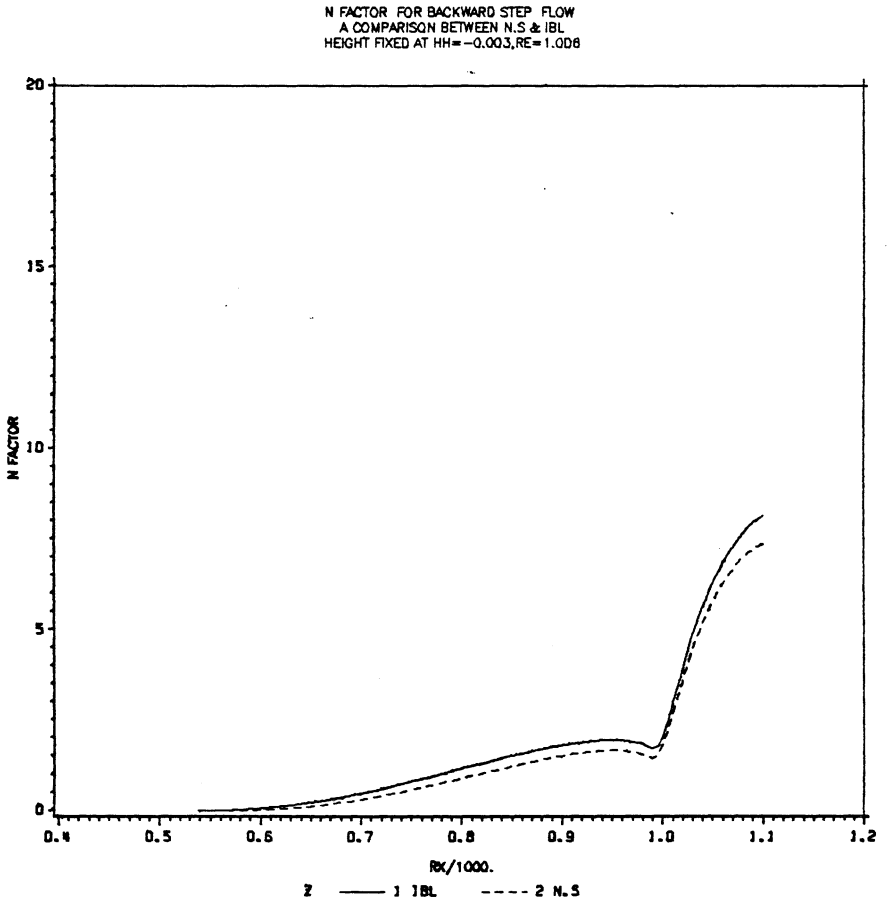

Figure 32. N-factor for backward step (M=0.8) for various Grids.

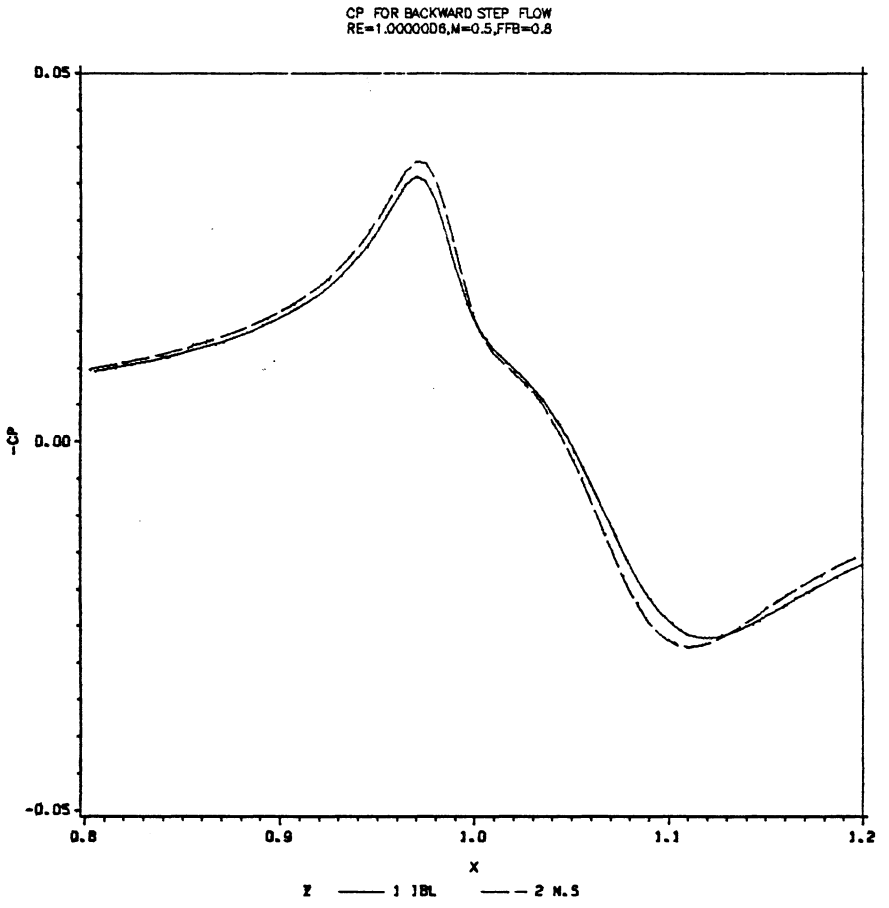

Figure 33. Cp at various far field Boundaries (M = 0.5)

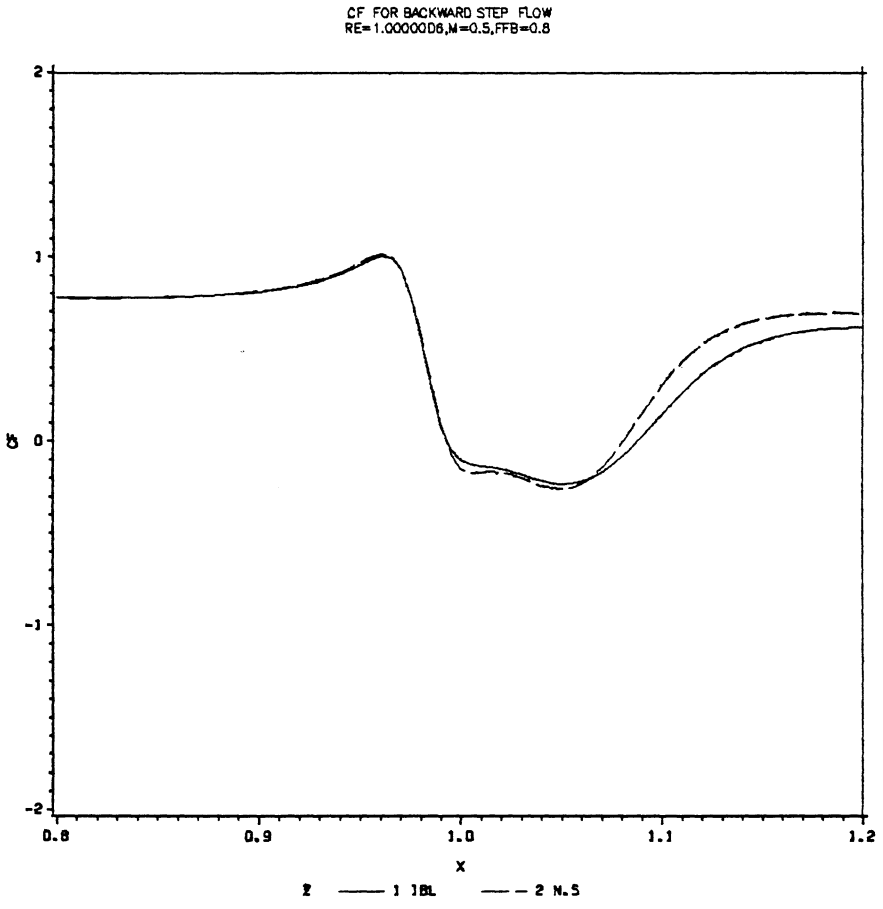

Figure 34. Cf at various far field Boundaries (M=0.5)

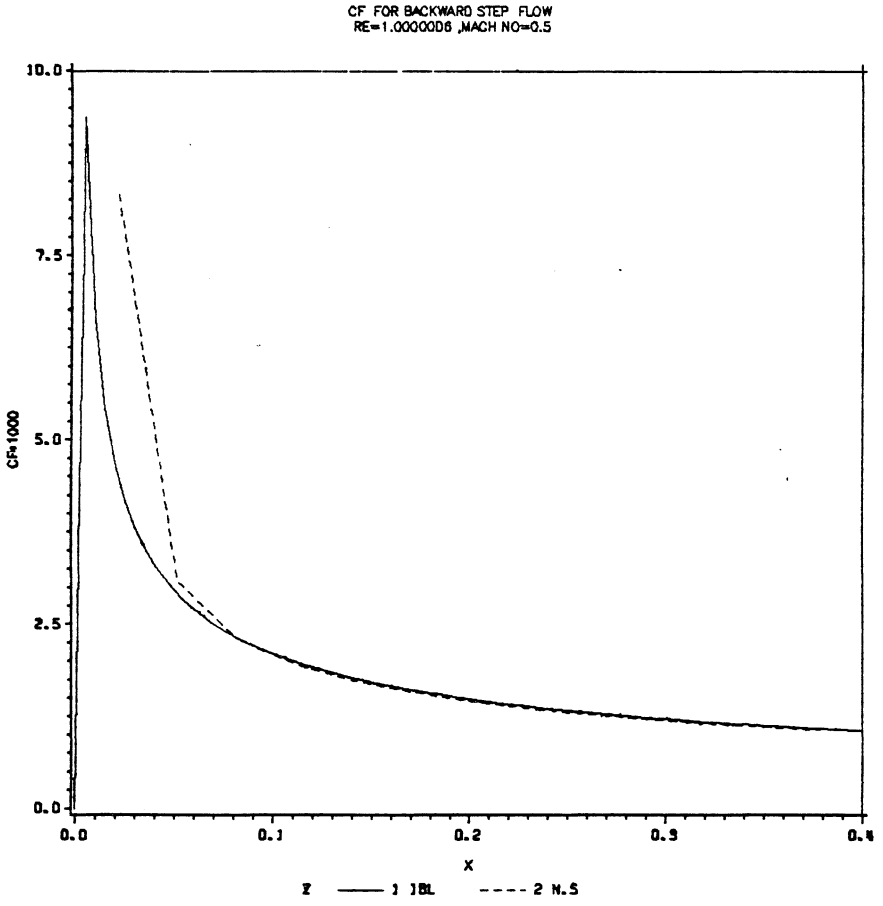

Figure 35. Cf for Backward step (M=0.5) at the leading edge.

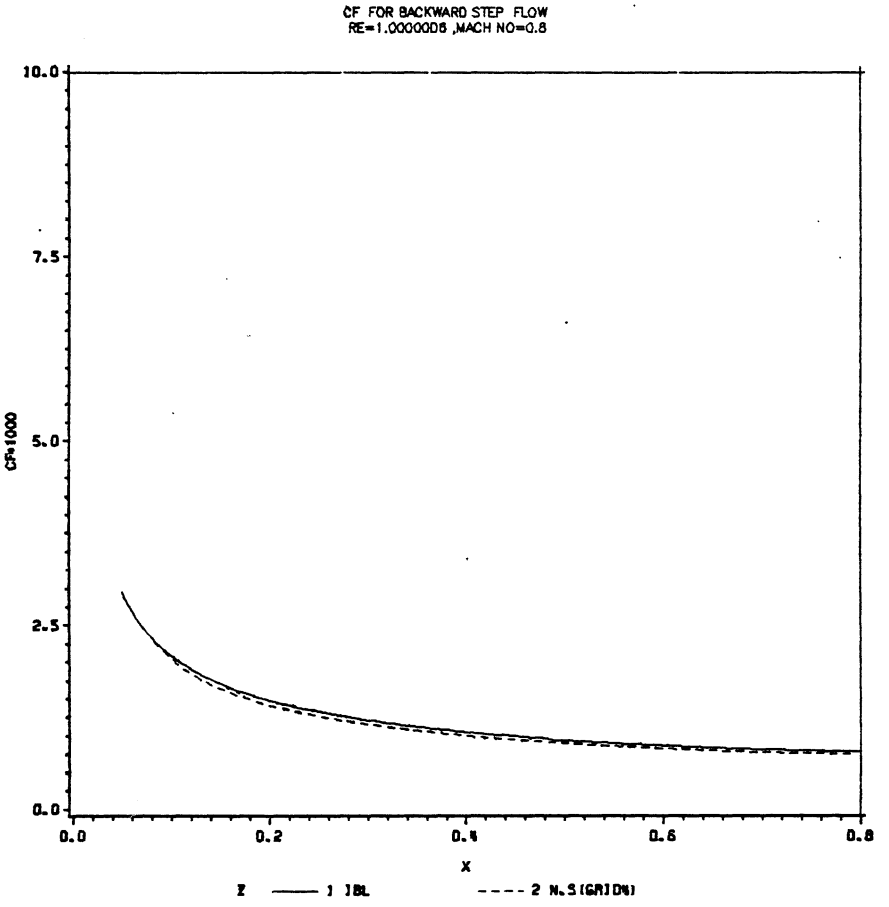

Figure 36. Cf for Backward step (M=0.8) at the leading edge.

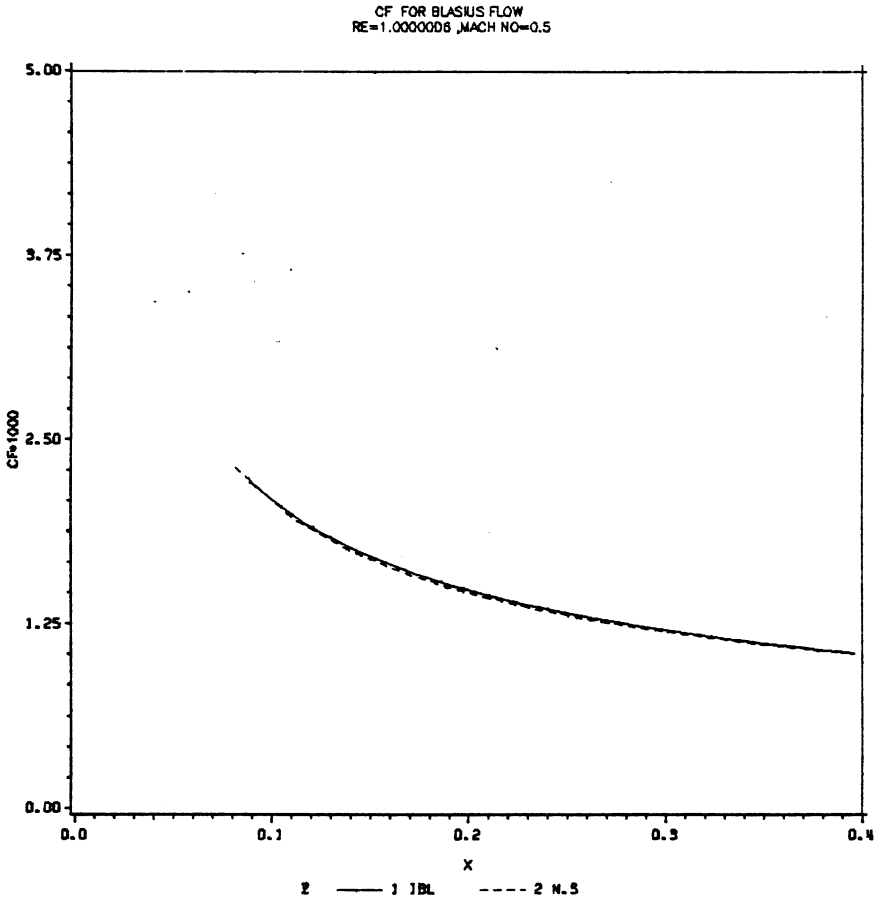

Figure 37. Cf for Blasius Flow (M = 0.5) at the leading edge

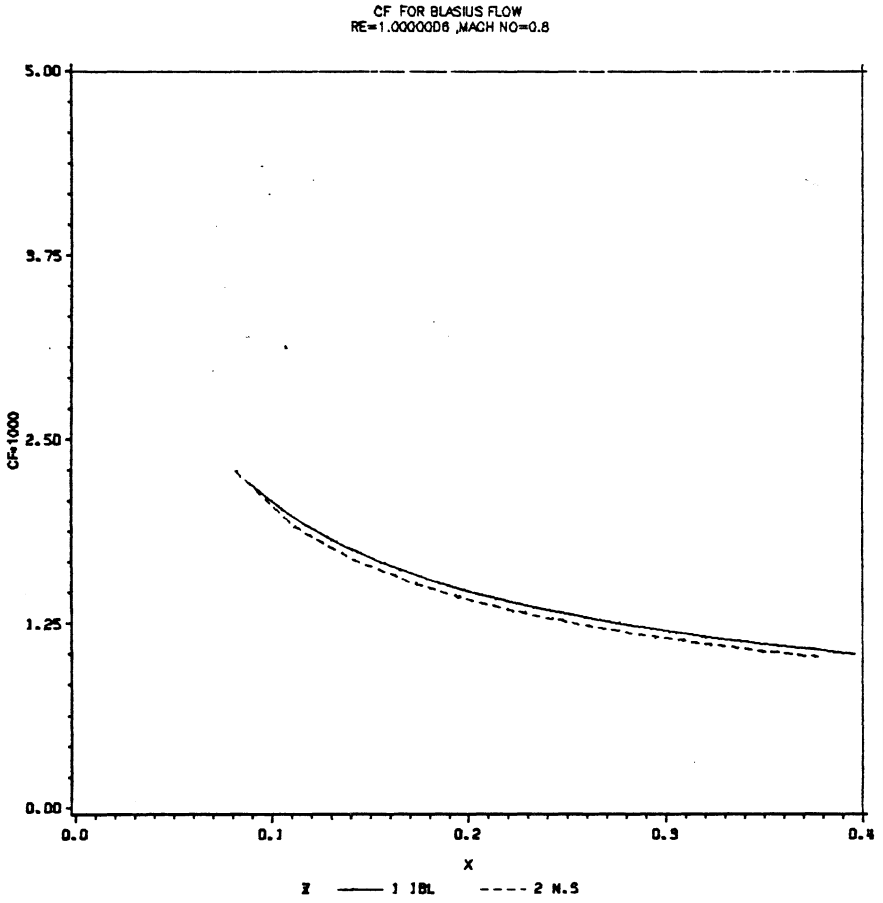

Figure 38. Cf for Blasius flow (M=0.8) at the leading edge

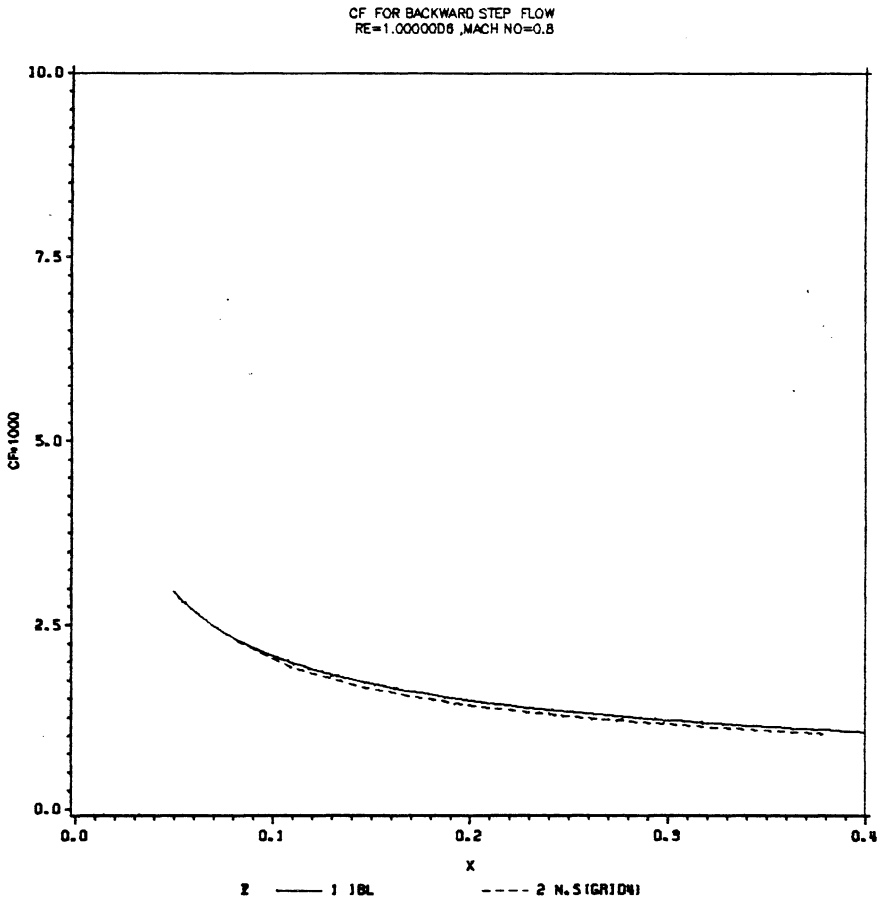

Figure 39. Cf for Backward step (M=0. 8) at the leading edge,

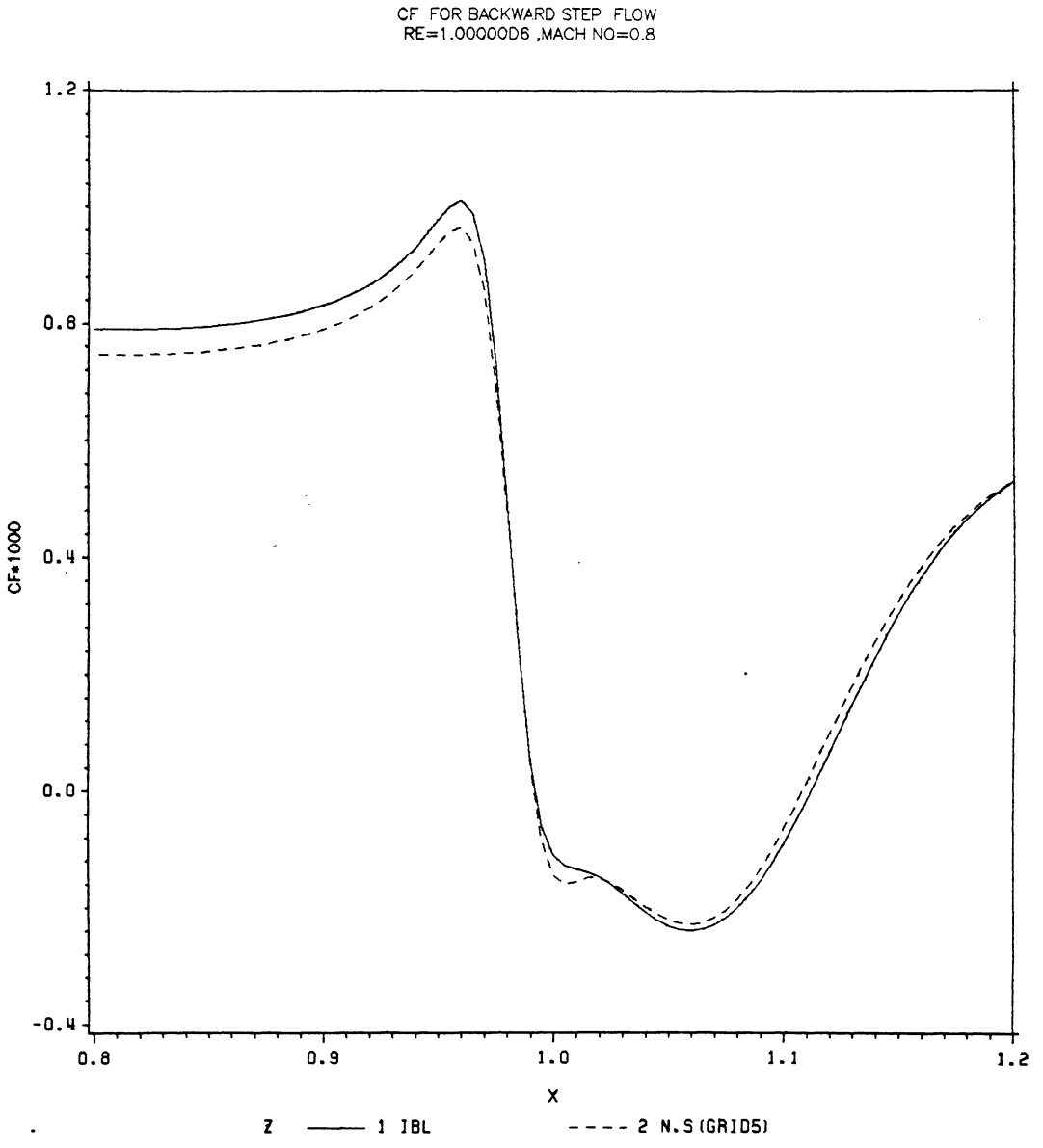

Figure 40. Cf for Backward step (M=0. 8) over the step

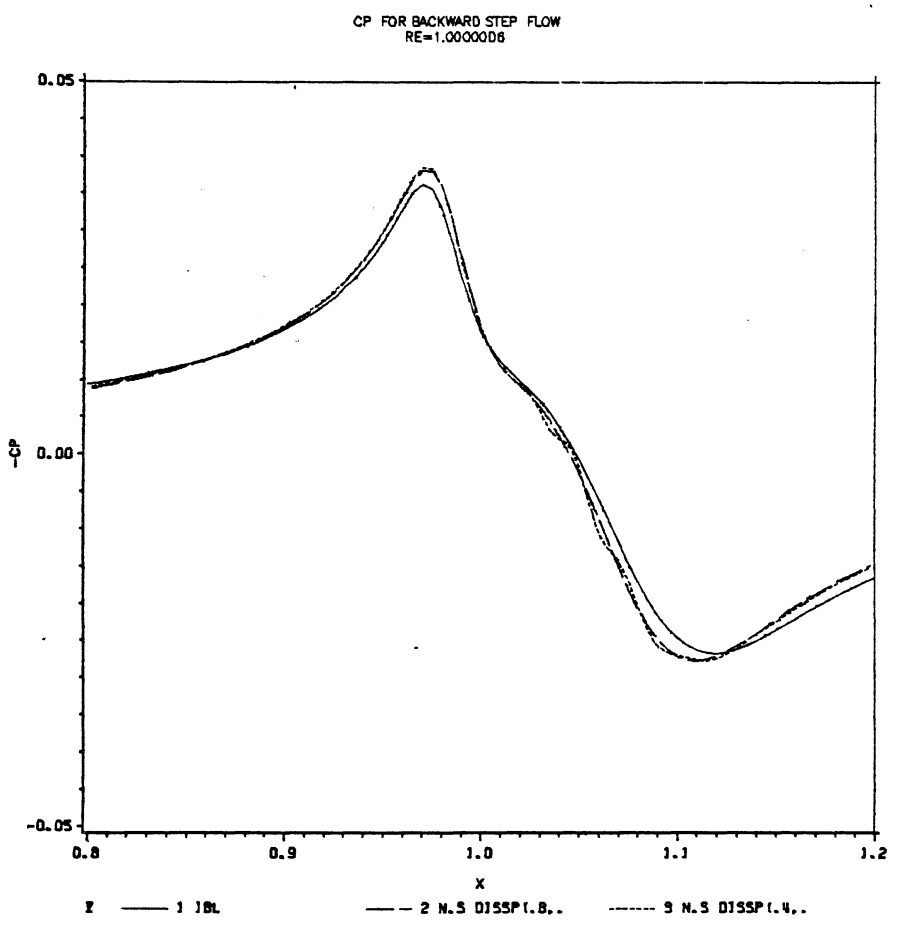

Figure 41. Cp ,Effect of Dissipation(M=0.8).

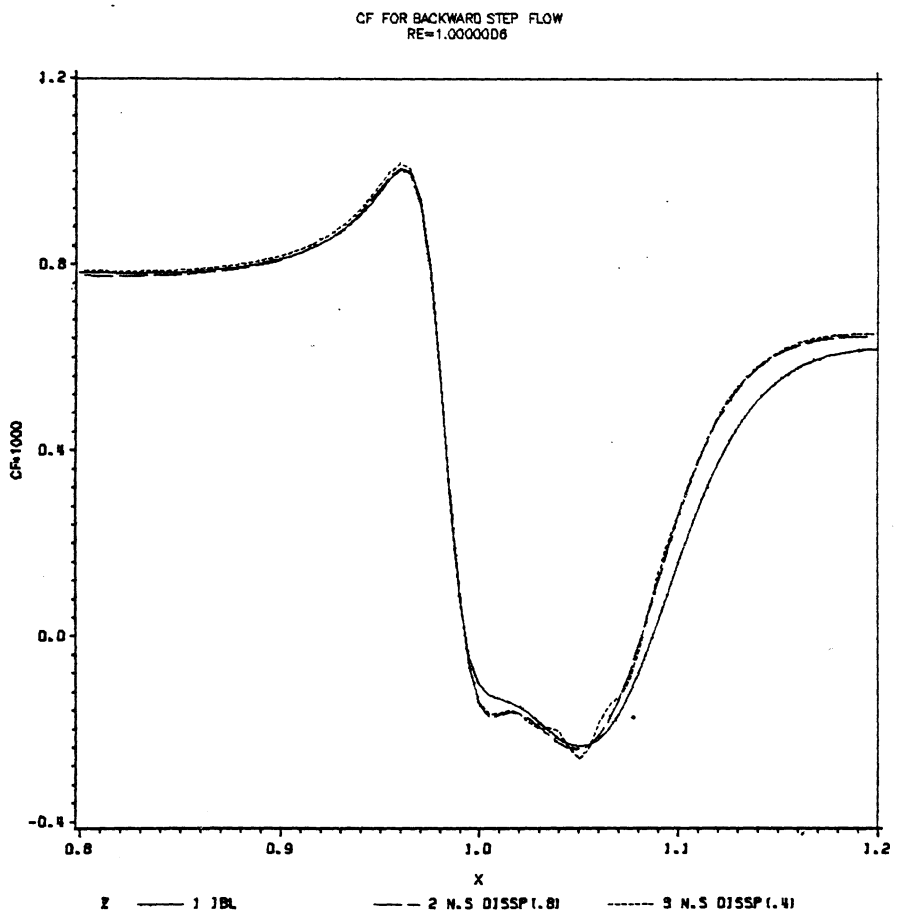

Figure 42. Cf ,Effect of Dissipation(M = 0.8).

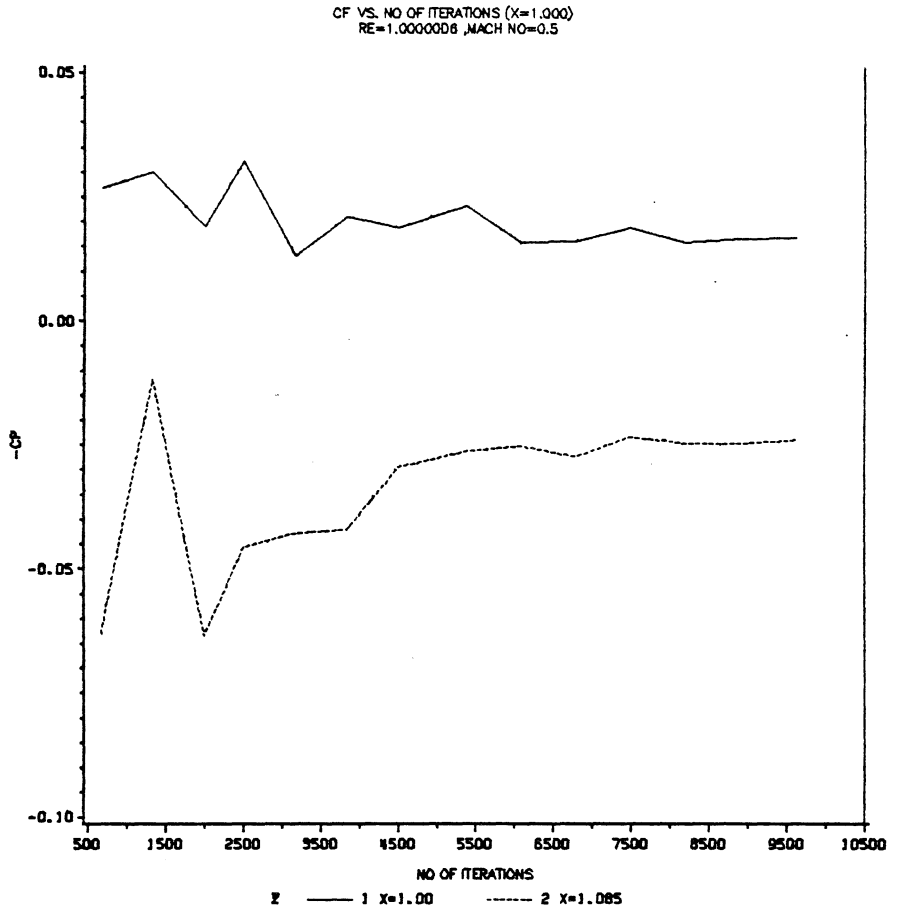

Figure 43. Cf Vs. Number of iterations (M = 0.5)

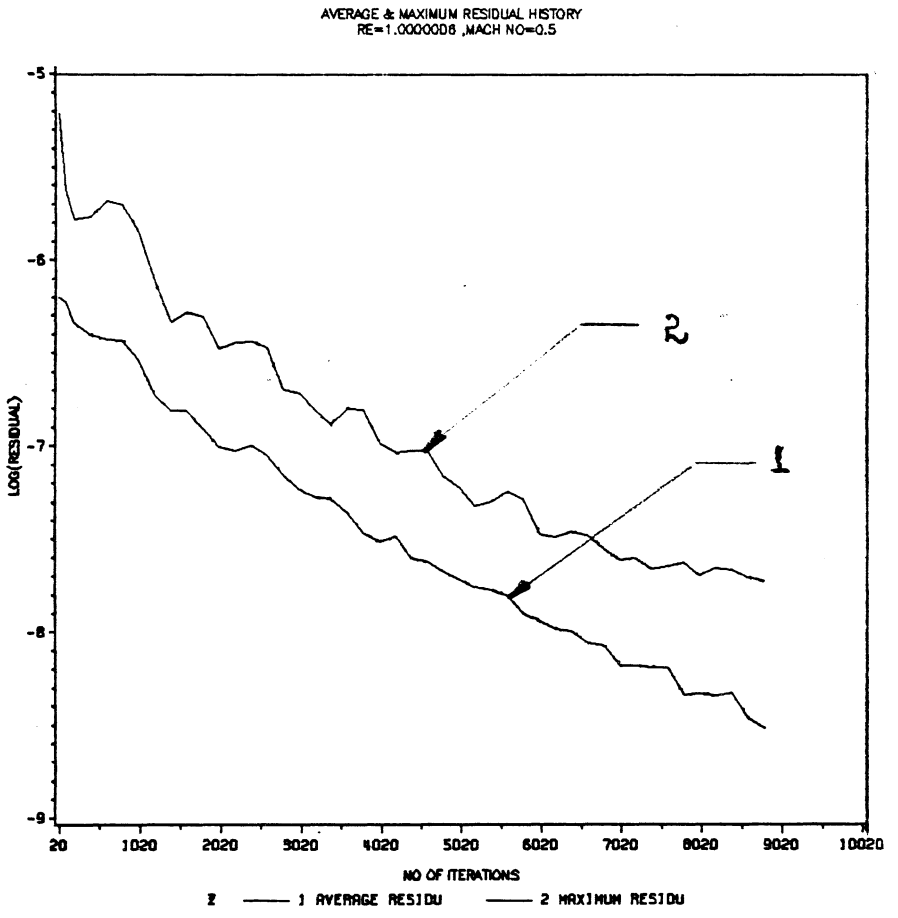

Figure 44. Average and residual History(M=0.5)

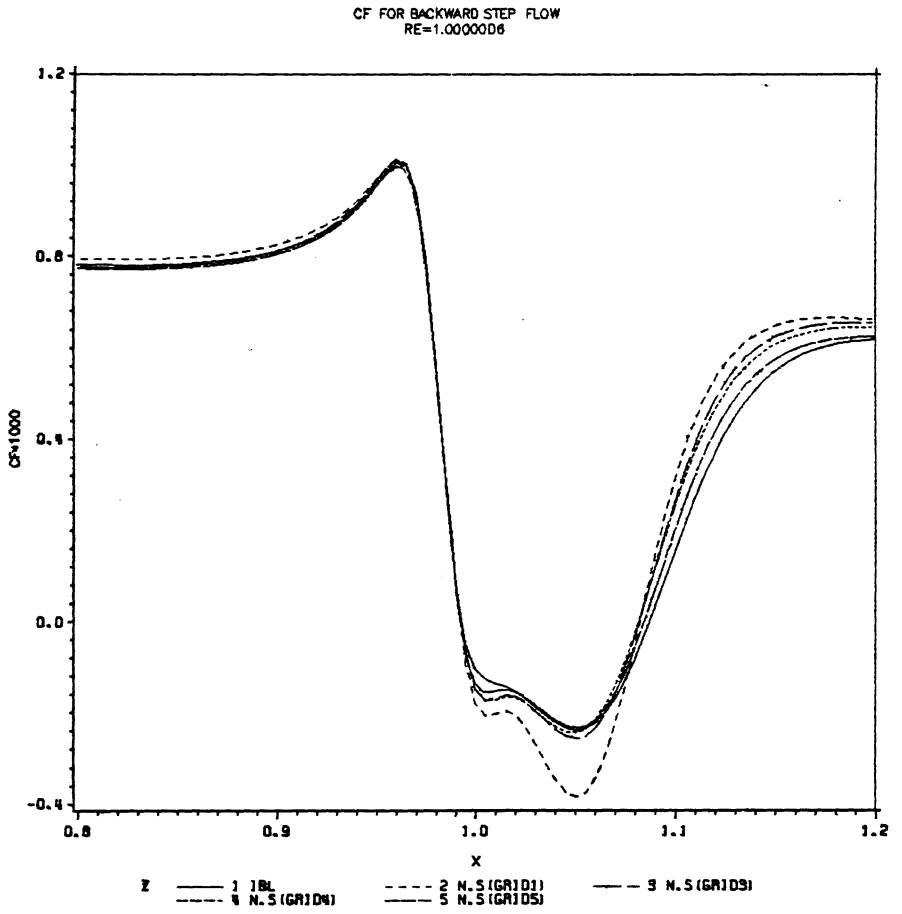

Figure 45. Cf For the Finest Grid (M=0. 5) and comparison with IBL

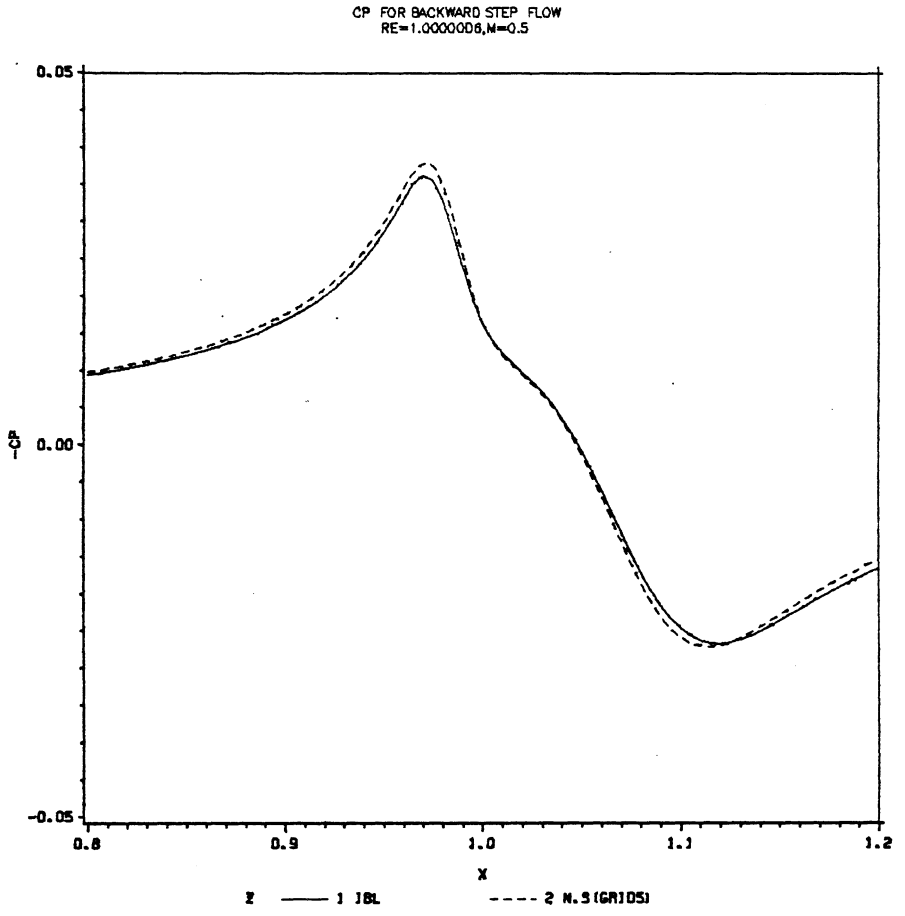

Figure 46. Cp for the finest Grid (M=0.5) and comparison with IBL

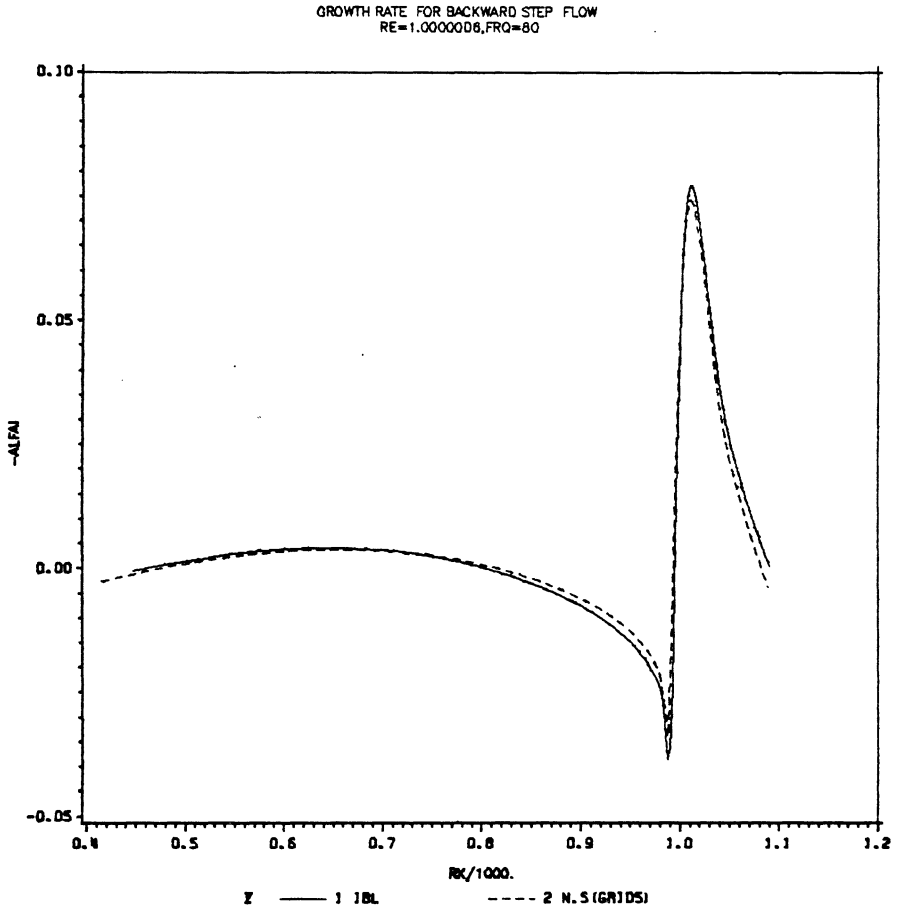

Figure 47. Growth rate (M = 0.5) comparison for finest grid

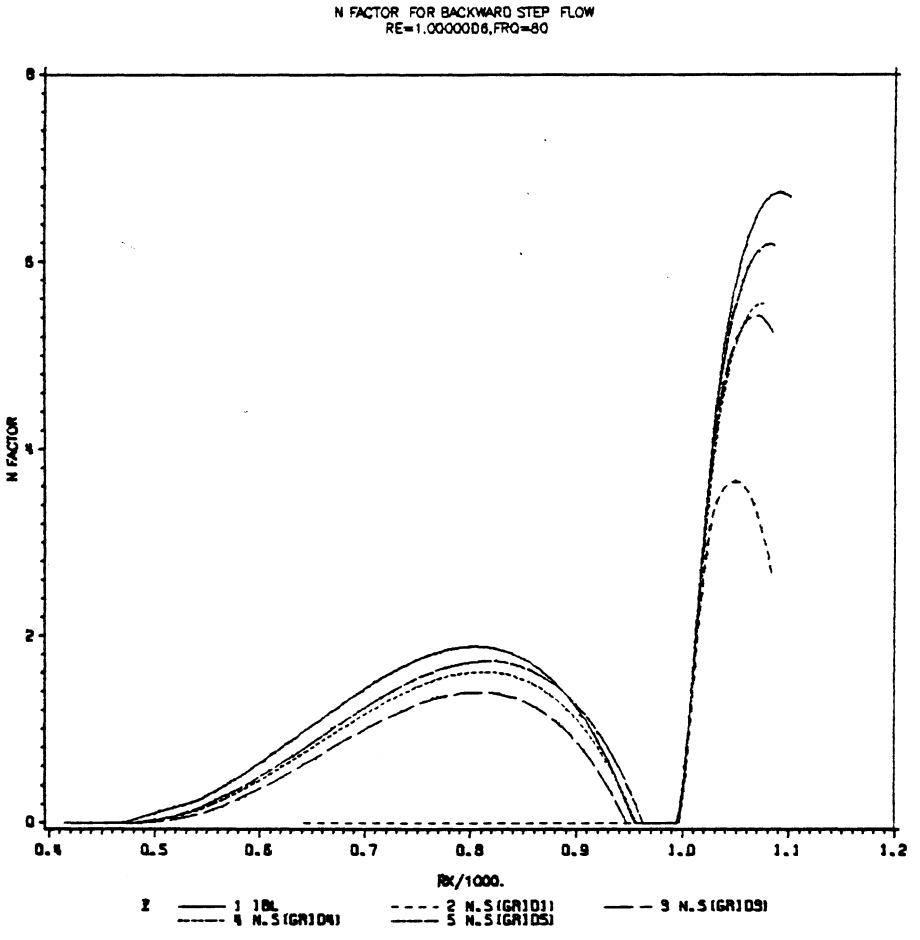

Figure 48. N factor (M=0. 5) comparison for finest grid

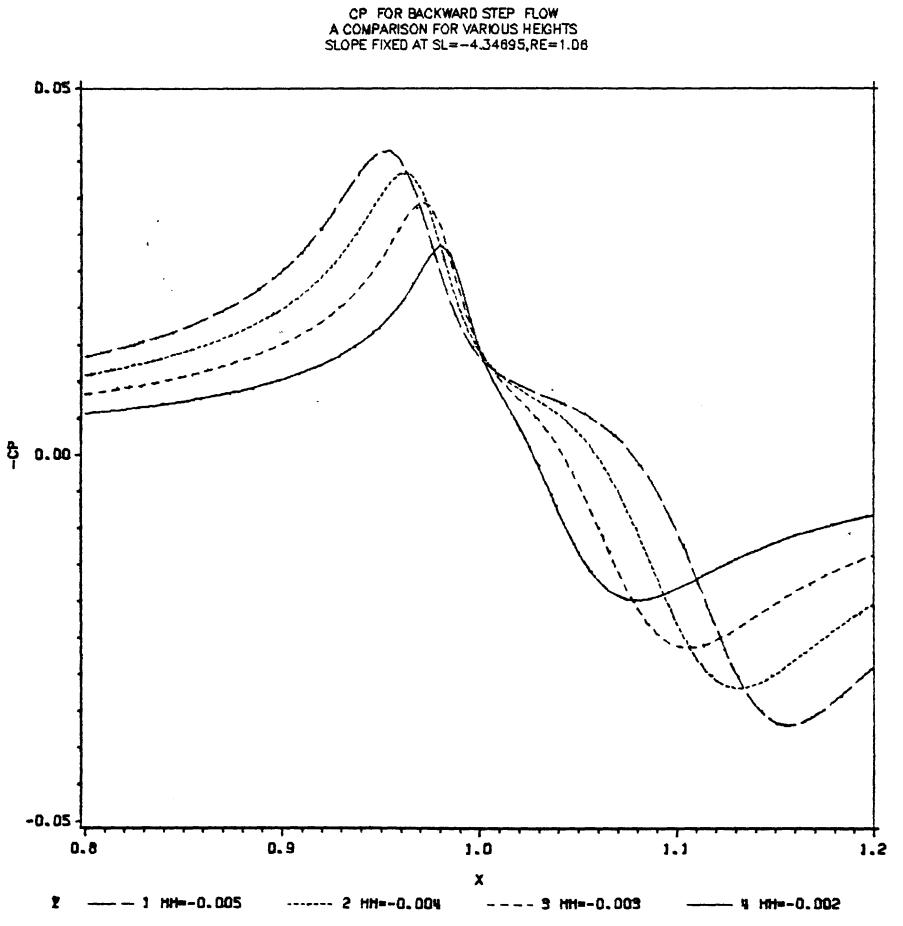

Figure 49. Cp for fixed slope and varying heights.(Backward step)

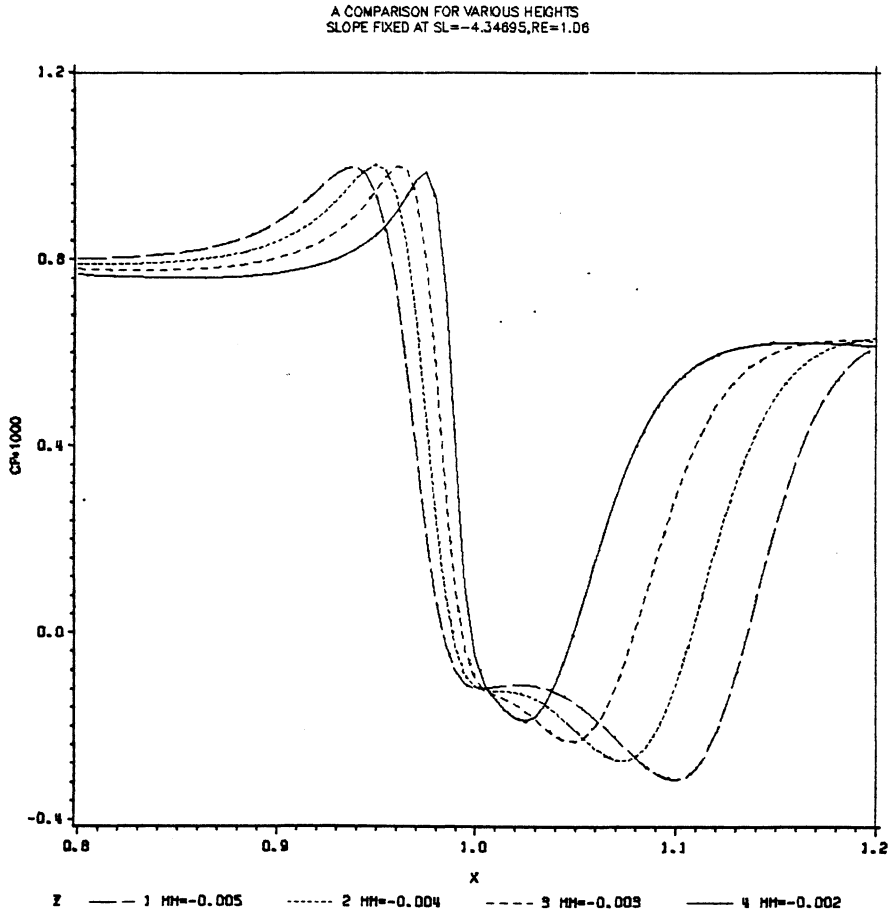

Figure 50. Cf for fixed slope and varying heights(Backward step)

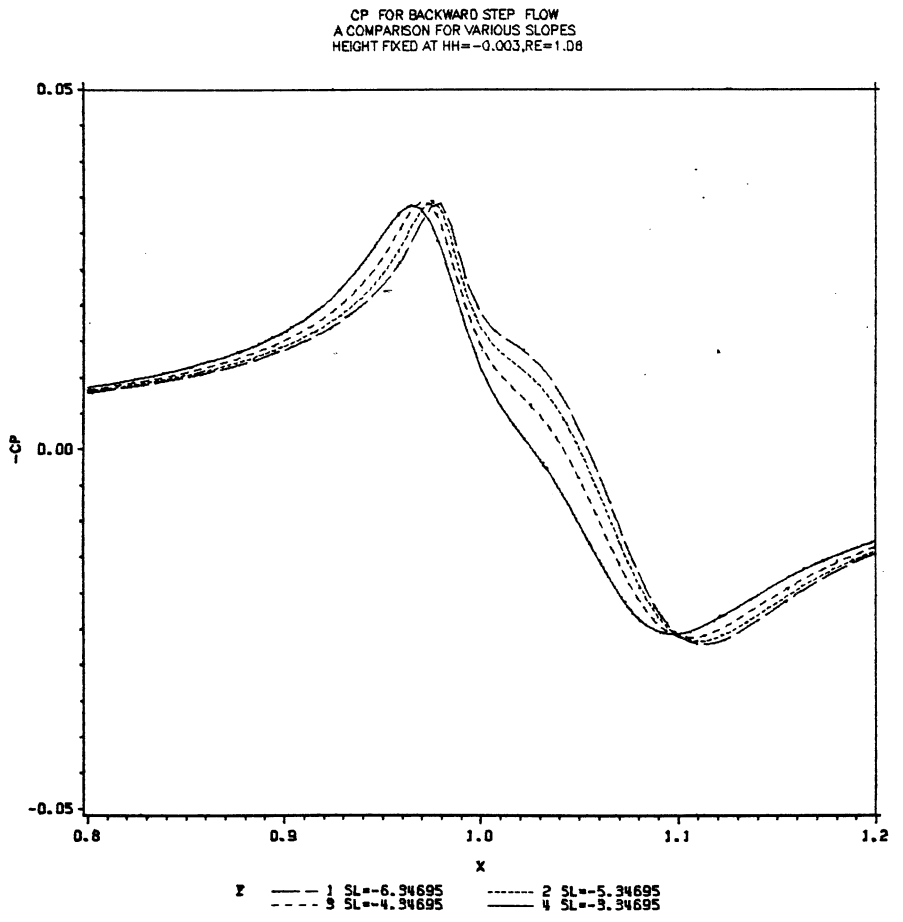

Figure 51. Cp for fixed heights and varying slopes(Backward step)

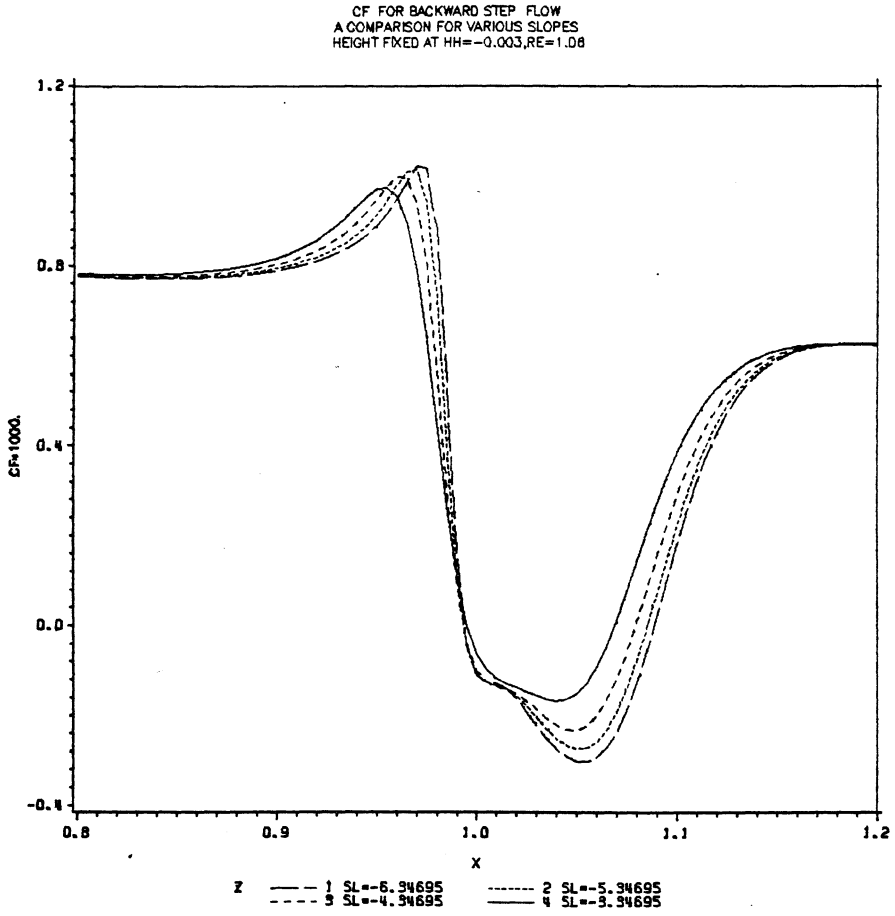

Figure 52. Cf for fixed heights and varying slopes(Backward step)

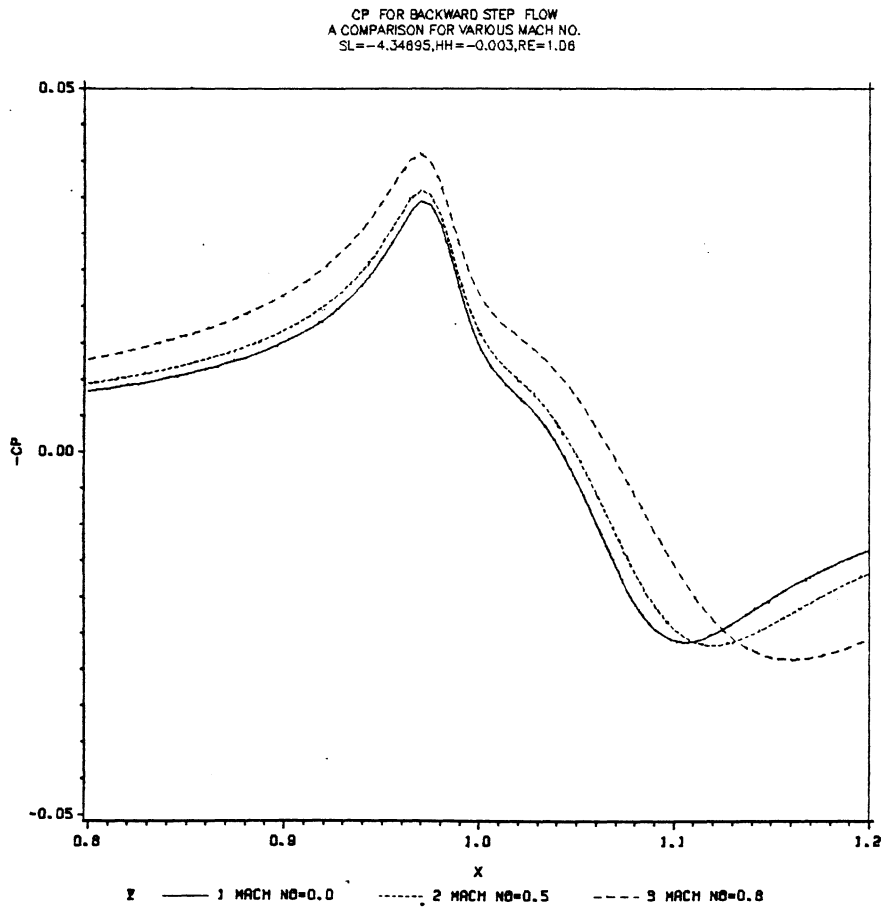

Figure 53. Cp for varying Mach numbers (Backward steps)

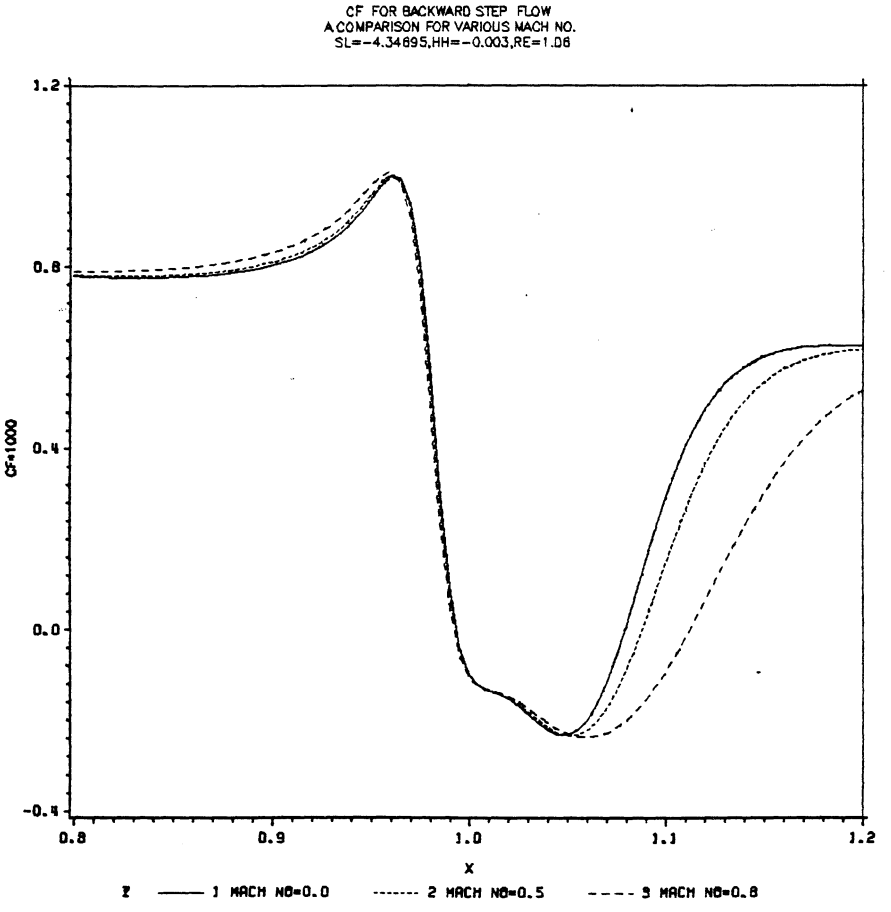

Figure 54. Cf for varying Mach numbers (Backward steps)

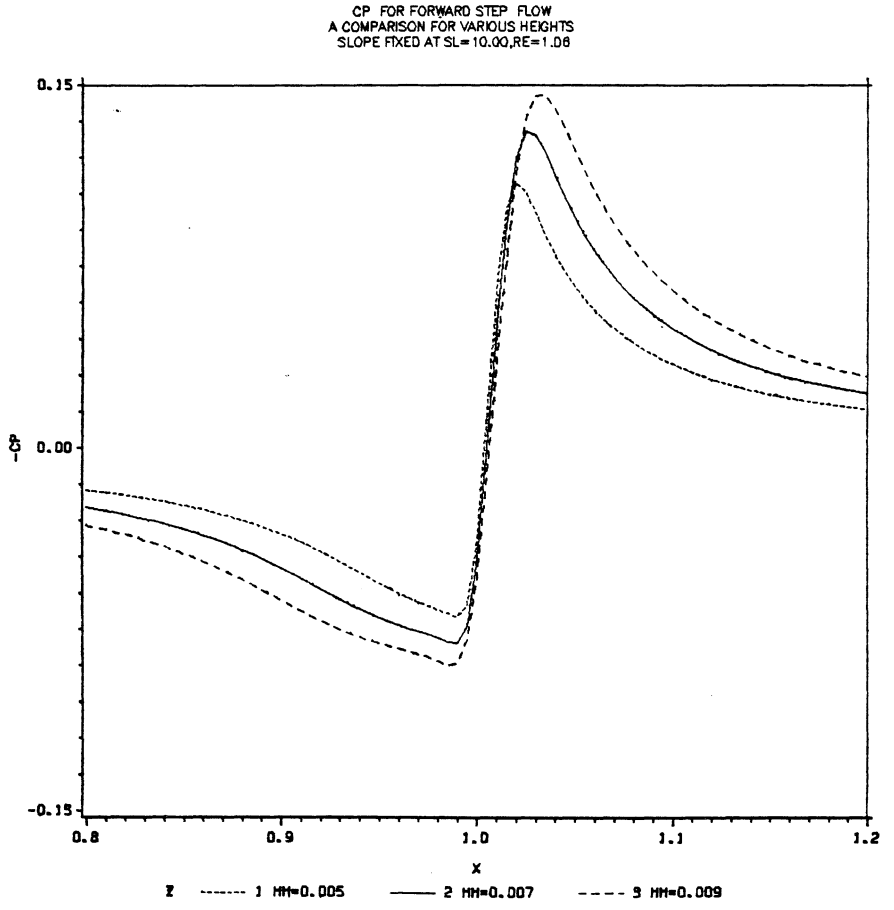

Figure 55. Cp for fixed slope and varying heights.(Forward step)

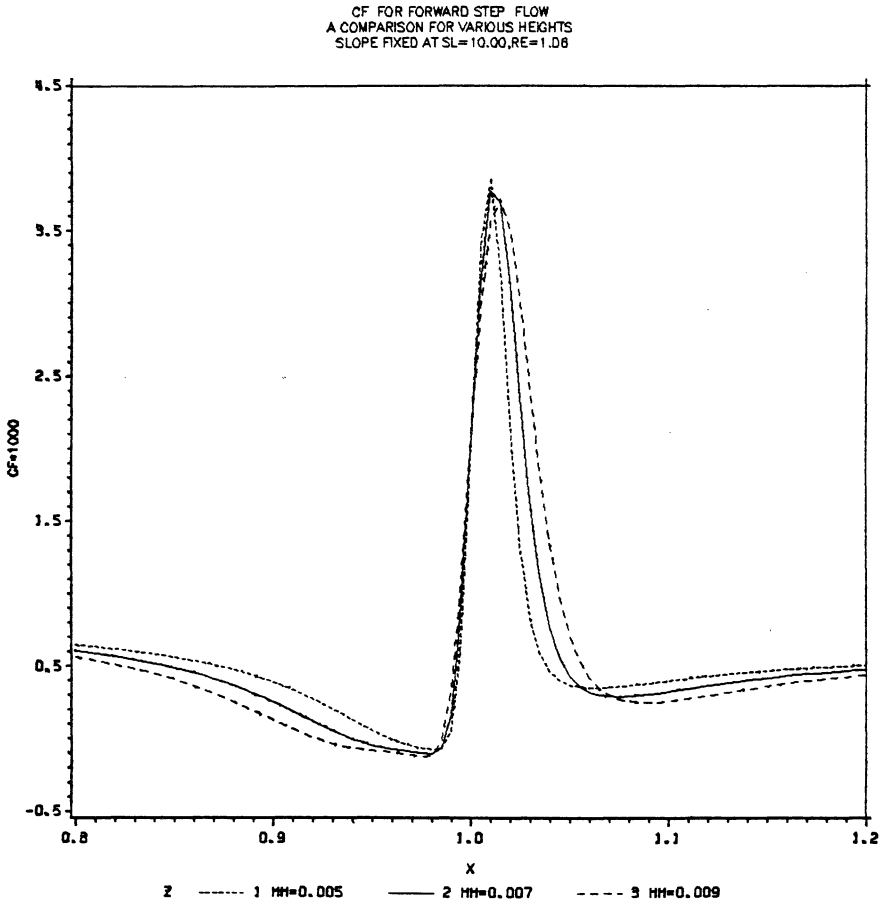

Figure 56. Cf for fixed slope and varying heights.(Forward step)

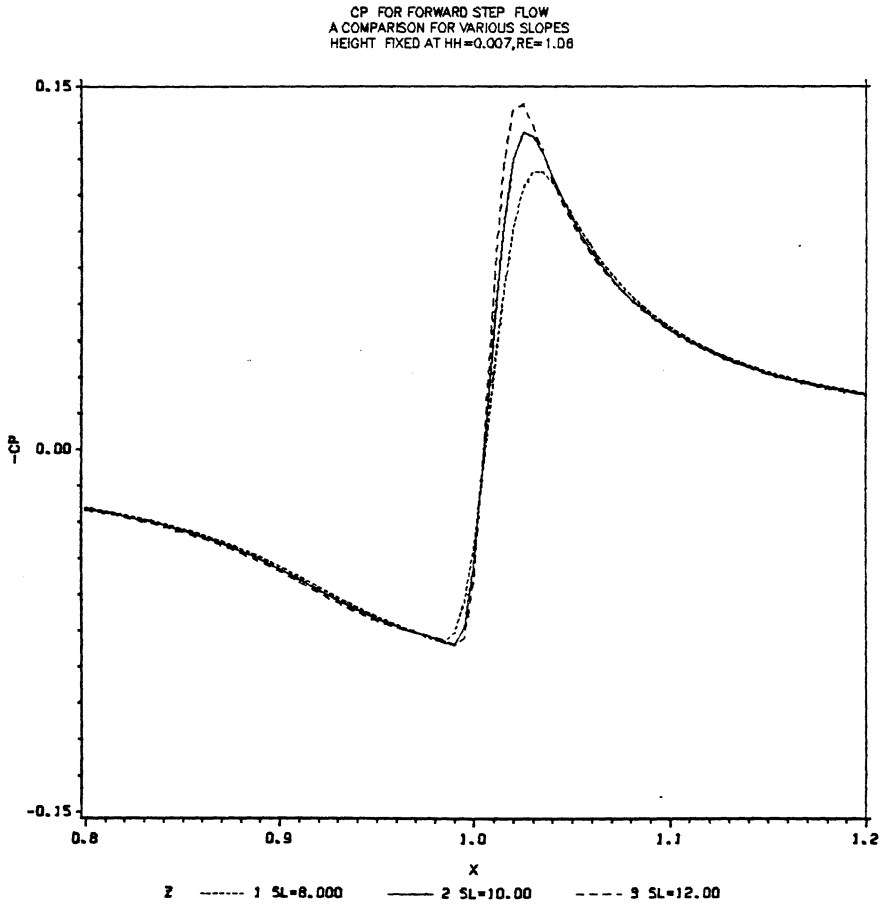

Figure 57. Cp for fixed heights and varying slopes(forward step)

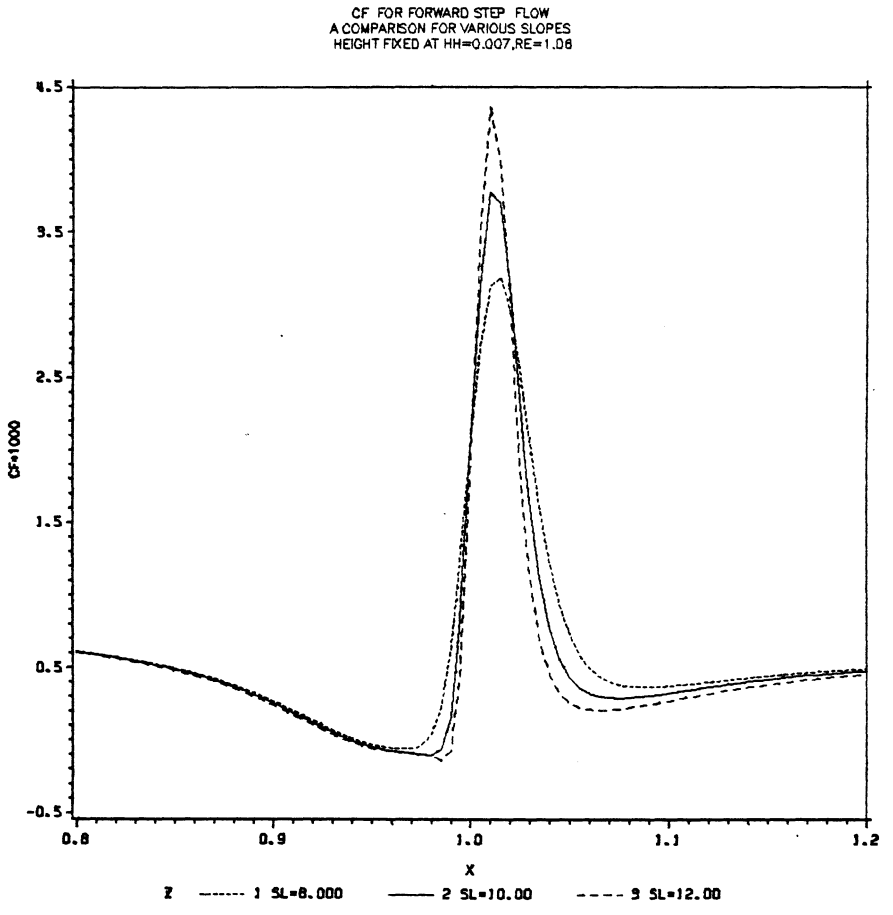

Figure 58. Cf for fixed heights and varying slopes(Forward step)

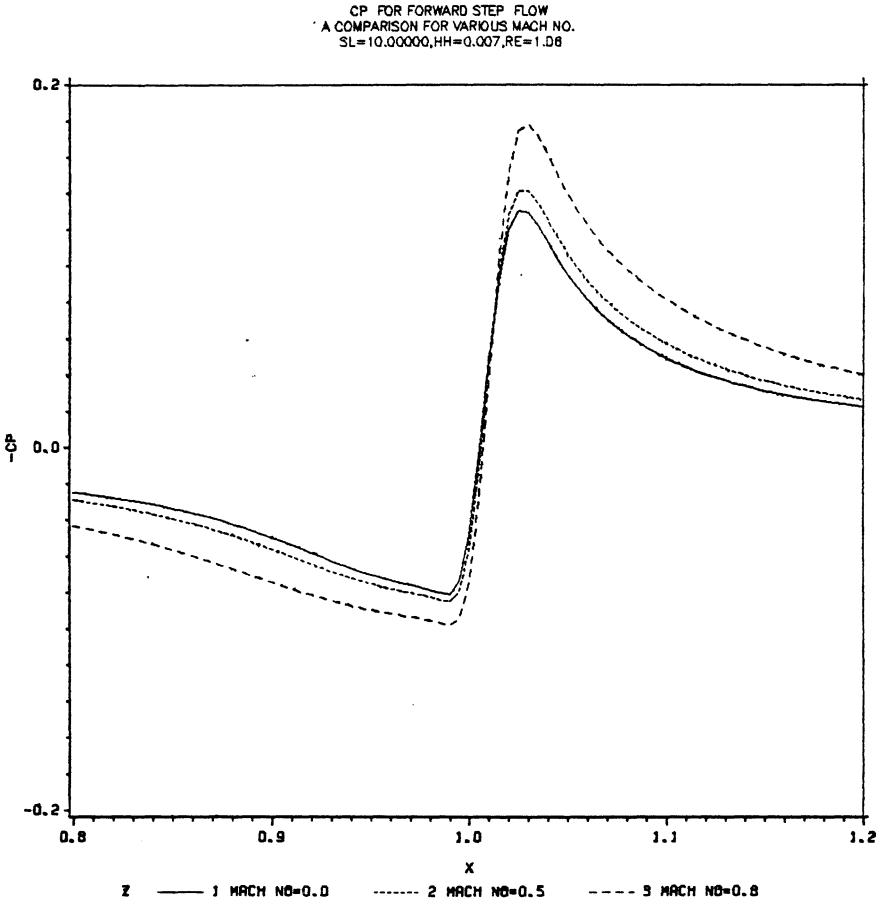

Figure 59. Cp for varying Mach numbers (Forward steps)

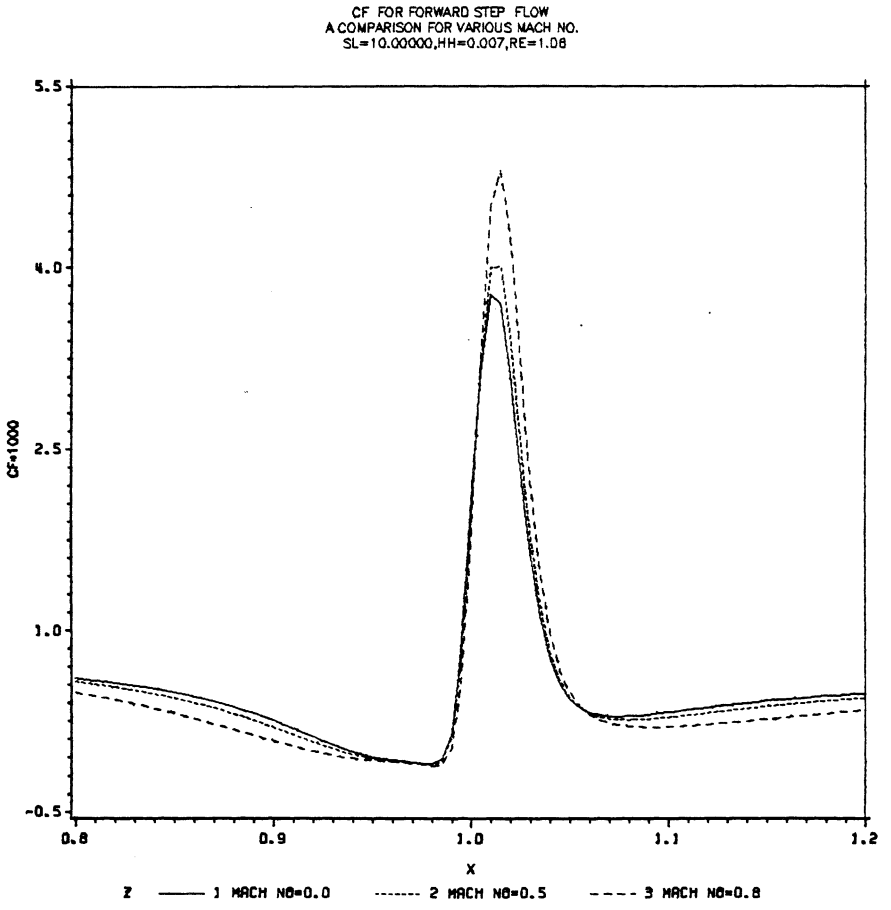

Figure 60. Cf for varying Mach numbers (Forward steps)

Height	Most Dangerous Frequency
-0.002	55
-0.003	60
-0.004	65
-0.005	70

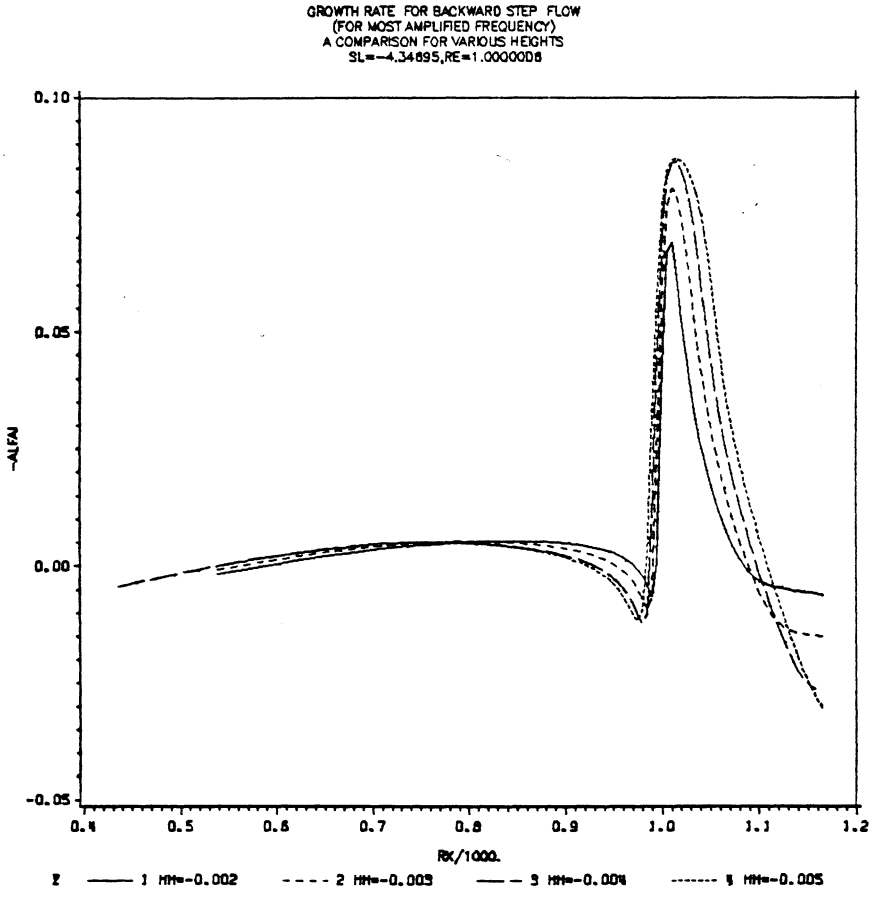

Figure 61. Growth rate for fixed slope (Backward step)

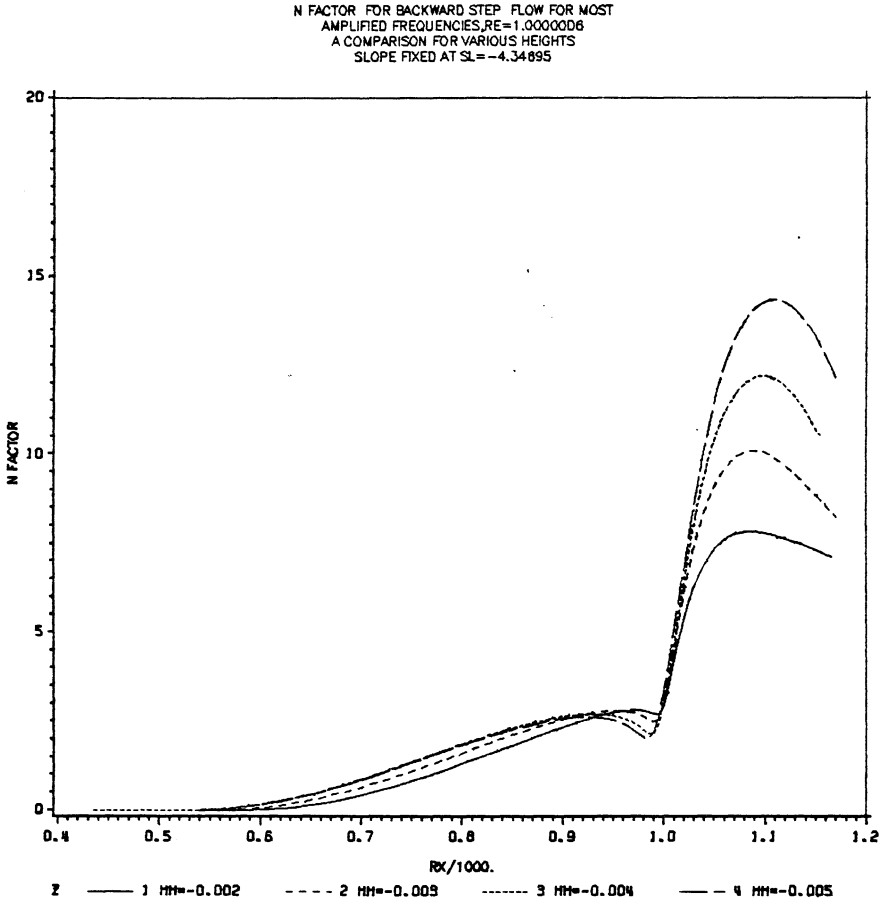

Figure 62. N-factor for fixed slope (Backward step)

Slope(degrees)	Most Dangerous Frequency
-3.34695	60
-4.34695	60
-5.34695	60
-6.34695	60

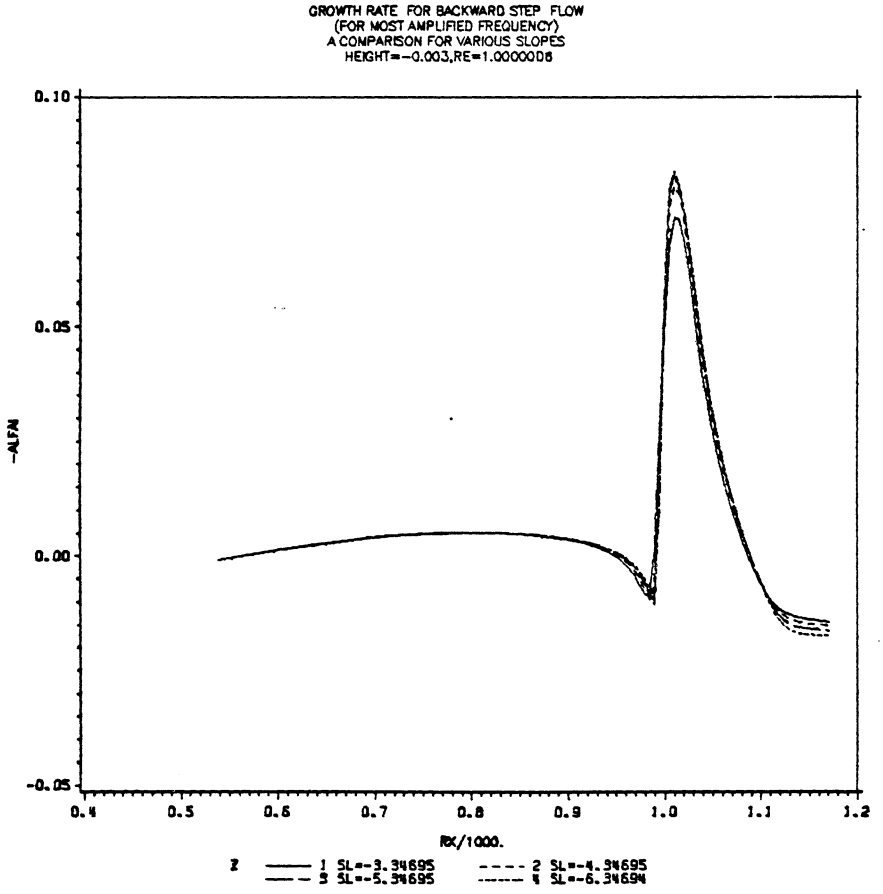

Figure 63. Growth rate for fixed heights (Backward step)

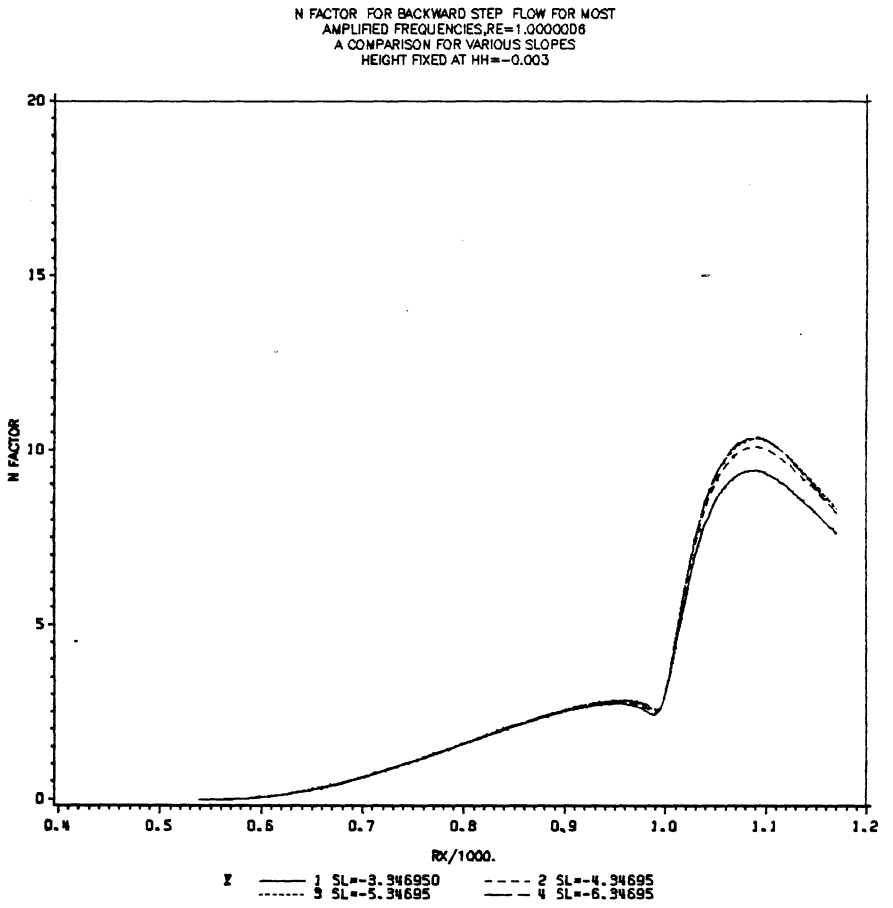

Figure 64. N-factor for fixed heights (Backward step)

Mach No.	Most Dangerous Frequency
0.0	60
0.5	55
0.8	50

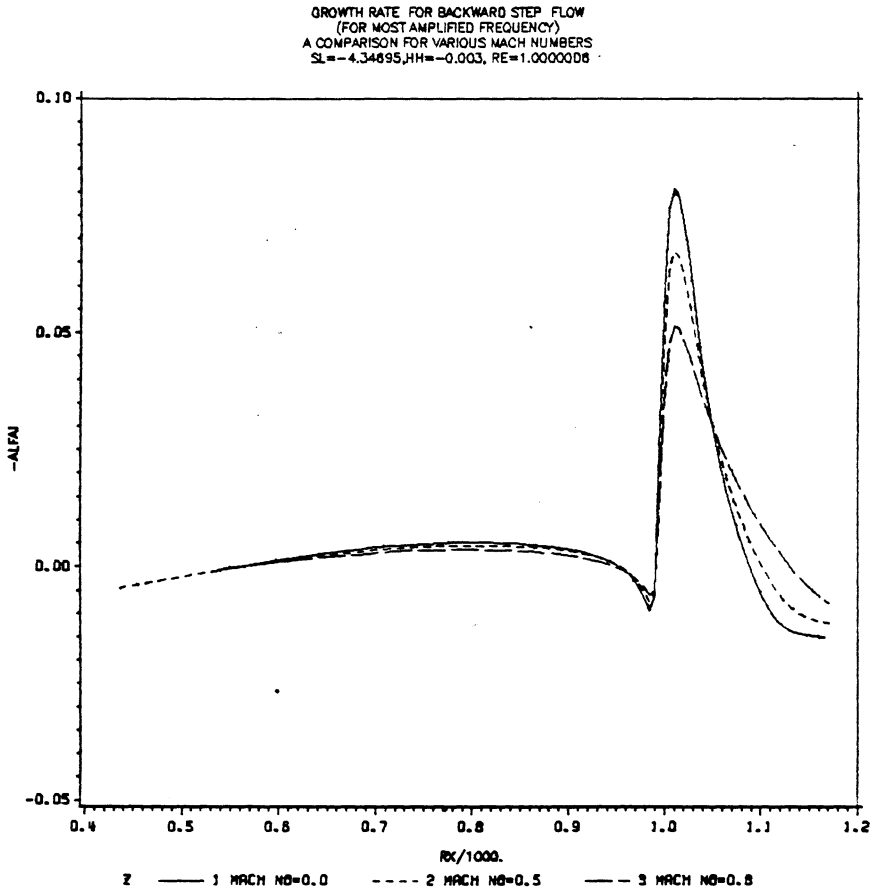

Figure 65. Growth rate for varying Mach numbers (Backward step)

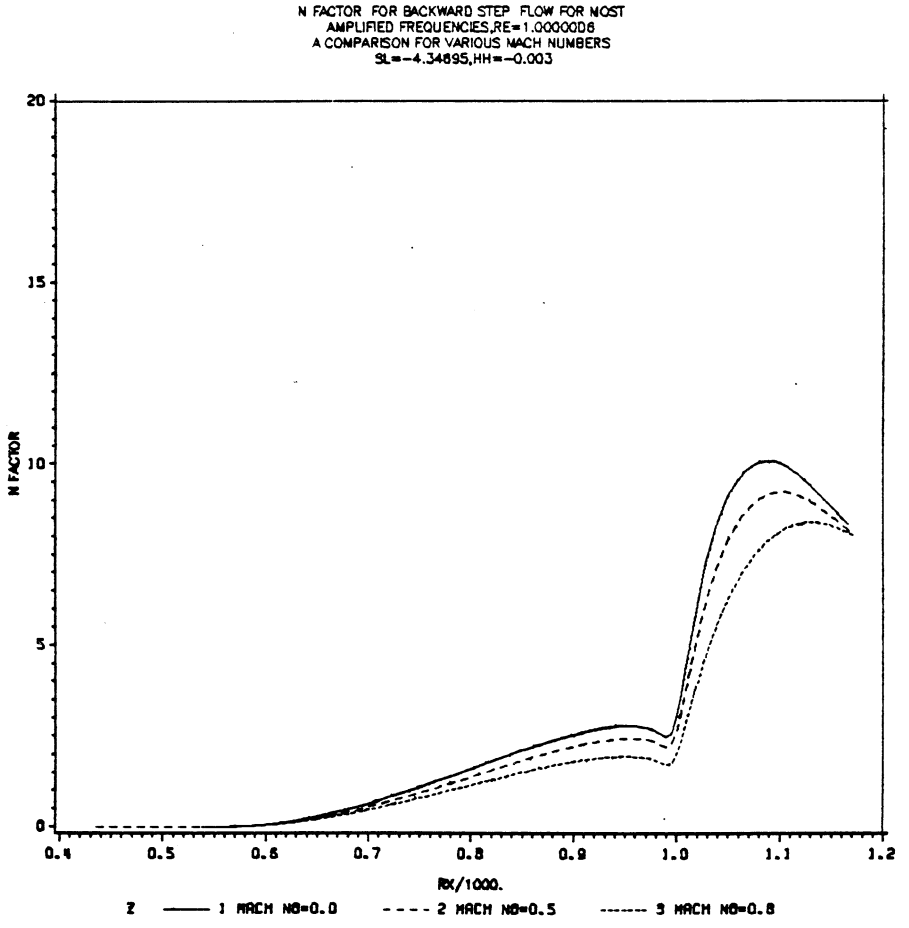

Figure 66. N-factor for varying Mach numbers (Backward step)

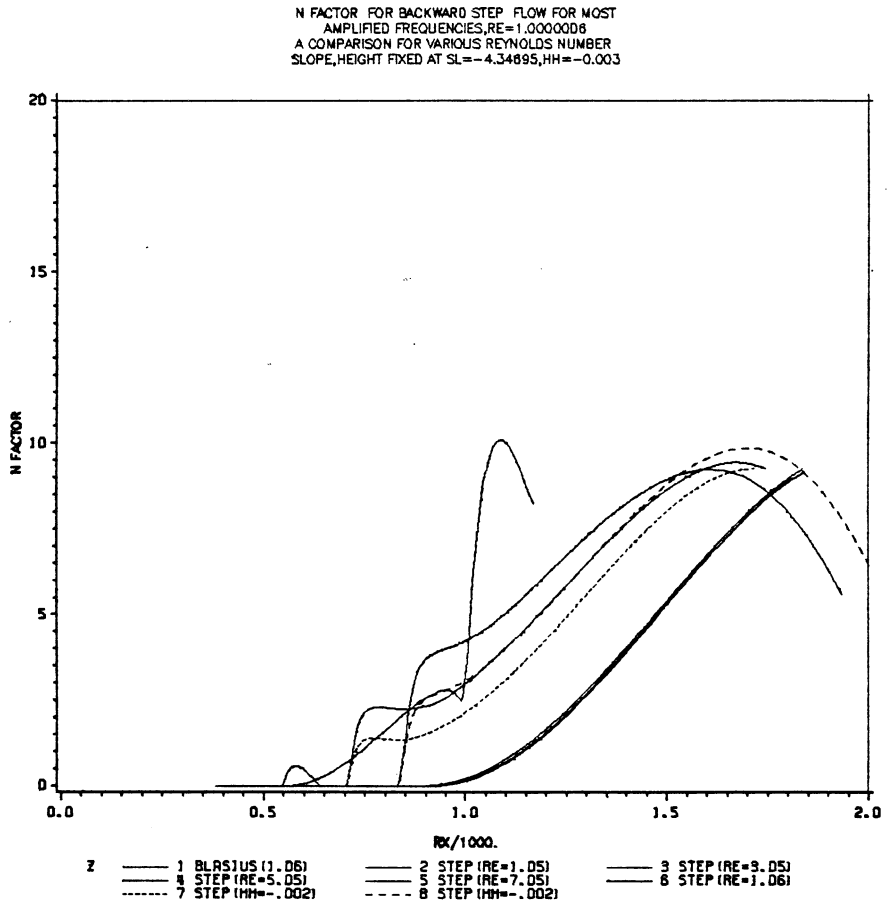

Figure 67. Effect of Reynolds number on the Stability (Backward step)

Height	Most Dangerous Frequency
0.005	45
0.007	50
0.009	55

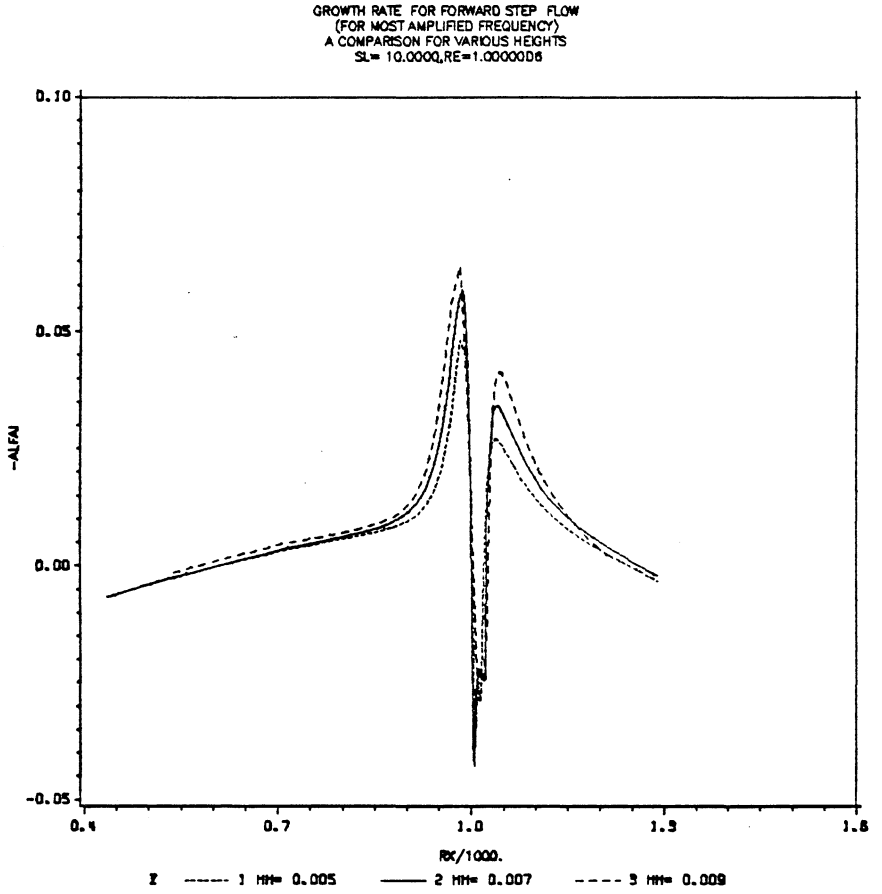

Figure 68. Growth rate for fixed slope (Forward step)

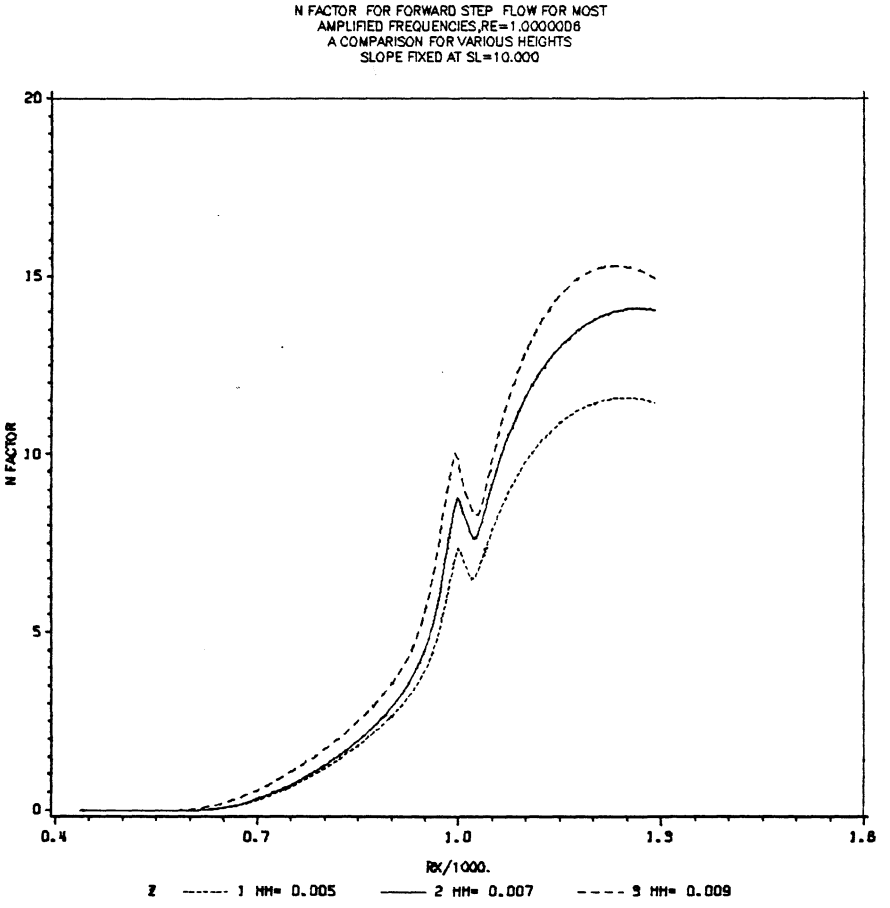

Figure 69. N-factor for fixed slope (Forward step)

Slope(degrees)	Most Dangerous Frequency
8.00	50
10.0	50
12.0	50

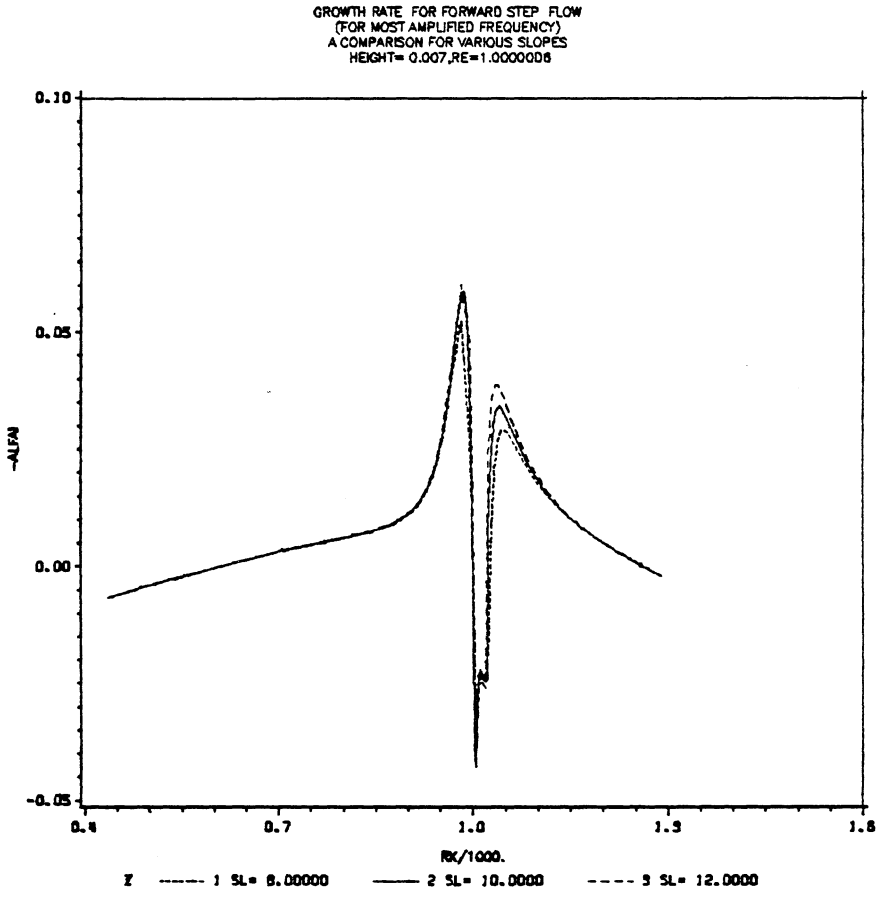

Figure 70. Growth rate for fixed heights (Forward step)

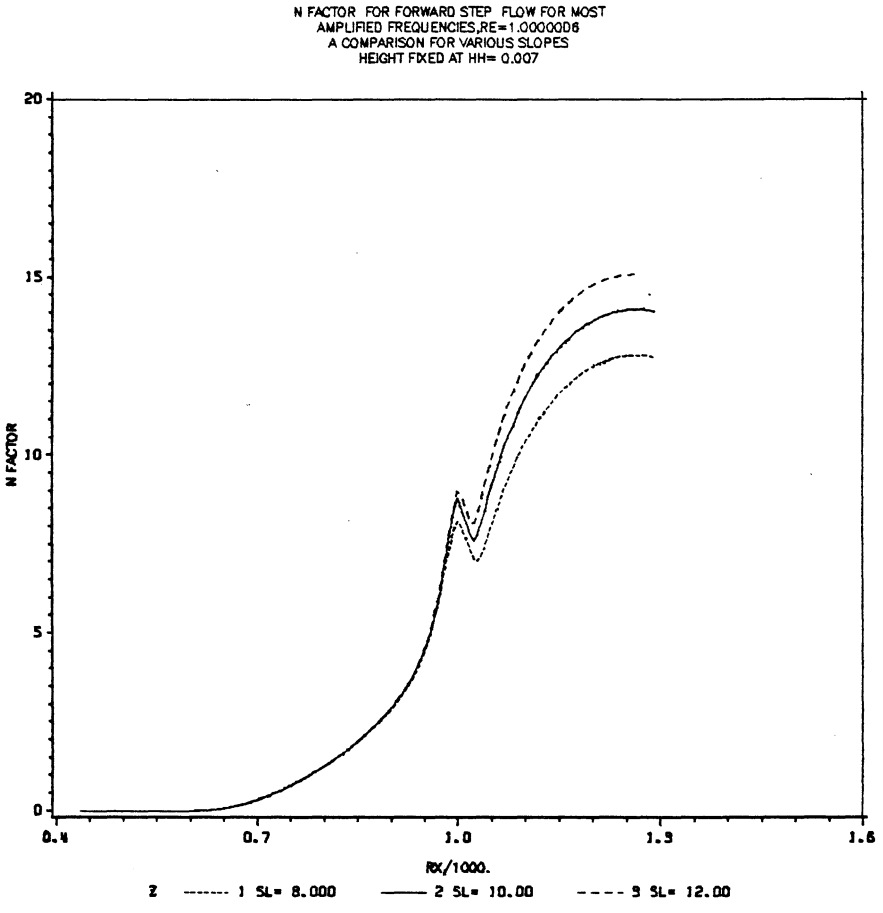

Figure 71. N-factor for fixed heights (Forward step)

Mach No.	Most Dangerous Frequency
0.0	50
0.5	45
0.8	40

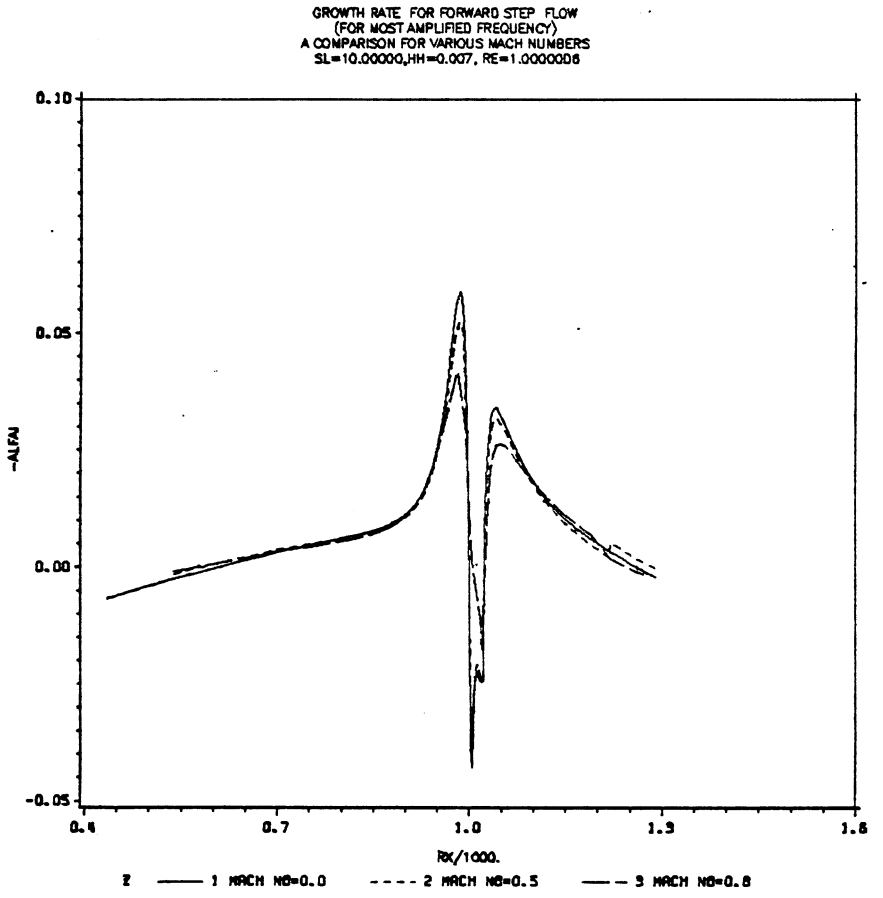

Figure 72. Growth rate for varying Mach numbers (Forward step)

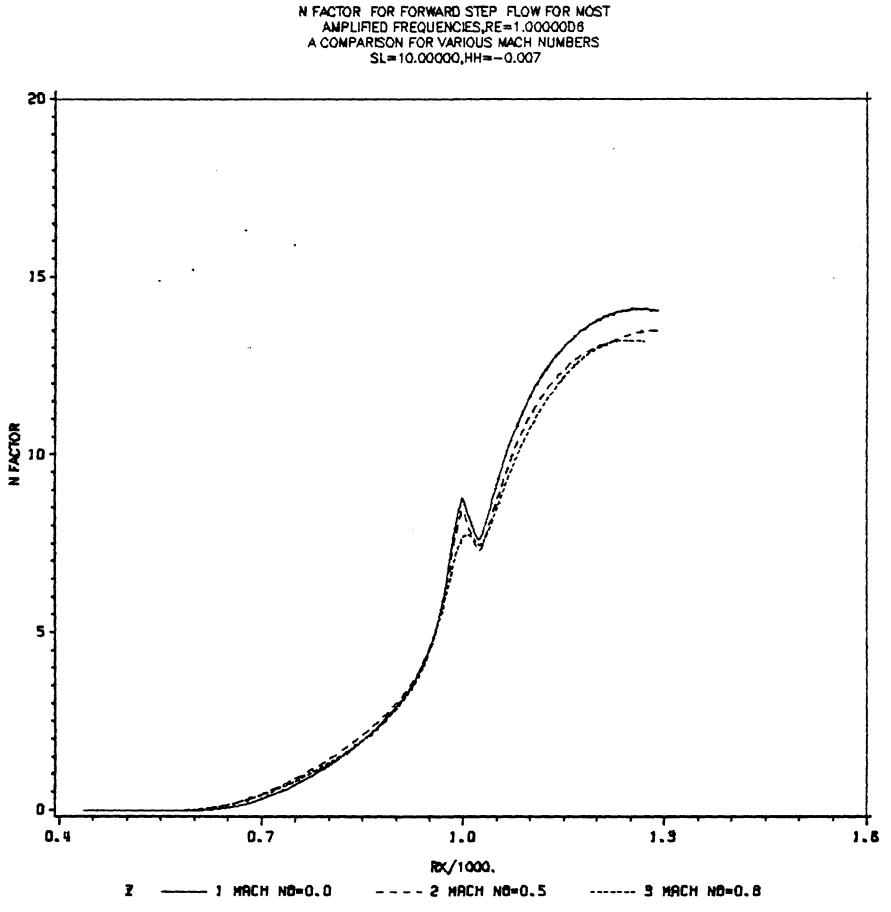

Figure 73. N-factor for varying Mach numbers (Forward step)

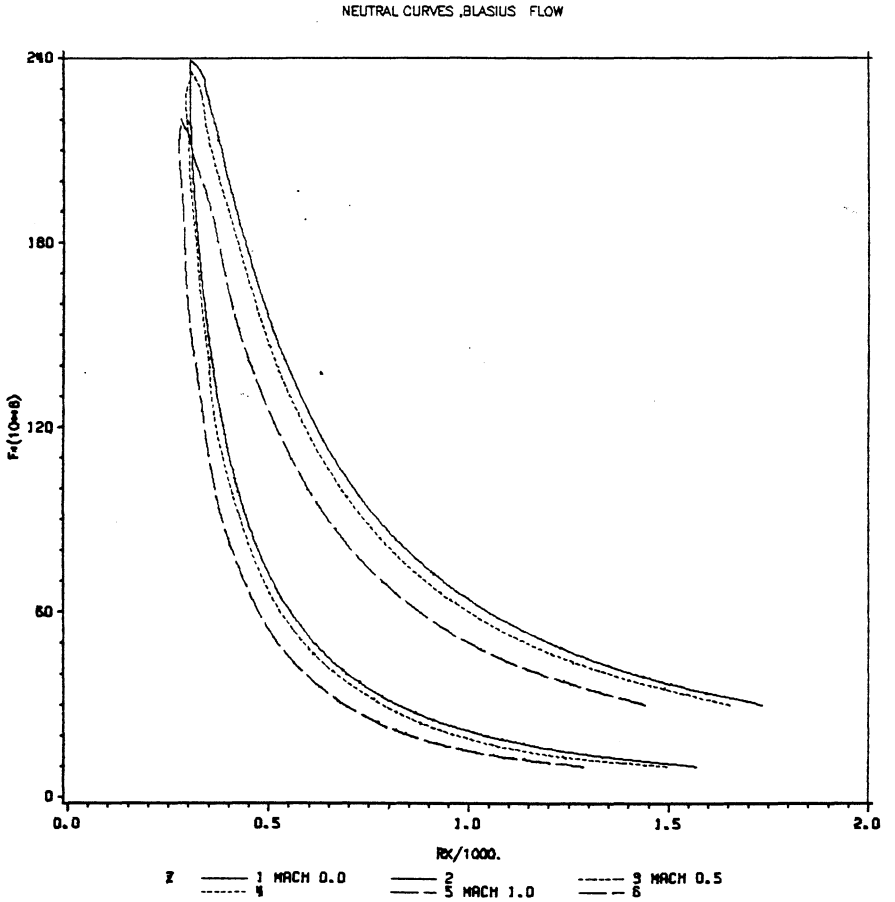

Figure 74. Neutral stability curves for Blasius flow

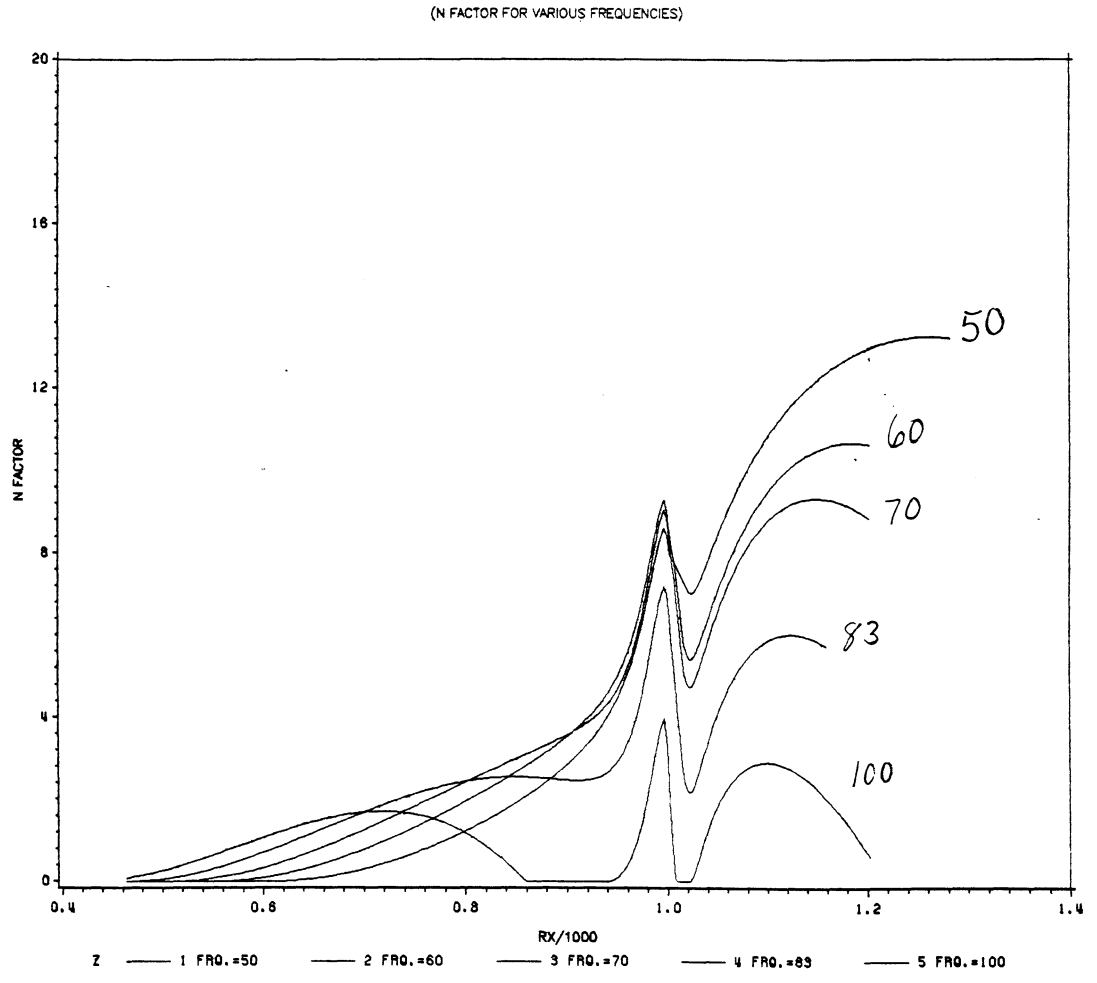

Figure 75. Most Dangerous Frequency Determination

The vita has been removed from the scanned document